

**Study on Structural Analysis of Nucleic Acids and
Energy Migration between Identical Chromophores
by using Orientation-dependent FRET System**

(配向依存 FRET システムを使用した
核酸構造解析と同種色素間エネルギー移動に関する研究)

KAWAI Hayato

河合 隼人

2023

TABLE OF CONTENTS

Chapter 1. General Introduction

1-1	Förster resonance energy transfer (FRET).....	1
1-2	Application of FRET using DNA -structure analysis-.....	3
1-3	Energy migration(homo-FRET)	7
1-4	Purpose of this study	10
1-5	References	12

Chapter 2. Analysis of structures and flexibilities of nicked and gapped DNA duplexes by using orientation-dependent FRET system

2-1	Abstract	16
2-2	Introduction	17
2-3	Results and discussions	20
2-3-1	Structural analysis of a canonical duplex	20
2-3-2	Structural analysis of DNA duplexes with nicks.....	23
2-3-3	Structural analysis of DNA duplexes with gaps.....	26
2-3-4	Melting temperatures (T_{ms}) of duplexes determined by FRET.....	29
2-4	Conclusions	31
2-5	Experimental section.....	33
2-6	References	39
2-7	Appendixes	42

Chapter 3. Structural analysis of photoactive DNA by using Perylene-Cy3 FRET system

3-1	Abstract	55
3-2	Introduction	56
3-3	Results and discussions	59
3-3-1	Orientation dependence of FRET between perylene-Cy3 pair.....	59
3-3-2	Structural analysis of stilbene modified DNA by using FRET system	66
3-3-3	Structural changes upon photodimerization between stilbene residues	71

3-3-4	Structural analysis of stilbene with spacers (1,3-propanediol) modified DNA by using FRET system.....	72
3-4	Conclusions	78
3-5	Experimental section	80
3-6	References	86
3-7	Appendixes	88

Chapter 4. Study of energy migration between the identical chromophores by using a DNA scaffold

4-1	Abstract	95
4-2	Introduction	96
4-3	Results and discussions	97
4-3-1	Sequence design in this study.....	97
4-3-2	Investigation of perylene separated from anthraquinone	99
4-3-3	Investigation of perylene next to anthraquinone	102
4-3-4	Melting temperatures (T_{ms}) of duplexes.....	104
4-3-5	Quantitative analysis of energy migration between two perylenes.	105
4-3-6	Comparison with Förster theory.....	111
4-3-7	Analysis of energy migration among four perylenes	113
4-4	Conclusions	120
4-5	Experimental section	121
4-6	References	129
4-7	Appendixes	131

Chapter 5. Quantitative analyses of homo FRET between two pyrenes

5-1	Abstract	143
5-2	Introduction	143
5-3	Results and discussions	146
5-3-1	Melting temperatures (T_{ms}) of duplexes.....	146
5-3-2	Emission spectra of each set of duplexes	147
5-3-3	Lifetime measurements of each set of duplexes.....	150
5-3-4	Quantitative analysis of energy migration between two pyrenes.....	152
5-3-5	Comparison with Förster theory.....	153
5-4	Conclusions	156

5-5	Experimental section	157
5-6	References	164
5-7	Appendixes	166
	List of Publications	175
	List of Presentations	175
	List of Awards	176
	Acknowledgements	177

Chapter 1. General Introduction

1-1 Förster resonance energy transfer (FRET)

Förster resonance energy transfer (FRET) is a nonradiative mechanism of energy transfer from a donor fluorophore to an acceptor via electronic dipole-dipole coupling. ^[1]

If the acceptor is a fluorophore, the acceptor emits light even though the donor has been excited. The FRET efficiency varies depending on both relative distance and orientation between the donor and acceptor. The rate constant of FRET (k_{ET} , energy transfer by Förster mechanism) represented by the following equation (1):

$$k_{ET} = \frac{9 \ln 10}{128 \pi^5 n^4 N_A \tau_D^0} \cdot \frac{\kappa^2}{R^6} \int f_D(\lambda) \varepsilon_A(\lambda) \lambda^4 d\lambda \quad (1)$$

where n is a refractive index, N_A is the Avogadro constant, τ_D^0 is radiative decay time of donor, and R is the distance between donor and acceptor. f_D and ε_A are donor emission spectra (normalize to 1) and acceptor absorption spectra.

The orientation factor, κ^2 , is calculated from the below equation (2):

$$\kappa^2 = (\cos \theta_T - 3 \cos \theta_D \cos \theta_A)^2 \quad (2)$$

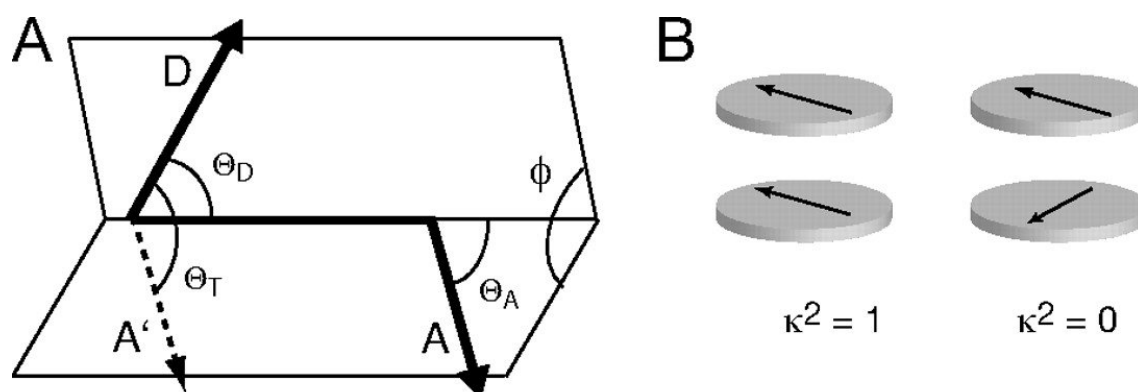


Figure 1-1.

(A) Schematic of the orientation factor κ^2 . (B) The orientation factor simplifies to $\kappa^2 = \cos^2 \theta_T$ and varies between 0 and 1 when the fluorophores lie in parallel planes. (Reprinted from Ref. 2.)

In FRET, there is no need for electron clouds to overlap between the two molecules, and energy transfer occurs even when the intermolecular distance is 10 nm. Due to its distance-dependence, FRET has been widely used as a “ruler” in chemistry and biology.^[3] Specifically, the interaction between proteins^[4] and the distance between molecules^[5] are clarified by FRET. However, the orientation dependence of FRET has usually not been taken into consideration, since it is difficult to precisely control the orientation of the fluorophores. To prevent the dye from fixing in an unexpected orientation, FRET systems are often designed with long linkers attached to the fluorophore to minimize orientation dependence^[5].

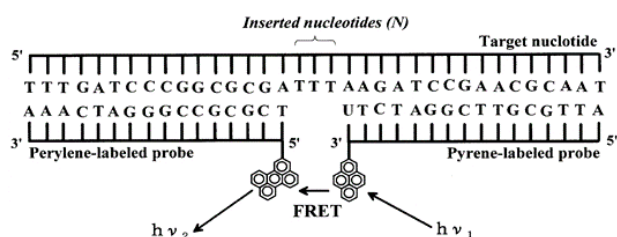


Figure 1-2.

Schematic of a FRET system that utilizes long linkers to prevent dye from fixing in an unexpected orientation. (Reprinted from Ref. 5.)

1-2 Application of FRET using DNA -structure analysis-

DNA scaffolds have been used to investigate orientation dependence of FRET. [2,6]

DNA is an effective scaffold as it forms a rigid double helical structure, enabling control of dye orientation. For example, Wilhelmsson and co-workers developed 2' - deoxyadenosine analogues qAN1 (donor) and qAnitro (acceptor) and the FRET orientation dependence was observed by simply replacing adenine with the analogues. [7a]

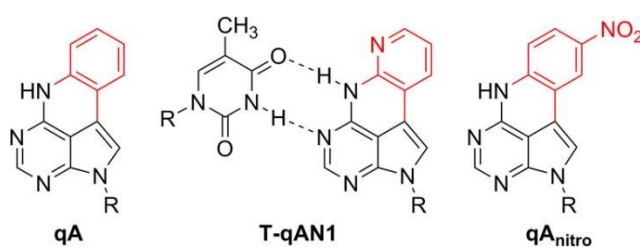


Figure 1-3.

Structure of qA, qAN1 (base paired with thymine (T)), and qAnitro. (Reprinted from Ref.7a)

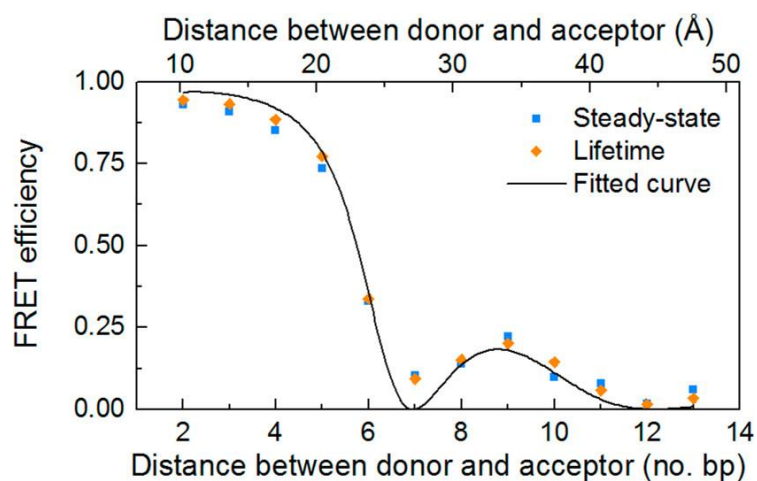


Figure 1-4.

The experimental FRET efficiency showed good agreement with the theoretical efficiency. (Reprinted from Ref.7a)

In another example, a FRET system using fluorescent thymidine and cytosine analogs has also been reported. [7b]

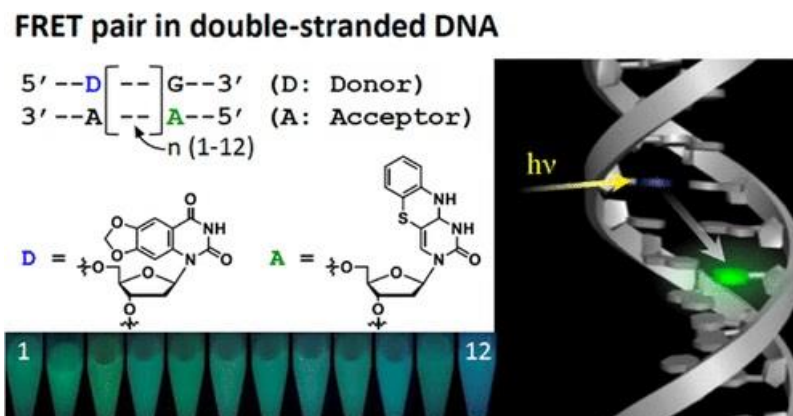


Figure 1-5.

Schematic of sequence and chemical structure of fluorescent thymidine and cytosine analogs. Photographs of FRET DNA in tubes and a structural model of the DNA are also shown. (Reprinted from Ref.7b)

Previous our research also showed a useful DNA-based FRET system, in which

pyrene and perylene were introduced into DNA via D-threoninol. [8] We have succeeded in control of fluorophores' orientations in DNA duplex as expected so that distance and orientation dependences of FRET efficiency were observed in this system. It is useful in that a wide range of dyes can be introduced.

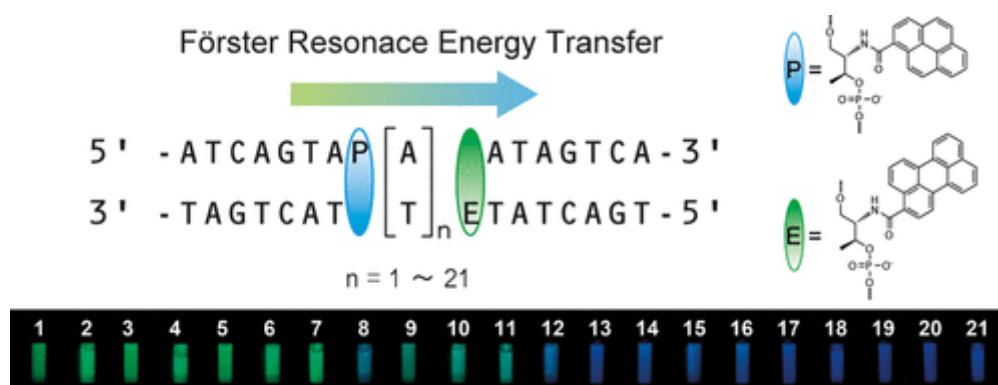


Figure 1-6.

Schematic of sequence design and chemical structure. Photographs showing changes in FRET efficiency are also shown. (Reprinted from Ref. 8)

The distance and orientation dependences FRET system employing the DNA scaffold enables detailed structural parameters to be obtained in solution.

X-ray crystallography and nuclear magnetic resonance (NMR) are powerful tools for analysis of DNA structures, but these techniques require a large amount of sample and are time consuming. Further, the X-ray crystal structures revealed may not reflect the structures found in biological milieu. Structural analysis of using a cryo-electron microscopy has also recently received broad attention due to the development of sample

preparation methods, detectors, image recognition using deep learning and so on. [9,10]

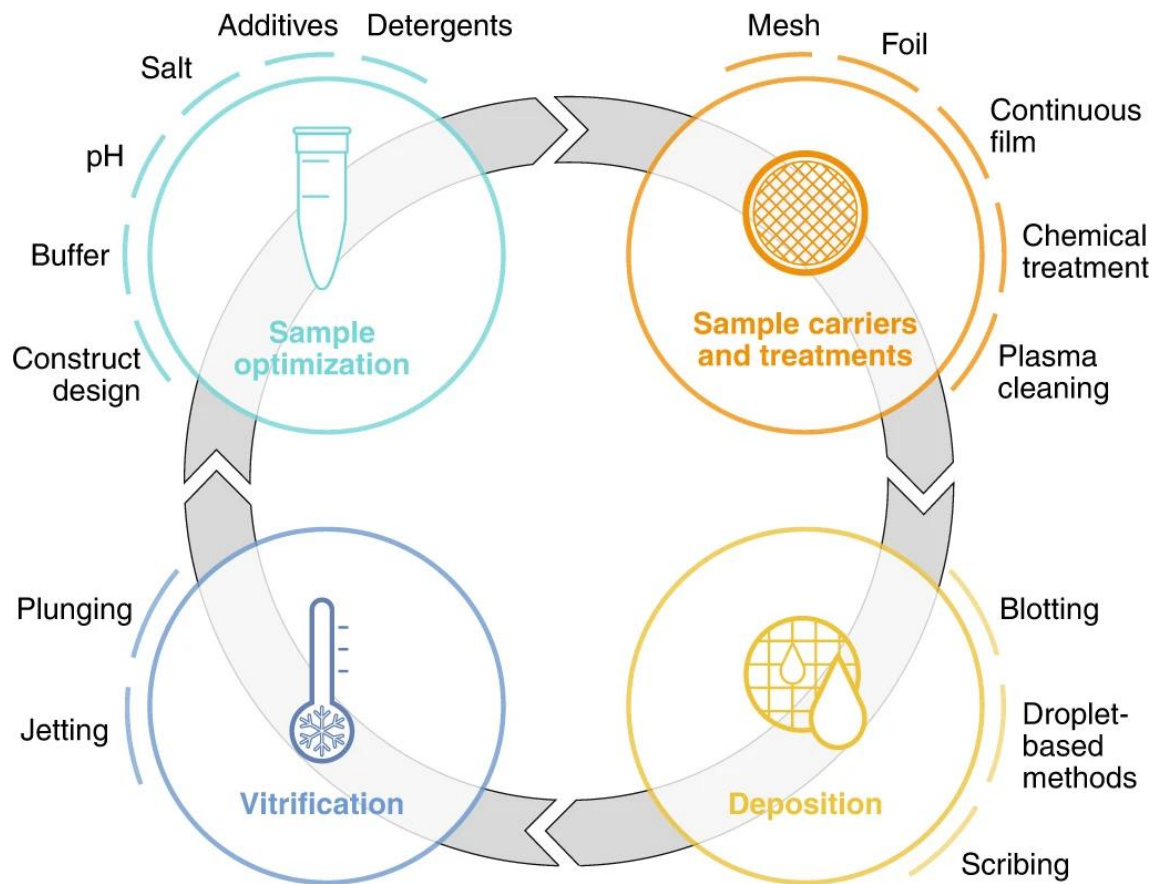


Figure 1-7.

Schematic of sample preparation for cryo-EM. (Reprinted from Ref.9)

It allows the analysis of the structure of biopolymers in solution. However, it has not yet become widespread as a general analytical method, and a simple structural analysis method is required.

1-3 Energy migration(homo-FRET)

Excitation energy migration (EM), also called excitation energy hopping or homo Förster resonance energy transfer (homo-FRET), is energy transfer among identical fluorophores. This type of transfer is a key process in natural photosynthesis since excitation energy can be transported without losing photon energy. In natural light-harvesting complexes, absorbed energy migrates first among a number of identical chlorophyll molecules and subsequently transfers to reaction center. Natural light-harvesting complexes achieve efficient solar energy conversion by tuning energy migration efficiency. ^[11]

Energy migration is also important in artificial light-harvesting systems, chemical sensing, photon energy conversion, and analyses of biomolecular probes. ^[12-15] It has been shown that EM efficiencies can be controlled to some extent through positioning of fluorophores via covalent or non-covalent bonds.

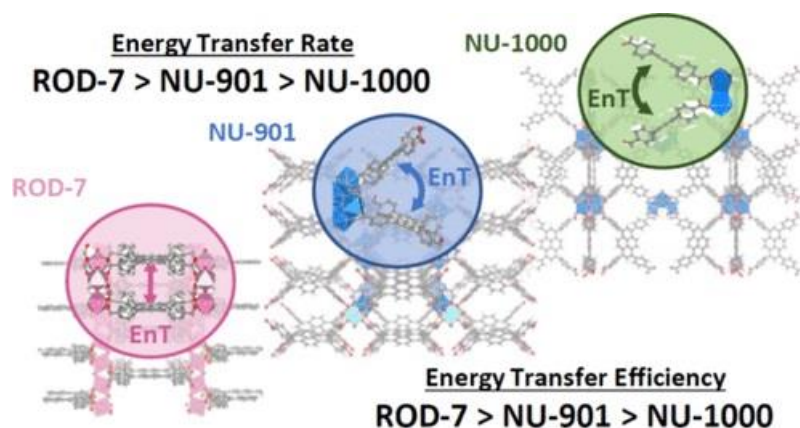


Figure 1-8.

Structure of metal–organic frameworks (MOFs) with pyrene and porphyrin. in which energy migration was studied. (Reprinted from Ref. 15)

However, precise control of distance and orientation of fluorophores over a wide range and an achievement of intended high efficiency EM still remains challenging.

DNA spontaneously forms a well-defined right-handed double helix, in which four nucleobases are aligned according to the sequence. Arrays of non-natural molecules with pre-determined size, distance, and even sequence can be easily prepared by incorporating unnatural monomer into DNA through covalent bonding.^[16,17] DNA has been widely used as a platform to prepare fluorophore arrays,^[18-22] and recently, photonic arrays and circuits based on DNA nano-structures have been reported.^[23-26]

In these structures, EM and hetero FRET play crucial roles in efficient energy harvesting and transport.^[27-37]

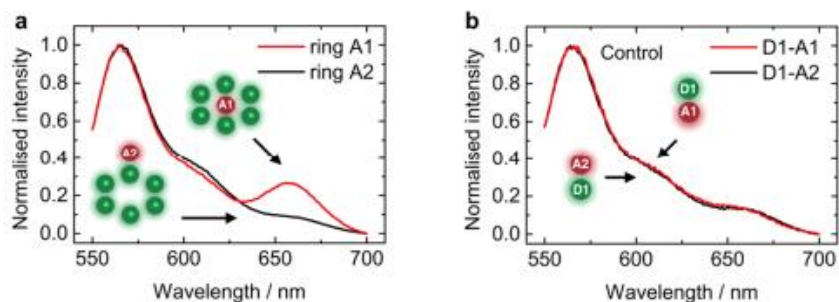


Figure 1-9.

a) Normalized fluorescence emission spectra with acceptor inside (ring A1, red line) and outside (ring A2, black line) the donor ring, b) Normalized fluorescence emission spectra of corresponding donor-acceptor pairs with donor fixed at D1 and acceptor at A1(D1-A1, red line) and at A2(D1-A2, black line.) (Reprinted from Ref. 35)

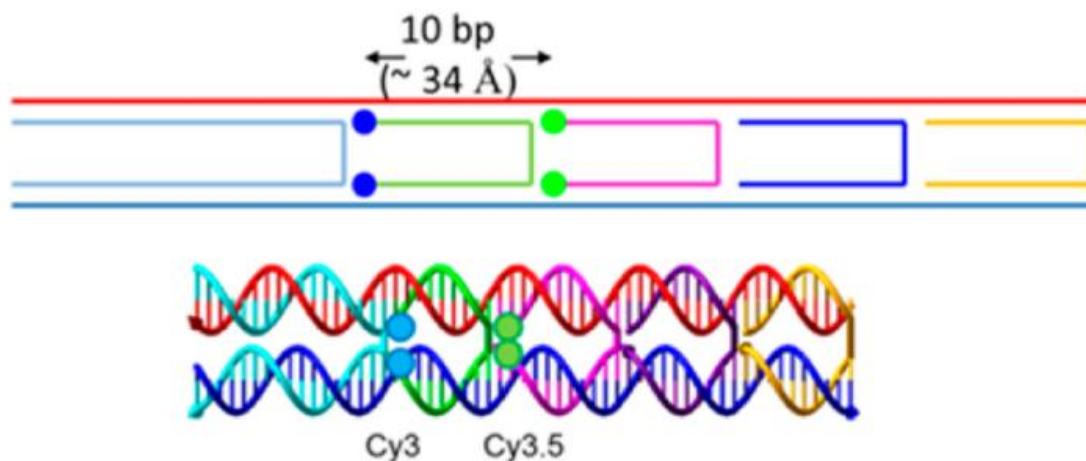


Figure 1-10.

Upper: Schematic of the dual rail DNA structure consisting of the self-assembly of seven DNA oligos, each depicted by a separate color. Lower: Schematic of the dual rail DNA structure showing the double crossover motif and positioning of the Cy3 and Cy3.5 fluorophores. (Reprinted from Ref. 36)

Several research groups, including ours, have utilized DNA scaffolds to quantify orientation and distance dependence of hetero FRET from a donor to an acceptor^[6-8]. On

the other hand, distance and orientation dependences of energy migration between identical fluorophores have not been elucidated. In EM, energy migration occurs among the identical fluorophores, and each fluorophore can function both as a donor and an acceptor. Such symmetry among the fluorophores makes it impossible to separate donor and acceptor emission. Time-resolved anisotropy measurement has been used to analyze EM; however, the analyses are model dependent, and kinetic parameters cannot be determined directly.^[38]

1-4 Purpose of this study

In this study, we developed several FRET applications by using orientation-dependent FRET system.

In chapter 2, we report the analysis results of differences in structures and flexibilities of nicked and gapped DNA duplexes. Differences in structures and flexibilities of DNA duplexes play important roles on recognition by DNA binding proteins. We introduced pyrene and perylene at the center of the DNA duplex via D-threoninol, and investigated DNA duplexes with nick and gaps, which are key intermediates in DNA repair systems. By taking advantage of orientation-dependent FRET, effects of gap size on structures and flexibilities were successfully revealed. Since our method is facile and sensitive, it could be widely used to analyze DNA structures containing damages and non-natural molecules.

In chapter 3, we used another fluorophore pair (perylene and Cy3) and investigated the structure of DNA containing a stilbene cluster. This pair allows analysis of large DNA structures and DNA duplex containing photoreactive molecules. Stilbene has unique photophysical properties and we also developed photo-switches by introducing clusters of stilbene derivatives into DNA. However, the structures of DNA containing stilbene clusters remain unclear.

In chapter 4 and 5, we experimentally analyzed the mechanism of energy transfer between identical fluorophores. In order to solve the problem that the fluorescence intensity and lifetime of the identical fluorophores do not change even if energy transfer occurs, a quencher is placed adjacent to one of the fluorophores. This attempted to distinguish the same fluorophores. The distance and orientation dependence of energy transfer was investigated from the fluorescence intensity and lifetime.

1-5 References

- [1] T. Förster, *Naturwissenschaften*, **1946**, *33*, 166–175.
- [2] A. Iqbal, S. Arslan, B. Okumus, T. J. Wilson, G. Giraud, D. G. Norman, T. Ha, D. M. J. Lilley, *Proc. Natl. Acad. Sci. USA*, **2008**, *105*, 11176–11181
- [3] R. M. Clegg, *Methods Enzymol.*, **1992**, *211*, 353–388.
- [4] J. Zhang, R. E. Campbell, A. Y. Ting, R. Y. Tsien, *Nat. Rev. Mol. Cell Biol.*, **2002**, *3*, 906–918.
- [5] M. Masuko, S. Ohuchi, K. Sode, H. Ohtani, A. Shimadzu, *Nucleic Acids Res.*, **2000**, *28*, e34.
- [6] a) F. D. Lewis, L. Zhang, X. Zuo., *J. Am. Chem. Soc.*, **2005**, *127*, 10002–10003; b) K. Börjesson, S. Preus, A. H. El-Sagheer, T. Brown, B. Albinsson, L. M. Wilhelmsson, *J. Am. Chem. Soc.*, **2009**, *131*, 4288–4293; c) S. Preus, K. Kilså, F.-A. Miannay, B. Albinsson, L. M. Wilhelmsson, *Nucleic Acids Res.* **2013**, *41*, e18; d) T. Fessl, D. M. J. Lilley, *Biophys. J.*, **2013**, *105*, 2175–2181; e) J. H. Han, S. Yamamoto, S. Park, H. Sugiyama, *Chem. Eur. J.*, **2017**, *23*, 7607–7613; f) H. Kashida, H. Kawai, R. Maruyama, Y. Kokubo, Y. Araki, T. Wada, H. Asanuma, *Commun. Chem.*, **2018**, *1*, 91; g) H. Kashida, Y. Kokubo, K. Makino, H. Asanuma, *Org. Biomol. Chem.*, **2019**, *17*, 6786–9789.
- [7] a) M. S. Wranne, A. F. Füchtbauer, B. Dumat, M. Bood, A. H. El-Sagheer, T. Brown, H. Gradén, M. Grötli, L. M. Wilhelmsson, *J. Am. Chem. Soc.*, **2017**, *139*, 9271–9280; b) S. Hirashima, H. Sugiyama, S. Park, *J. Phys. Chem. B*, **2020**, *124*, 8794–8800
- [8] T. Kato, H. Kashida, H. Kishida, H. Yada, H. Okamoto, H. Asanuma, *J. Am. Chem. Soc.*, **2013**, *135*, 741–750.
- [9] G. Weissenberger, R. J. M. Henderikx, P. J. Peters, *Nature Methods*, **2021**, *18*, 463–

- 471.
- [10] X. Wang, E. Alnabati, T. W. Aderinwale, S. R. M. V. Subramaniya, G. Terashi, D. Kihara, *Nature Communications*, **2021**, *12*, 2302.
- [11] G. McDermott, S. M. Prince, A. A. Freer, A. M. Hawthornthwaite-Lawless, M. Z. Papiz, R. J. Cogdell, N. W. Isaacs, *Nature*, **1995**, *374*, 517–521.
- [12] M. R. Wasielewski, *Acc. Chem. Res.*, **2009**, *42*, 1910–1921.
- [13] N. Aratani, D. Kim, A. Osuka, *Acc. Chem. Res.*, **2009**, *42*, 1922–1934.
- [14] A. N. Bader, S. Hoetzl, E. G. Hofman, J. Voortman, P. M. P. van B. en Henegouwen, G. van Meer, H. C. Gerritsen, *ChemPhysChem*, **2011**, *12*, 475–483.
- [15] S. M. Shaikh, S. Ilic, B. J. Gibbons, X. Yang, E. Jakubikova, A. J. Morris, *J. Phys. Chem. C*, **2021**, *125*, 22998–23010
- [16] M. R. Jones, N. C. Seeman, C. A. Mirkin, *Science*, **2015**, *347*, 1260901.
- [17] M. Komiyama, K. Yoshimoto, M. Sisido, K. Ariga, *Bull. Chem. Soc. Jpn.*, **2017**, *90*, 967–1004.
- [18] V. L. Malinovskii, D. Wengera, R. Häner, *Chem. Soc. Rev.*, **2010**, *39*, 410–422.
- [19] Y. N. Teo, E. T. Kool, *Chem. Rev.*, **2012**, *112*, 4221–4245.
- [20] H. Kashida, H. Asanuma, *Phys. Chem. Chem. Phys.*, **2012**, *14*, 7196–7204.
- [21] P. Ensslen, H.-A. Wagenknecht, *Acc. Chem. Res.*, **2015**, *48*, 2724–2733.
- [22] E. Stulz, *Acc. Chem. Res.*, **2017**, *50*, 823–831.
- [23] I. H. Stein, C. Steinhauer, P. Tinnefeld, *J. Am. Chem. Soc.*, **2011**, *133*, 4193–4195.
- [24] E. Graugnard, D. L. Kellis, H. Bui, S. Barnes, W. Kuang, J. Lee, W. L. Hughes, W. B. Knowlton, B. Yurke, *Nano Lett.* **2012**, *12*, 2117–2122.

- [25] S. B-White, C. M. Spillmann, W. R. Algar, A. Khachatryan, J. S. Melinger, E. R. Goldman, M. G. Ancona, I. L. Medintz, *Nat. Commun.*, **2014**, *5*, 5615.
- [26] É. Boulais, N. P. D. Sawaya, R. Veneziano, A. Andreoni, J. L. Banal, T. Kondo, S. Mandal, S. Lin, G. S. Schlau-Cohen, N. W. Woodbury, H. Yan, A. Aspuru-Guzik, M. Bathe, *Nat. Mater.*, **2017**, *17*, 159–166.
- [27] Y. Ohya, K. Yabuki, M. Hashimoto, A. Nakajima, T. Ouchi, *Bioconjugate Chem.*, *2003*, **14**, 1057–1066.
- [28] S. Vyawahare, S. Eyal, K. D. Mathews, S. R. Quake, *Nano Lett.*, **2004**, *4*, 1035–1039.
- [29] A. L. Benveniste, Y. Creeger, G. W. Fisher, B. Ballou, A. S. Waggoner, B. A. Armitage, *J. Am. Chem. Soc.*, **2007**, *129*, 2025–2034.
- [30] J. K. Hannestad, P. Sandin, B. Albinsson, *J. Am. Chem. Soc.*, **2008**, *130*, 15889–15895.
- [31] C. V. Kumar, M. R. Duff, *J. Am. Chem. Soc.*, **2009**, *131*, 16024–16026.
- [32] P. K. Dutta, R. Varghese, J. Nangreave, S. Lin, H. Yan, Y. Liu, *J. Am. Chem. Soc.*, **2011**, *133*, 11985–11993.
- [33] M.Sc. Florian Garo, R. Häner, *Angew. Chem. Int. Ed.*, **2012**, *51*, 916–919.
- [34] K. Pan, E. Boulais, L. Yang, M. Bathe, *Nucleic Acids Res.*, **2014**, *42*, 2159–2170.
- [35] E. A. Hemmig, C. Creatore, B. Wünsch, L. Hecker, P. Mair, M. A. Parker, S. Emmott, P. Tinnefeld, U. F. Keyser, A. W. Chin, *Nano Lett.*, **2016**, *16*, 2369–2374.
- [36] J. S. Melinger, A. Khachatryan, M. G. Ancona, S. B.-White, E. R. Goldman, C. M. Spillmann, I. L. Medintz, P. D. Cunningham, *ACS Photonics*, **2016**, *3*, 659–669.
- [37] F. Nicoli, A. Barth, W. Bae, F. Neukirchinger, A. H. Crevenna, D. C. Lamb, T.

Lied, *ACS Nano*, **2017**, *11*, 11264–11272.

- [38] S. E. Bradforth, R. Jimenez, F. van Mourik, R. van Grondelle, G. R. Fleming, *J. Phys. Chem.*, **1995**, *99*, 16179–16191.

Chapter 2. Analysis of structures and flexibilities of nicked and gapped DNA duplexes by using orientation-dependent FRET system

2-1 Abstract

In chapter 2, we report the analysis results of differences in structures and flexibilities of nicked and gapped DNA duplexes by using orientation-dependent FRET system. Differences in structures and flexibilities of DNA duplexes play important roles on recognition by DNA binding proteins. This chapter presents a novel method for structural analyses of DNA duplexes. We first analyzed canonical B-form duplex to validate this method and the experimental FRET efficiencies were in excellent agreement with theoretical values calculated based on the reported parameters. We then investigated DNA duplexes with nick and gaps, which are key intermediates in DNA repair systems. Effects of gap size on structures and flexibilities were successfully revealed. Since our method is facile and sensitive, it could be widely used to analyze DNA structures containing damages and non-natural molecules.

2-2 Introduction

Structural anomalies in DNA double-helical structures play important roles in biological processes. For example, DNA repair enzymes to find damaged sites among a huge number of intact base pairs. This DNA repair is also an important factor in genome editing technology. Genomes cleaved by the CRISPR / Cas9 system are genetically edited when DNA repair errors occur.^[1] Recent studies have indicated that DNA-binding proteins can recognize differences in structures and flexibilities of DNA duplexes.^[2,3] We previously reported a novel distance and orientation dependent FRET system in which donor and acceptor are incorporated into DNA through D-threoninol linkers.^[4] Here, we applied this FRET system for analyses of DNA double helical structures. In contrast to the previous study, we determined structural parameters of various DNA structures from experimentally determined FRET efficiencies. We first analyzed the canonical B-form double helix by using orientation-dependent FRET and then evaluated nicked and gapped DNA duplexes, which are key intermediates in DNA repair systems.^[5,6] Not only the structures but also the flexibility of DNA in solution were revealed using orientation-dependent FRET. To the best of our knowledge, differences between both structures and flexibilities of nicked/gapped duplexes are revealed for the first time. Sequences of oligonucleotides used in this study are shown in Figure 2-1.

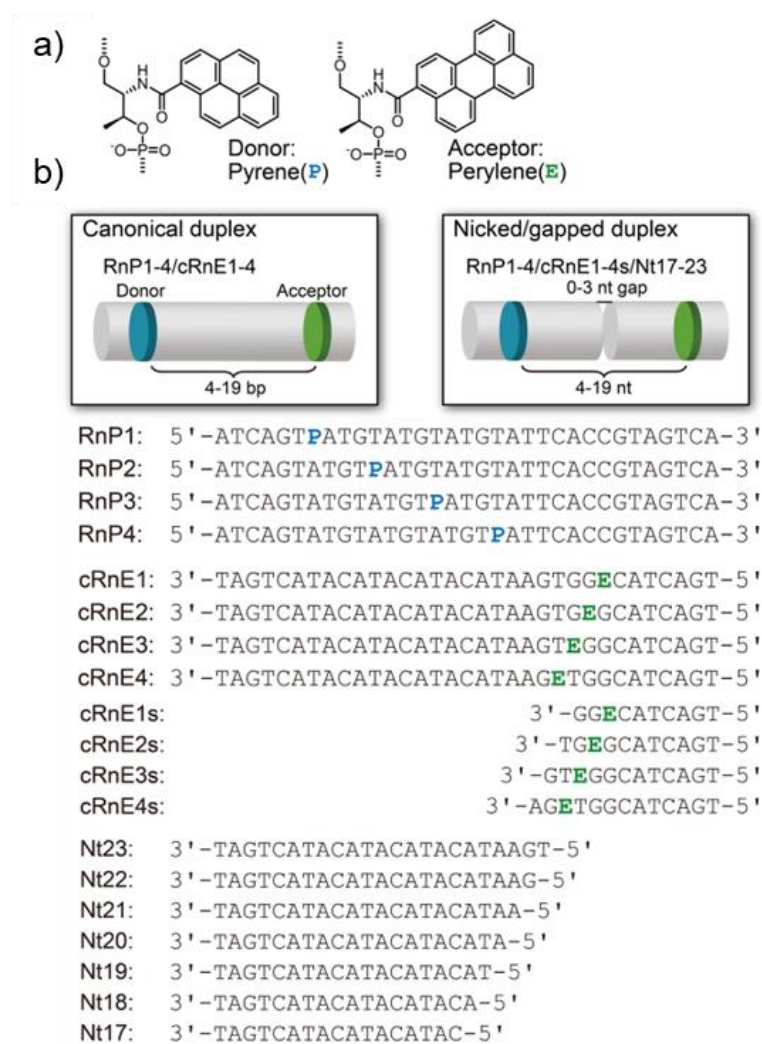


Figure 2-1.

a) Chemical structures of donor and acceptor. b) Sequences of oligonucleotides used in this study. Schematic illustrations of canonical and nicked/gapped duplexes are also shown.

Pyrene and perylene were incorporated into DNA via D-threoninol as a donor and an acceptor, respectively. In general, it was difficult to control dye orientation because dyes were usually introduced into terminal or extrahelical positions of DNA. On the other hand, molecules can intercalate between base pairs when they are introduced into the middle

positions of DNA through D-threosinol.^[7] Therefore, their orientations can be strictly controlled through stacking interaction with neighboring base pairs. No abasic sites were incorporated at the counter positions of dyes because we have revealed that additional incorporation of dyes does not distort DNA structures. We varied the number of base pairs between the pyrene donor and the perylene acceptor and measured FRET efficiencies. The FRET plot of the efficiency versus the number of base pairs was then fit to structural parameters obtained based on a cylinder model of the B-form duplex. There are several advantages of our method; (i) detailed structural parameters in solution can be easily obtained by using not only distance dependence but also orientation dependence of FRET. (ii) Since orientation is strictly controlled in our FRET system, experimental FRET efficiencies showed excellent agreement with theoretically calculated values (*vide infra*). Therefore, even bending and flexibility of DNA duplex can be estimated by monitoring deviations from the cylinder model. (iii) Dye pairs with relatively long Forster radius can be used with our method so that large DNA structures can be analyzed (Studies using different dye pairs are shown in chapter 3).

2-3 Results and discussions

2-3-1 Structural analysis of a canonical duplex

We first analyzed the structure of a canonical duplex to validate the accuracy of our method. We synthesized four strands tethering pyrene (**RnP1-4**) and four complementary strands tethering perylene (**cRnE1-4**) shown in Figure 2-1. The two base pairs flanking pyrene were identical in all duplexes, and this resulted in pyrene quantum yields that were within experimental error for all duplexes (Figure S2-1). The number of base pairs between the two dyes can be varied from 4 to 19 bp by combining these strands appropriately (Table S2-1). We measured fluorescent emission spectra of duplexes (Figure S2-2) and calculated FRET efficiencies from decrease in donor emission. FRET efficiency between dyes in canonical duplexes as a function of distance in base pairs is not monotonous, but periodic, demonstrating orientation dependence of FRET (Figure 2-2b). Three variables were used to calculate FRET efficiencies: rise, rotation, and the sum of angles between dyes and neighboring base pairs (Figure 2-1a).

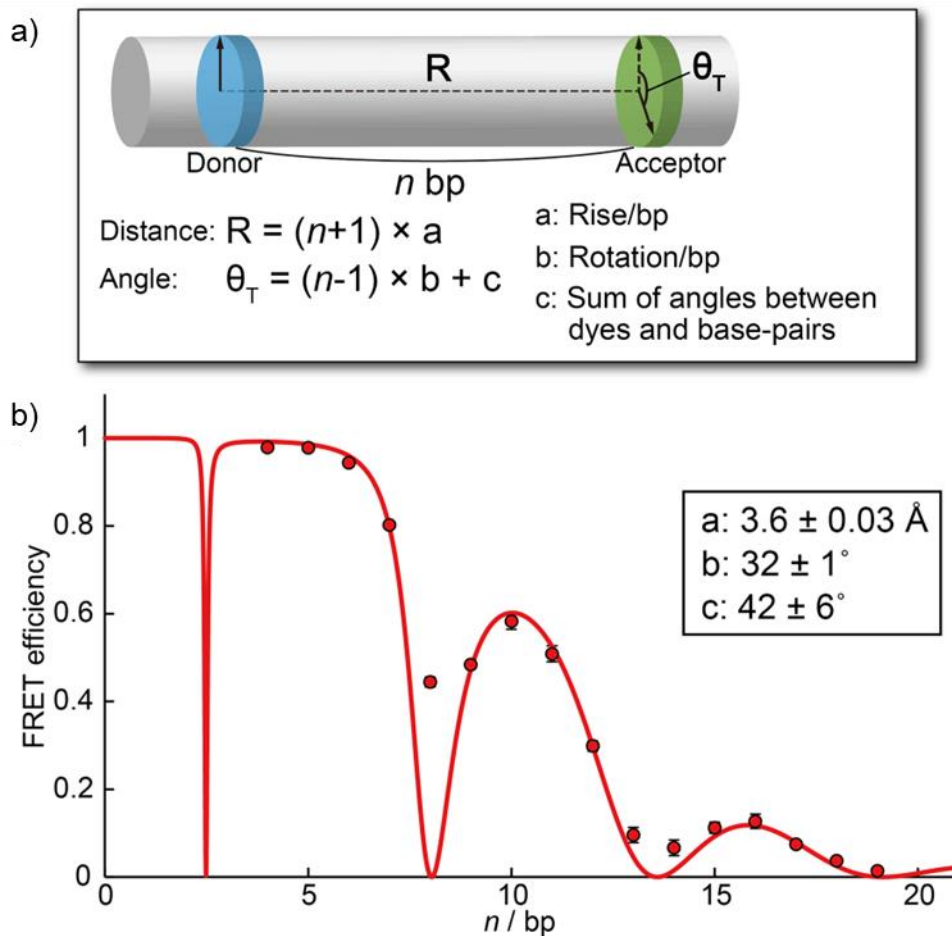


Figure 2-2.

Analysis of structural parameters of a canonical DNA duplex. a) Equations used for calculation of distance and angle between dyes. b) FRET plot of a canonical DNA duplex. The x-axis is the number of base pairs between donor and acceptor. Experimental data are shown as circles. The line is FRET efficiencies theoretically calculated by using determined parameters shown in the inset.

Parameters were determined by using least-squares method. Theoretically calculated FRET efficiencies using these parameters are shown in a line in Figure 2-1b. It should be noted that a large error from a theoretically calculated value was observed at 8 bp.

Although we calculated FRET efficiencies by assuming that the relative angle between dyes has a Gaussian distribution, large differences at base pair separations other than 8 bp were still observed (Figure S2-3). Therefore, we concluded that the difference at 8 bp was not caused by the incomplete fixation of dye orientations. It was reported based on a theoretical analysis that the point dipole approximation fails when the distance between molecules is short. Consequently, the orientation factor cannot be zero even if molecules are perpendicular.^[8] We believe that large difference between the experimentally determined FRET efficiency at 8 bp and the efficiency expected based on the cylindrical model is due to a non-zero orientation factor caused by failure of dipole approximation. From this reason, we did not use FRET efficiency at 8 bp to determine structural parameters. For other base pair separations, experimental values agreed well with the curve generated based on the model of B-form DNA (Figure 2-2b), clearly demonstrating that orientation of dyes is strictly controlled in our system. The rise per base pair calculated based on FRET data was 3.6 ± 0.03 Å and rotation per base pair was $32 \pm 1^\circ$, almost identical to those of a canonical B-form DNA duplex (3.4 Å and 34° , respectively). The difference of the rise could be explained by a refractive index. There is an inversely proportional relationship between the rise and the refractive index. If the refractive index is set to 1.5, rise per base pair decreases to 3.4 Å. The difference of rise per base pair

indicates that the refractive index of natural base pairs are higher than 1.4. In contrast, rotation angle is not dependent on physical parameters. X-ray crystallography has shown that rotation angle is highly dependent on sequence although averaged angle is usually 34–36°.^[9-11] Therefore, the difference from typical rotation angle could be due to its strong sequence dependence. To the best of our knowledge, an orientation dependent FRET system showing such an excellent agreement with theory over a long distance has not been reported previously. We also analyzed a duplex containing an A-tract using a similar system (Figure S2-4). In the case of A-tract duplex, larger differences between experimental FRET efficiencies and calculated values based on the B-form cylinder model were observed. In particular, the observed efficiencies at longer distance were higher than expected values. As reported previously, an A-tract induces a bend in DNA^[12-14] so that the actual distance between donor and acceptor is shorter than expected from the cylinder model. Although more detailed investigation is required to clarify the detailed structure of A-tract, bending was clearly detected by using our FRET system.

2-3-2 Structural analysis of DNA duplexes with nicks

We subsequently analyzed DNA duplexes with nicks and gaps using our FRET system. Nicked and gapped duplexes were prepared by hybridizing short acceptor-containing

strands (**cRnE1s-4s**) and donor-containing strands (**RnP1-4**) with a longer DNA (**Nt17-23**) as shown in Figure 2-1. Fluorescent emission spectra and emission intensities of nicked duplexes are shown in Figure S2-5a and S2-5e. FRET efficiencies of nicked duplexes showed a nonmonotonous dependence on the number of base pairs between donor and acceptor dyes (Figure 2-3).

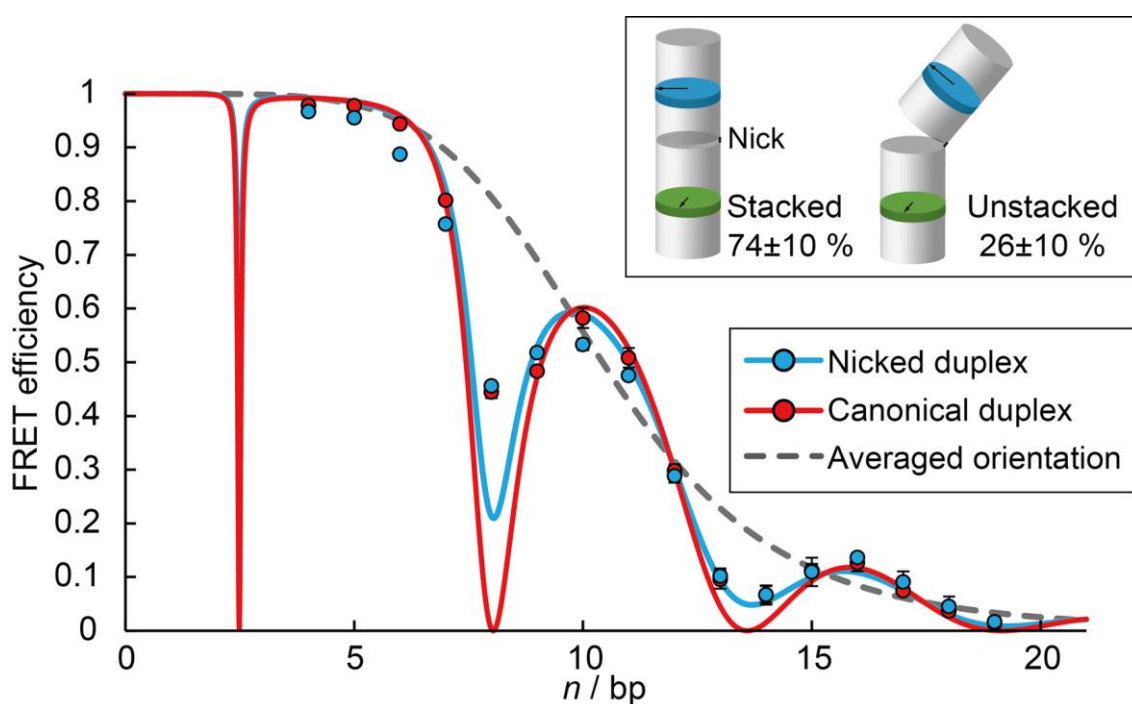


Figure 2-3.

FRET plot of nicked (blue) and canonical (red) duplexes. The blue line curve was generated by assuming 26% of duplexes adopt an unstacked.

This indicated that the relative orientation between the donor and the acceptor was not averaged. The positions of minima and maxima in the FRET plot were the same as

those of canonical duplex, showing that despite the nick, the duplex maintains a canonical B-form duplex geometry. However, the nicked duplex had lower maximum and higher minimum FRET efficiencies compared with canonical duplex. This weakened orientation dependence strongly indicated that the nick imparted flexibility. The higher flexibility of nicked duplex was also observed by using other methodologies such as gel electrophoresis and NMR.^[15-18] We analyzed the conformational flexibility of nicked duplex by simply assuming an equilibrium between stacked and unstacked duplex conformations.^[17,19] Our calculations indicated that when 26% of duplexes adopted an unstacked structure at the nick, calculated efficiencies showed better agreement with experimental values. This is a rough calculation because it is difficult to estimate the precise orientation factors of unstacked structure. However, we believe this assumption is useful to estimate relative flexibilities of various DNA structures. From these results, we concluded that a nicked duplex has higher conformational flexibility than the canonical duplex. X-ray crystallography demonstrated that nicked duplex adopts B-form duplex.^[20] Our study also indicates that the nicked duplex adopts a B-form conformation in solution and was able to provide a measure of the enhanced flexibility of a nicked DNA duplex relative to that of an intact duplex

2-3-3 Structural analysis of DNA duplexes with gaps

We then investigated the structure of gapped duplexes. Fluorescent emission spectra and emission intensities of gapped duplexes are shown in Figure S2-5b~d and S2-5f~h. The FRET plot of a duplex with a single nucleotide gap is shown in Figure 2-4a. The minima in the FRET plots were different in nicked duplexes and the duplexes with 1-nt gaps; a minimum was observed at 8 bp with the nicked duplex and at 6 nt with 1-nt gapped duplex. This shift strongly indicated that insertion of a gap altered the orientation between the two dyes. As an orientation dependence of FRET efficiency was observed with 1-nt gapped duplexes, the two duplex regions separated by a 1-nt gap are stacked. The difference in dye orientation from the nicked duplex is probably due to rotation and/or bending at the gap. Actually, NMR analysis indicated that there are two conformations with 1-nt gapped duplex; one is close to B-DNA and the other is kinked.^[18] Interestingly, the decline of FRET efficiency was observed at 6, 10 and 14 nt in the case of 1-nt gapped duplex. Because we used four kinds of gapped sequences (**cRnE1s-4s** and **Nt19-22**) as shown in Table S2-4, this result indicated that structure of 1-nt gapped DNA duplex depends on its sequence.

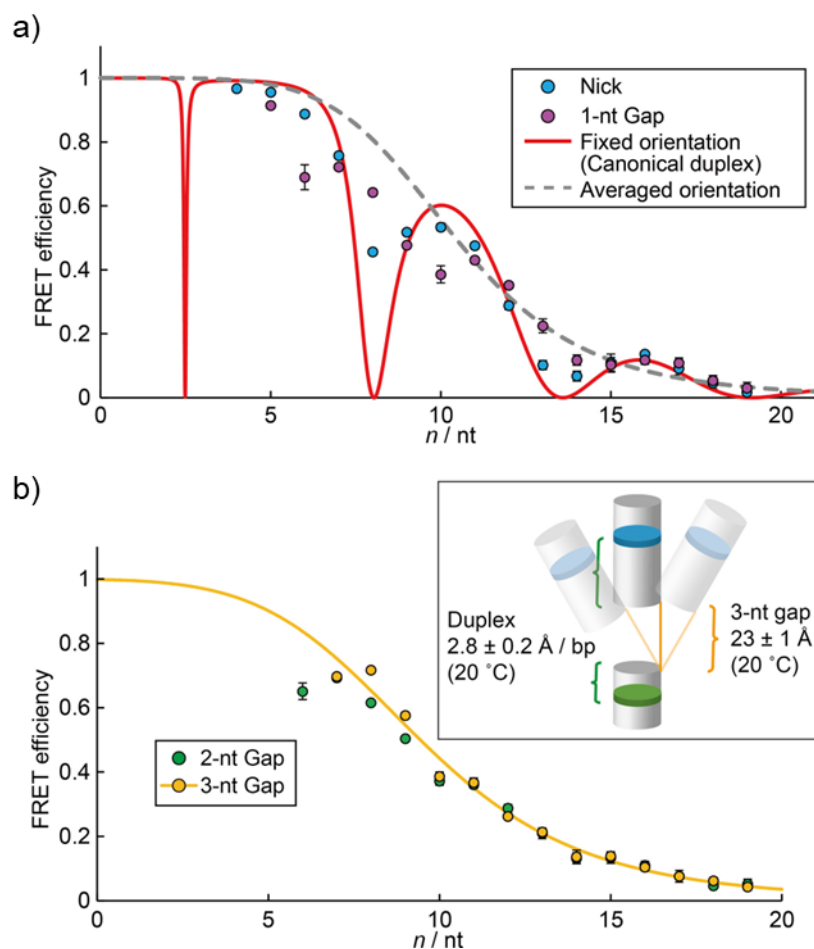


Figure 2-4.

a) FRET plots of nicked duplex and duplex with a 1-nt gap. Red line shows the fitting curve used to determine structural parameters of canonical duplex. Dotted line shows theoretical curve assuming averaged orientation of dyes in canonical duplex. b) FRET plots of duplexes with 2-nt and 3-nt gaps. Curve in orange was calculated by assuming FRET efficiencies of 3-nt gapped duplexes were dependent not on orientation but on distance between dyes. Determined structural parameters of duplex with 3-nt gap at 20°C are shown in inset. See Figure S2-7 for structural parameters determined from FRET efficiencies at 0°C .

The FRET plot of structure with the 2-nt gap showed smaller orientation dependence.

FRET efficiency monotonously decreased as the number of nucleotides between the dyes

increased (Figure 2-4b, green circles). Thus, stacking interactions between two duplexes is very weak when there is a 2-nt gap. Almost no orientation dependence was observed when the gap was 3 nt (Figure 2-4b, orange circles), suggesting little stacking and an averaged dye orientation. Similar results were reported by using gel electrophoresis where electrophoretic mobility decreased by insertion of two or more nucleotide gap.^[17,21] We estimated the length of 3-nt gap and of the complex of the three oligonucleotides by assuming a random orientation. FRET efficiencies of duplexes with 3-nt gaps were in excellent agreement with a model based on this assumption (Figure 2-4b, orange circles and line). The length of 3-nt gap was estimated to be $23 \pm 1 \text{ \AA}$, indicating that the gapped bases are stretched. Masuko et al. previously reported an equation to calculate the length of gap by using distance dependent FRET system.^[22] According to their equation, the length of 3-nt gap was calculated as 19.1 \AA , which is shorter than our result. We also measured emission spectra and determined FRET efficiencies at 0°C (Figure S2-7). A total of 3-nt gapped duplexes at 0°C showed higher FRET efficiencies than those at 20°C , and the length of 3-nt gap at 0°C was estimated as $19 \pm 2 \text{ \AA}$. These results indicated that breathing effect of acceptor strand or high mobility of 3-nt gap might contribute to the stretching of DNA. In contrast, length of double-helical portion increases by $2.8 \pm 0.2 \text{ \AA}$ per base pair, which was much shorter than canonical duplex ($3.6 \pm 0.03 \text{ \AA}$). The rise

represents the averaged increment of the distance between a donor and an acceptor and the decrease is probably due to the movement of 3-nt gap inserted between double helices. From these results, we concluded that two duplexes move freely when a 3-nt gap is inserted between the regions.

2-3-4 Melting temperatures (T_{ms}) of duplexes determined by FRET

In order to further investigate the stacking interaction between two double helices, melting temperatures (T_{ms}) of the duplexes were determined using FRET. Melting curves were obtained by monitoring emission intensity at 500 nm with excitation wavelength of 345 nm so that only hybridization of short perylene-containing strand was monitored (Figure S2-8). This allowed the stacking interaction between the two helices to be evaluated since the melting temperature of perylene-containing strand depends on whether the two duplexes stack. The T_{ms} of nicked duplexes were much higher than those of gapped duplexes, supporting our hypothesis that a stable stacking interaction occurs in the nicked duplexes (Figure 2-5). The T_{ms} of the duplexes with 1 and 2-nt gaps were within experimental error although T_m of **cRnE3s** slightly decreased. This result indicated that stacking interaction between two duplexes separated by 1-nt gap is weak whereas its strength partially depended on its sequence.^[23] Furthermore, 3-nt gapped duplexes showed same T_{ms} as 2-nt gapped duplexes, supporting that two duplexes are no longer

stacked in those structures. Overall, the melting analyses support the conclusions drawn

from FRET that the duplexes do not stack strongly when separated by a gap of 2 nt.

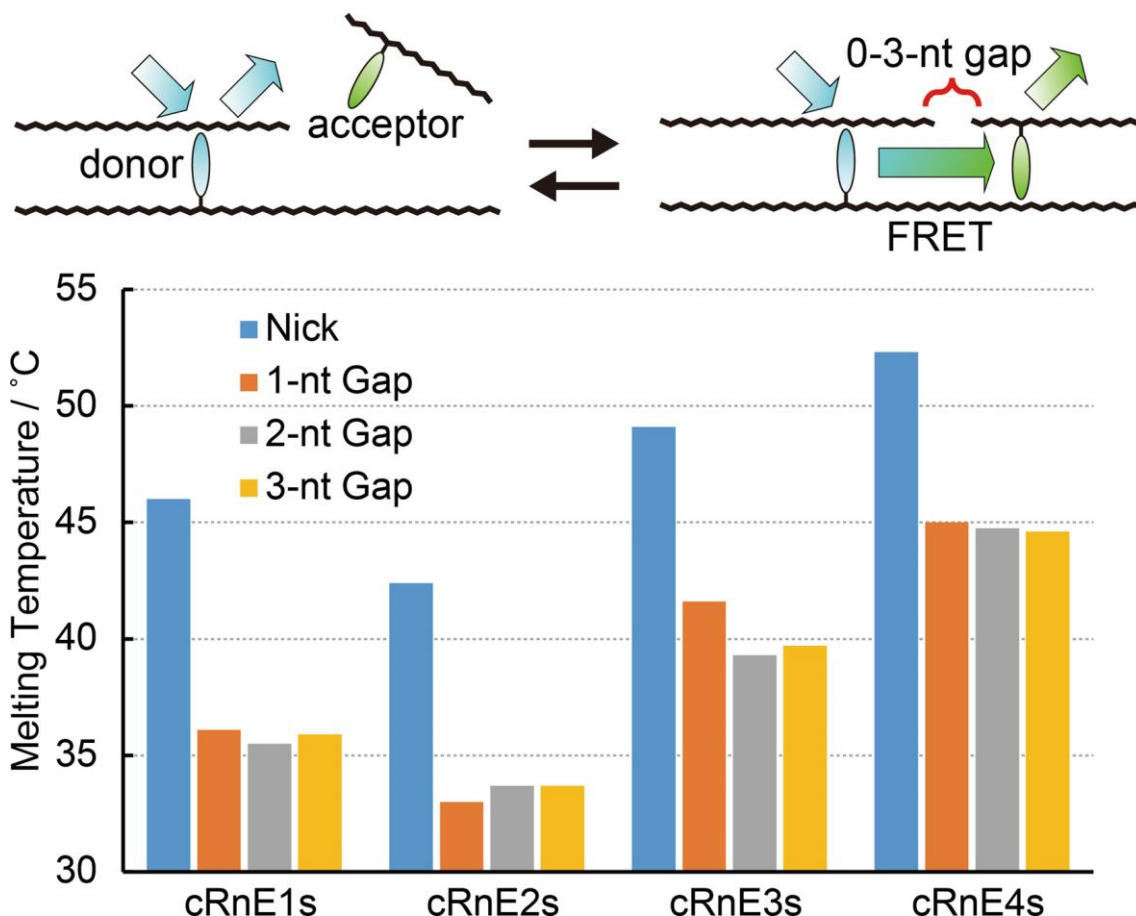


Figure 2-5.

Melting temperatures of strand containing perylene in the context of nicked or gapped duplex. These melting temperatures were determined from melting curves obtained by monitoring 500 nm emission with 345 nm excitation such that only melting of the perylene-containing strand is observed.

2-4 Conclusions

We developed a novel method for analyses of DNA structures by using the orientation-dependent FRET system. Structural parameters of canonical B-form duplex were precisely obtained by using this system. Large deviation from a cylinder model probably due to bending was observed with A-tract duplex. Moreover, differences in structures and flexibilities among nicked and gapped duplexes were revealed in detail. Although nicked duplex has high flexibility, it maintains a canonical B-form geometry. However, insertion of 1-nt gap altered the dye orientation although orientation dependence was still observed. 2-nt and 3-nt gapped duplexes showed almost no orientation dependence in FRET plot, indicating weak stacking between two duplexes separated by a gap. DNA repair enzymes, such as ligases and DNA polymerases, can recognize nicked or gapped duplexes, although the recognition of gaps depends on the gap size.^[24-27] Differences in structure and flexibility, which were revealed in this study, likely enable recognition by these enzymes. Importantly, our results demonstrated that the orientation of dyes is strictly controlled in our FRET system. Furthermore, other dye pairs can be incorporated into DNA via D-threoninol. We believe our FRET system will prove to be a facile and versatile tool for analysis of DNA structures in solution. This system could, for example, be used to analyze structures of DNA duplexes with various types of

damage, such as radiation-induced lesions, epigenetically modified nucleobases, and non-natural molecules. ^[28,29] Moreover, structural changes in DNA duplexes induced by protein binding could be analyzed using this FRET system.

2-5 Experimental section

Materials

All conventional phosphoramidite monomers, CPG columns, and reagents for DNA synthesis, and Poly-Pak II cartridges were purchased from Glen Research. Other reagents for the syntheses of phosphoramidite monomers were purchased from Tokyo Chemical Industry, Wako, and Aldrich. Unmodified oligonucleotides were purchased from Integrated DNA Technologies. Native oligodeoxyribonucleotides (ODNs) were purchased from Integrated DNA Technologies. ODNs tethering pyrene or perylene were synthesized on an automated DNA synthesizer (H-8-SE, Gene World) as we reported previously.^[30,31] ODNs were purified by reversed-phase HPLC and characterized by MALDI-TOF MS (Autoflex II, Bruker Daltonics) and HPLC.

The MALDI-TOFMS data for the modified DNA were as follows: **RnP1**: Obsd. 10220 (Calcd. for [**RnP1**+H⁺]: 10220). **RnP2**: Obsd. 10219 (Calcd. for [**RnP2** +H⁺]: 10220). **RnP3**: Obsd. 10220 (Calcd. for [**RnP3** +H⁺]: 10220). **RnP4**: Obsd. 10220 (Calcd. for [**RnP4** +H⁺]: 10220). **cRnE1**: Obsd. 10257 (Calcd. for [**cRnE1** +H⁺]: 10257). **cRnE2**: Obsd. 10257 (Calcd. for [**cRnE2** +H⁺]: 10257). **cRnE3**: Obsd. 10257 (Calcd. for [**cRnE3** +H⁺]: 10257). **cRnE4**: Obsd. 10257 (Calcd. for [**cRnE4** +H⁺]: 10257). **AtP1**: Obsd.

10297 (Calcd. for [**AtP1**+H⁺]: 10300). **AtP2**: Obsd. 10300 (Calcd. for [**AtP2** +H⁺]: 10300). **AtP3**: Obsd. 10298 (Calcd. for [**AtP3** +H⁺]: 10300). **AtP4**: Obsd. 10299 (Calcd. for [**AtP4** +H⁺]: 10300). **AtP5**: Obsd. 10300 (Calcd. for [**AtP5** +H⁺]: 10300). **cAtE1**: Obsd. 10168 (Calcd. for [**cAtE1** +H⁺]: 10170). **cAtE2**: Obsd. 10169 (Calcd. for [**cAtE2** +H⁺]: 10170). **cAtE3**: Obsd. 10169 (Calcd. for [**cAtE3** +H⁺]: 10170). **cRnE1s**: Obsd. 3184 (Calcd. for [**cRnE1s** +H⁺]: 3184). **cRnE2s**: Obsd. 3487 (Calcd. for [**cRnE2s** +H⁺]: 3488). **cRnE3s**: Obsd. 3816 (Calcd. for [**cRnE3s** +H⁺]: 3817). **cRnE4s**: Obsd. 4130 (Calcd. for [**cRnE4s** +H⁺]: 4130).

Fluorescence measurements

Fluorescence spectra were measured on JASCO models FP-6500 or FP-8500. The excitation wavelength was 345 nm Band widths were 3 nm (FP-6500) or 2.5 nm (FP-8500) for excitation and emission. Before measurements, sample solutions containing DNA duplex were heated at 80 °C, then slowly cooled down to 20 or 0 °C at a rate of 4 °C min⁻¹. Fluorescence spectra were measured at 80 to 20 or 0 °C at 10 °C intervals after 4 min incubations. Sample solutions contained 100 mM NaCl, 10 mM phosphate buffer, pH 7.0. Concentrations of ODNs were 0.2 μM donor strand (**RnP1-4** or **AtP1-5**) and 0.4 μM acceptor strand (**cRnE1-4** or **cAtE1-3**). For analyses of nicked and gapped

duplexes, 0.2 μM donor strand (**RnP1-4**), 0.4 μM acceptor strand (**cRnE1s-4s**) and 0.6 μM **Nt23-17** were used.

Melting Temperature Measurements

The melting curves were measured with a UV-1800 (Shimadzu) by monitoring 260 nm absorbance versus temperature. For nicked or gapped duplex, the melting curve was obtained with a JASCO model FP-6500 by measuring emission intensity at 500 nm with 345 nm excitation. The melting temperature (T_m) was determined from the maximum in the first derivative of the melting curve. Both the heating and the cooling curves were measured, and the calculated T_m agreed to within 1.0 $^{\circ}\text{C}$. The temperature ramp was 0.5 $^{\circ}\text{C min}^{-1}$. The sample solutions for melting analyses from absorbance contained 100 mM NaCl, 10 mM phosphate buffer, pH 7.0, 1.0 μM each DNA. The sample solutions for melting analyses from emission contained 100 mM NaCl, 10 mM phosphate buffer, pH 7.0, 0.2 μM donor strand (**RnP1-4**), 0.4 μM acceptor strand (**cRnE1s-4s**) and 0.6 μM **Nt23-17**.

Calculation of FRET efficiency

FRET efficiency (Φ_T) was experimentally calculated from the following equations (1):

$$\Phi_T = 1 - I_{DA}/I_D \quad (1)$$

where I_{DA} is emission intensity of a duplex containing a donor and an acceptor at 405 nm, and I_D is that of donor only duplex at 405 nm. Emission intensities were measured 20°C.

Each emission intensity was normalized at the intensity of 80°C in order to eliminate the effects of concentration errors. Error bars of FRET efficiencies show standard deviations of three independent experiments.

Determination of structural parameters

FRET efficiency (Φ_T) was theoretically calculated from the following equations (2)~ (4):

$$\Phi_T = \frac{1}{1 + (R/R_0)^6} \quad (2)$$

$$R_0 = 0.2108[J(\lambda)\kappa^2 n^{-4} \Phi_D]^{1/6} \quad (3)$$

$$\kappa^2 = (\cos \theta_T - 3 \cos \theta_D \cos \theta_A)^2 \quad (4)$$

where R is the distance between donor and acceptor, and R_0 is a Förster radius (the distance where $\Phi_T = 0.5$). $J(\lambda)$ is integral of spectral overlap between donor emission and acceptor absorption at λ nm. n is a refractive index, which is typically assumed to be 1.4 for biomolecules, ^[32] and Φ_D is a donor quantum yield. The orientation factor, κ^2 , was calculated from the above equation, where θ_T is the angle between transition dipoles of donor and acceptor, and θ_D and θ_A are the angles between these dipoles and the separation vector.

In our FRET system of duplex, donor and acceptor are in parallel planes since they are intercalated into the DNA duplex. Thus, the orientation factor is simply represented by the following equation (5):

$$\kappa^2 = \cos^2\theta_T \quad (5)$$

By using these equations, FRET efficiency was calculated from the distance (R) and the angle (θ_T) between dyes.

For analyses of double helical structures, we used three variables, rise per base pair (a in Å), angle per base pair (b in °) and the angle between dyes and flanking base pairs (c in °). Consequently, the distance and the angle can be expressed by using the number of base pairs (n) between donor and acceptor as follows (6) and (7):

$$R = a \times (n + 1) \quad (6)$$

$$\theta_T = b \times (n - 1) + c \quad (7)$$

These three variables were determined by fitting experimental FRET efficiencies with values calculated from these equations. Values were determined from the least-squares method using Solver tool in Microsoft Excel. Errors were estimated from standard errors calculated by using KaleidaGraph (Synergy software).

For analyses of nicked duplex, we assumed an equilibrium between stacked and unstacked structures. In the stacked structure, the structure was assumed to be the same as that of the duplex without a nick. In unstacked duplex, a randomized orientation ($\kappa^2 = 2/3$) was assumed. Percentages of stacked and unstacked structures were estimated using the least-squares method using the Solver tool in Excel. For analyses of duplexes with 3-nt gaps, we assumed that the orientation was not fixed and, thus, that the orientation factor (κ^2) was $2/3$. The distance (R) was calculated from the following equation (8):

$$R = d \times (n - 1) + e \quad (8)$$

where d (in Å) is rise per base pair in duplexed portion of 3-nt gapped structure. And, e (in Å) is the length of 3-nt gap (i.e. the distance between duplex regions).

2-6 References

- [1] F. A. Ran, P. D. Hsu, J. Wright, V. Agarwala, D. A. Scott, F. Zhang, *Nature Protocols*, **2013**, 8, 2281–2308.
- [2] W. Yang, *Cell Res.*, **2008**, 18, 184–197
- [3] M.W. Germann, C.N. Johnson, A.M. Spring, *Med. Res. Rev.*, **2012**, 32, 659–683
- [4] T. Kato, H. Kashida, H. Kishida, H. Yada, H. Okamoto, H. Asanuma, *J. Am. Chem. Soc.* 2013, 135, 741–750
- [5] A. Sancar, L.A. Lindsey-Boltz, K. Ünsal-Kaçmaz, S. Linn, *Annu. Rev. Biochem.*, **2004**, 73, 39–85
- [6] T. Lindahl, R.D. Wood, *Science*, **1999**, 286, 1897–1905
- [7] X. Liang, H. Asanuma, H. Kashida, A. Takasu, T. Sakamoto, G. Kawai, M. Komiyama, *J. Am. Chem. Soc.*, **2003**, 125, 16408–16415
- [8] A. Muñoz-Losa, C. Curutchet, B.P. Krueger, L.R. Hartsell, B. Mennucci, *Biophys. J.*, **2009**, 96, 4779–4788
- [9] R.E. Dickerson, H.R. Drew, *J. Mol. Biol.*, **1981**, 149, 761–786
- [10] T.A. Larsen, M.L. Kopka, R.E Dickerson, *Biochemistry*, **1991**, 30, 4443–4449
- [11] K. Grzeskowiak, *Chem. Biol.*, **1996**, 3, 785–790
- [12] H.-M. Wu, D.M. Crothers, *Nature*, **1984**, 308, 509–513
- [13] H.C.M. Nelson, J.T. Finch, B.F. Luisi, A. Klug, *Nature*, **1987**, 330, 221–226
- [14] A.D. DiGabriele, T.A. Steitz, *J. Mol. Biol.*, **1993**, 231, 1024–1039
- [15] P. Furrer, J. Bednar, A.Z. Stasiak, V. Katritch, D. Michoud, A. Stasiak, J. Dubochet, *J. Mol. Biol.*, **1997**, 266, 711–721
- [16] Y. Zhang, D.M. Crothers, *Proc. Natl. Acad. Sci. U.S.A.*, **2003**, 100, 3161–3166
- [17] P. Yakovchuk, E. Protozanova, M.D. Frank-Kamenetskii, *Nucleic Acids Res.*,

- 2006**, *34*, 564–574
- [18] C. Roll, C. Ketterlé, V. Faibis, G.V. Fazakerley, Y. Boulard, *Biochemistry*, **1998**, *37*, 4059–4070
- [19] E. Protozanova, P. Yakovchuk, M.D. Frank-Kamenetskii, *J. Mol. Biol.*, **2004**, *342*, 775–785
- [20] J. Aymami, M. Coll, G.A. van der Marel, J.H. van Boom, A.H. Wang, A. Rich, *Proc. Natl. Acad. Sci. U.S.A.*, **1990**, *87*, 2526–2530
- [21] J.B. Mills, J.P. Cooper, P.J. Hagerman, *Biochemistry*, **1994**, *33*, 1797–1803
- [22] M. Masuko, S. Ohuchi, K. Sode, H. Ohtani, A. Shimadzu, *Nucleic Acids Res.*, **2000**, *28*, e34.
- [23] The 1-nt gapped duplex of **cRnE3s** has consecutive two thymidines at the gapped site (see Table S2-4 for actual sequence). This duplex can adopt a bulge like structure rather than a gapped structure. We believe this structure contribute to the relatively high stability of 1-nt gapped duplex with **cRnE3s**.
- [24] J.A. Brown, L.R. Pack, L.E. Sanman, Z. Suo, *DNA Repair*, **2011**, *10*, 24–33
- [25] F. Karimi-Busheri, J. Lee, M. Weinfeld, A.E. Tomkinson, *Nucleic Acids Res.*, **1998**, *26*, 4395–4400
- [26] C.K. Ho, J.L. Van Etten, S. Shuman, *J. Virol.*, **1997**, *71*, 1931–1937
- [27] Y. Liu, W.A. Beard, D.D. Shock, R. Prasad, E.W. Hou, S.H. Wilson, *J. Biol. Chem.*, **2005**, *280*, 3665–3674
- [28] K.S. Gates, *Chem. Res. Toxicol.*, **2009**, *22*, 1747–1760
- [29] T. Carell, C. Brandmayr, A. Hienzsch, M. Müller, D. Pearson, V. Reiter, I. Thoma, P. Thumbs, M. Wagner, *Angew. Chem. Int. Ed.*, **2012**, *51*, 7110–7131

- [30] H. Asanuma, M. Akahane, N. Kondo, T. Osawa, T. Kato, H. Kashida, *Chem. Sci.*, **2012**, *3*, 3165–3169
- [31] T. Doi, T. Sakakibara, H. Kashida, Y. Araki, T. Wada, H. Asanuma, *Chem. Eur. J.*, **2015**, *21*, 15974–15980
- [32] J.R. Lakowicz, *Principles of Fluorescence Spectroscopy*, **2006**, Springer, NY

2-7 Appendixes

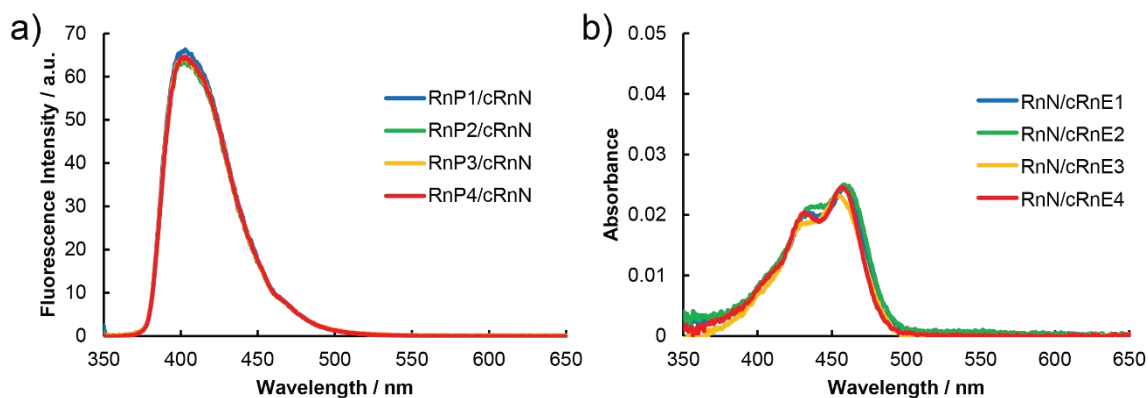


Figure S2-1. a) Emission spectra of pyrene in DNA duplex (RnP1-4/cRnN). cRnN is a native DNA without an acceptor. b) Absorption spectra of acceptor strands. RnN is a native DNA without a donor.

cRnN: 5'-TGACTACGGTGAATACATACATACTGAT-3'

RnN: 5'-TCAGTATGTATGTATGTATTCACCGTAGTCA-3'

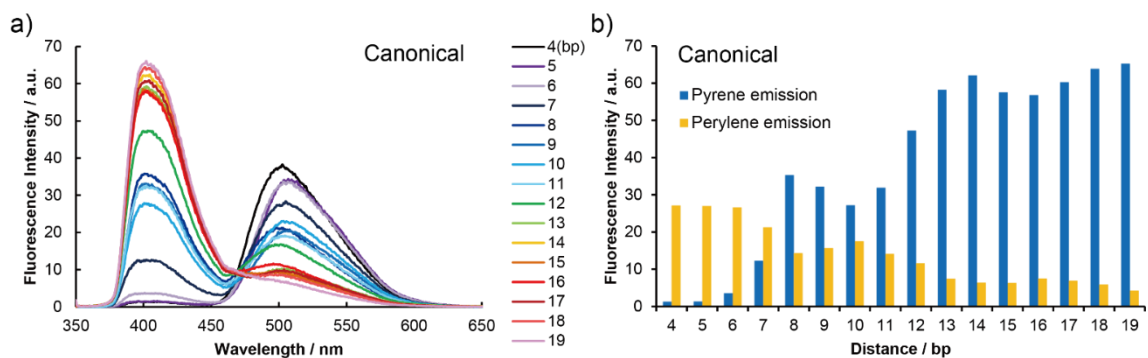


Figure S2-2. a) Emission spectra and emission intensities of canonical duplexes. b) Emission intensities of pyrene were monitored at 405 nm, whereas those of perylene were monitored at 530 nm.

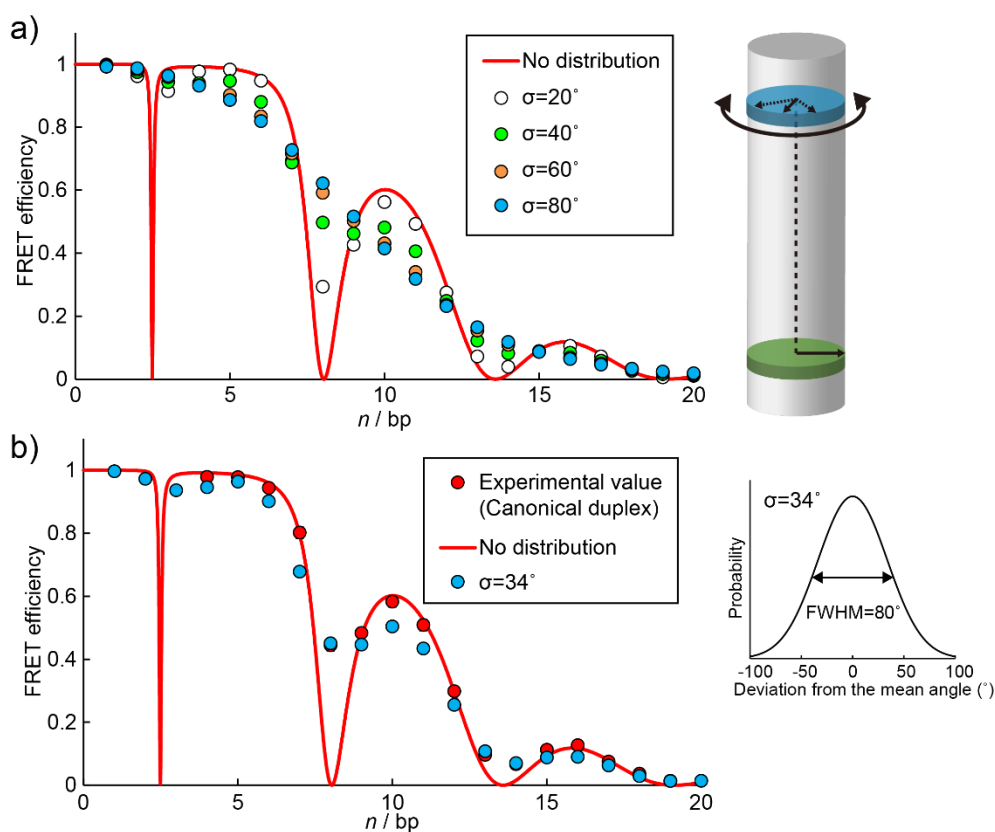


Figure S2-3. FRET efficiencies theoretically-calculated by assuming a Gaussian distribution of the dye angle. a) Theoretically-calculated FRET efficiencies assuming that the relative angle between dyes has no distribution (red line) or Gaussian distribution with various standard deviations (σ). b) Comparison of experimentally-determined FRET efficiencies of canonical duplex (red circles) with calculated values assuming Gaussian distribution ($\sigma=34^\circ$; blue circles). Although FRET efficiencies at 8bp agreed with each other, large differences at other points were still observed. Distribution of the relative angle between dyes at σ of 34° is also shown.

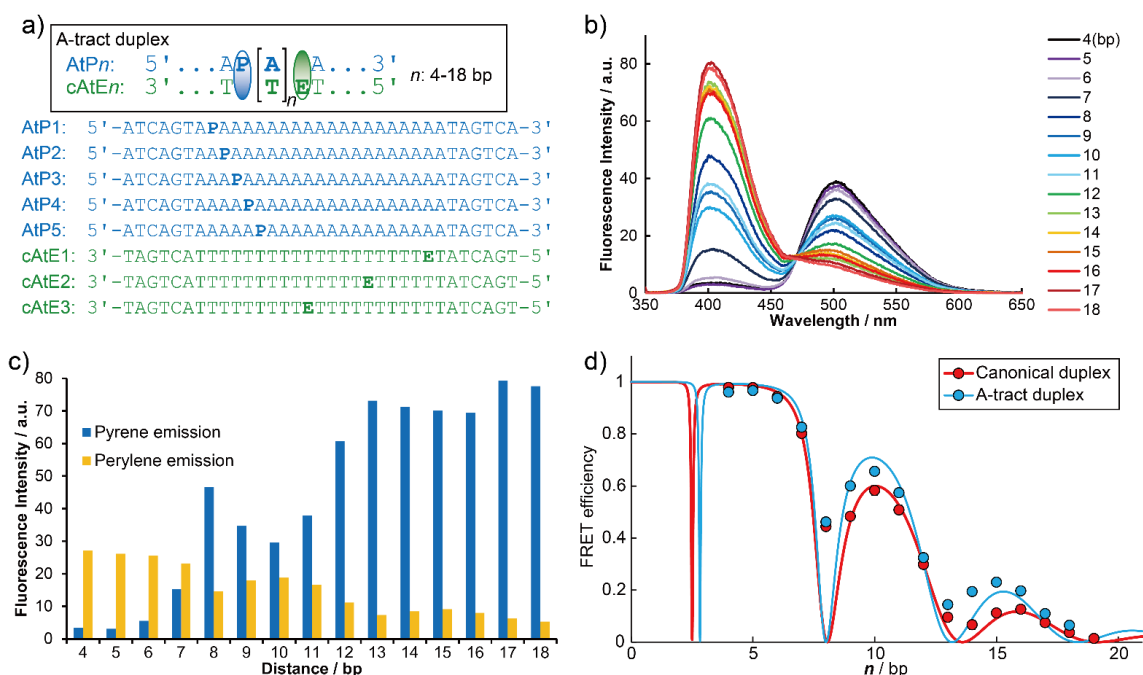


Figure S2-4. Analysis of DNA duplex containing A-tract. a) Sequence design. The number of A:T base pairs was varied from 4 to 18. b) Emission spectra of duplexes. c) Emission intensities of pyrene were monitored at 405 nm, whereas those of perylene were monitored at 530 nm. d) FRET plot of A-tract duplex (blue circles). Fitting curve of A-tract duplex based on a cylinder model is shown in a blue line. Results of canonical duplexes are also shown for comparison.

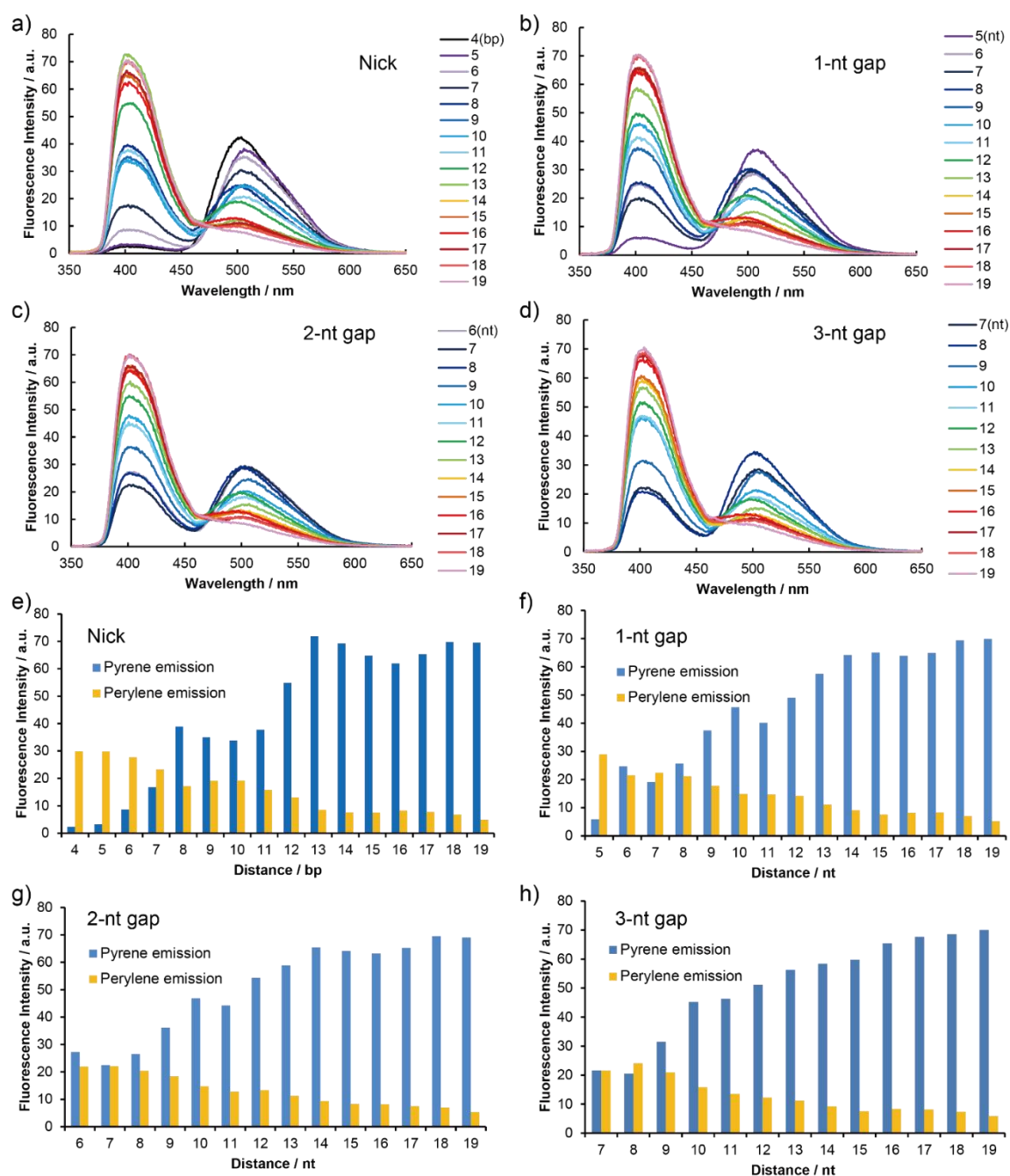


Figure S2-5. Emission spectra and emission intensities of nicked and gapped duplexes. a-d) Fluorescence emission spectra of nicked duplex and duplexes with 1, 2, and 3-nt gaps. e-h) Emission intensities of nicked duplex and duplexes with 1, 2, and 3-nt gaps. Emission intensities of pyrene were monitored at 405 nm, whereas those of perylene were monitored at 530 nm.

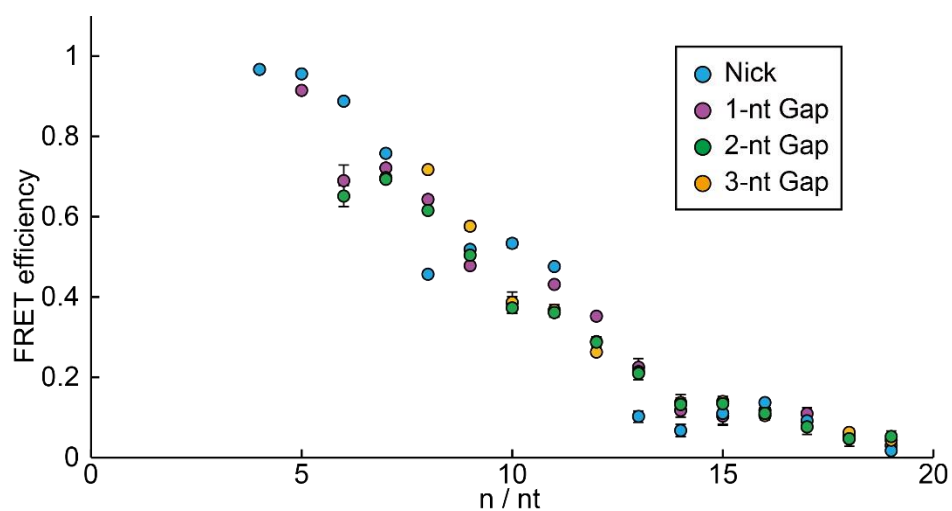


Figure S2-6. FRET plots of nicked and gapped duplexes.

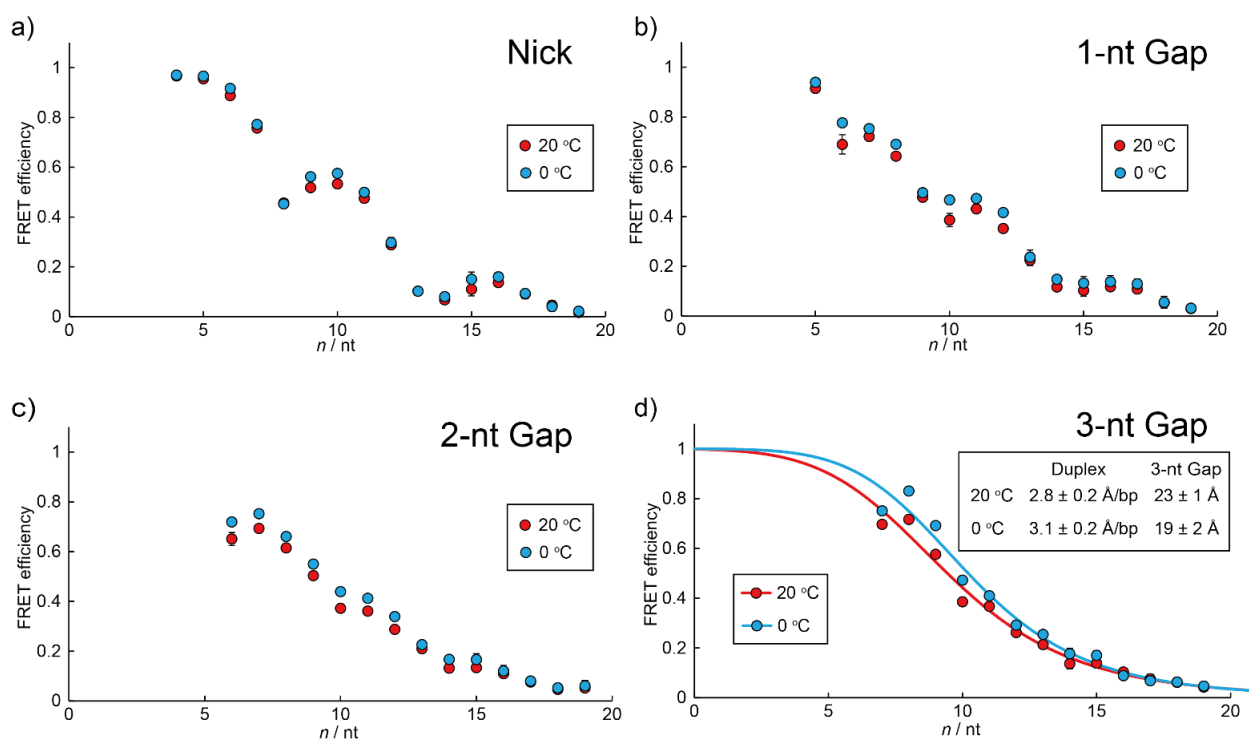


Figure S2-7. Temperature dependence of FRET plots of nicked or gapped duplexes. Determined parameters for 3-nt gapped duplex at 0 and 20 °C are also shown in the inset of d).

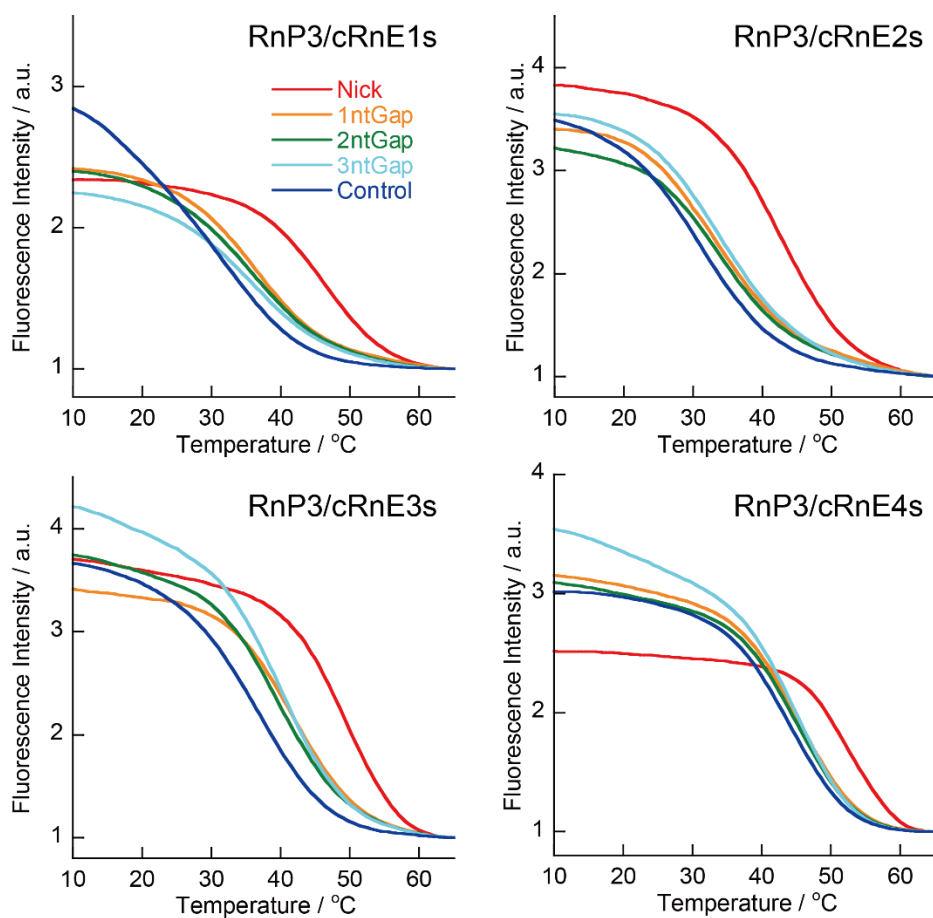


Figure S2-8. Melting curves of nicked or gapped duplexes monitored by FRET.

Table S2-1. FRET efficiencies and melting temperatures of canonical duplexes.

Distance	Sequence	Φ_T^a	$T_m / ^\circ\text{C}^b$
19 bp	RnP1 ATCAGT P ATGTATGTATGTATTCACC-GTAGTCA (5' → 3')	0.014 ± 0.007	71.3
	cRnE1 TAGTCA-TACATACATACATAAGTGG E CATCAGT (3' ← 5')		
18 bp	RnP1 ATCAGT P ATGTATGTATGTATTCAC-CGTAGTCA (5' → 3')	0.037 ± 0.007	68.6
	cRnE2 TAGTCA-TACATACATACATAAGTGG E CATCAGT (3' ← 5')		
17 bp	RnP1 ATCAGT P ATGTATGTATGTATTCAC-CCGTAGTCA (5' → 3')	0.075 ± 0.005	70.0
	cRnE3 TAGTCA-TACATACATACATAAGT E GGCATCAGT (3' ← 5')		
16 bp	RnP1 ATCAGT P ATGTATGTATGTATTC-ACCGTAGTCA (5' → 3')	0.127 ± 0.016	71.2
	cRnE4 TAGTCA-TACATACATACATAAG E TGGCATCAGT (3' ← 5')		
15 bp	RnP2 ATCAGTATGT P ATGTATGTATTCACC-GTAGTCA (5' → 3')	0.112 ± 0.012	70.3
	cRnE1 TAGTCATACA-TACATACATAAGTGG E CATCAGT (3' ← 5')		
14 bp	RnP2 ATCAGTATGT P ATGTATGTATTCAC-CGTAGTCA (5' → 3')	0.067 ± 0.018	66.5
	cRnE2 TAGTCATACA-TACATACATAAGTGG E CATCAGT (3' ← 5')		
13 bp	RnP2 ATCAGTATGT P ATGTATGTATTCAC-CCGTAGTCA (5' → 3')	0.096 ± 0.017	66.9
	cRnE3 TAGTCATACA-TACATACATAAGT E GGCATCAGT (3' ← 5')		
12 bp	RnP2 ATCAGTATGT P ATGTATGTATTC-ACCGTAGTCA (5' → 3')	0.298 ± 0.011	68.1
	cRnE4 TAGTCATACA-TACATACATAAG E TGGCATCAGT (3' ← 5')		
11 bp	RnP3 ATCAGTATGTATGT P ATGTATTCACC-GTAGTCA (5' → 3')	0.508 ± 0.018	71.2
	cRnE1 TAGTCATACATACA-TACATAAGTGG E CATCAGT (3' ← 5')		
10 bp	RnP3 ATCAGTATGTATGT P ATGTATTCAC-CGTAGTCA (5' → 3')	0.583 ± 0.019	68.4
	cRnE2 TAGTCATACATACA-TACATAAGTGG E CATCAGT (3' ← 5')		
9 bp	RnP3 ATCAGTATGTATGT P ATGTATTCAC-CCGTAGTCA (5' → 3')	0.484 ± 0.009	69.0
	cRnE3 TAGTCATACATACA-TACATAAGT E GGCATCAGT (3' ← 5')		
8 bp	RnP3 ATCAGTATGTATGT P ATGTATTC-ACCGTAGTCA (5' → 3')	0.444 ± 0.011	69.7
	cRnE4 TAGTCATACATACA-TACATAAG E TGGCATCAGT (3' ← 5')		
7 bp	RnP4 ATCAGTATGTATGTATGT P ATTCACC-GTAGTCA (5' → 3')	0.802 ± 0.004	66.8
	cRnE1 TAGTCATACATACATACA-TAAGTGG E CATCAGT (3' ← 5')		
6 bp	RnP4 ATCAGTATGTATGTATGT P ATTCAC-CGTAGTCA (5' → 3')	0.944 ± 0.001	64.4
	cRnE2 TAGTCATACATACATACA-TAAGTGG E CATCAGT (3' ← 5')		
5 bp	RnP4 ATCAGTATGTATGTATGT P ATTCAC-CCGTAGTCA (5' → 3')	0.978 ± 0.001	65.0
	cRnE3 TAGTCATACATACATACA-TAAGT E GGCATCAGT (3' ← 5')		
4 bp	RnP4 ATCAGTATGTATGTATGT P ATTC-ACCGTAGTCA (5' → 3')	0.979 ± 0.001	66.4
	cRnE4 TAGTCATACATACATACA-TAAG E TGGCATCAGT (3' ← 5')		

Table S2-2. FRET efficiencies and melting temperatures of A-tract duplexes.

Distance	Sequence	Φ_T	$T_m / ^\circ\text{C}^a$
18 bp	AtP1 ATCAGTAPAAAAAAAAAAAAAAAAAAAAA-ATAGTCA (5'→3') cAtE1 TAGTCAT-TTTTTTTTTTTTTTTTTTETATCAGT (3'←5')	0.07	58.5
17 bp	AtP2 ATCAGTAAAPAAAAAAAAAAAAAAAAAAAAA-ATAGTCA (5'→3') cAtE1 TAGTCATT-TTTTTTTTTTTTTTTTTTETATCAGT (3'←5')	0.11	61.1
16 bp	AtP3 ATCAGTAAAAPAAAAAAAAAAAAAAAAAAAAA-ATAGTCA (5'→3') cAtE1 TAGTCATTT-TTTTTTTTTTTTTTTTTTETATCAGT (3'←5')	0.20	61.3
15 bp	AtP4 ATCAGTAAAAAPAAAAAAAAAAAAAAAAAAAAA-ATAGTCA (5'→3') cAtE1 TAGTCATTTT-TTTTTTTTTTTTTTTTTTETATCAGT (3'←5')	0.23	61.0
14 bp	AtP5 ATCAGTAAAAAPAAAAAAAAAAAAAAAAAAAAA-ATAGTCA (5'→3') cAtE1 TAGTCATTTT-TTTTTTTTTTTTTTTTTTETATCAGT (3'←5')	0.19	61.3
13 bp	AtP1 ATCAGTAPAAAAAAAAAAAAAAAAAAAAA-AAAAAATAGTCA (5'→3') cAtE2 TAGTCAT-TTTTTTTTTTTTTTETTTTTTATCAGT (3'←5')	0.14	58.1
12 bp	AtP2 ATCAGTAAAPAAAAAAAAAAAAAAAAAAAAA-AAAAAATAGTCA (5'→3') cAtE2 TAGTCATT-TTTTTTTTTTTTTTETTTTTTATCAGT (3'←5')	0.32	61.1
11 bp	AtP3 ATCAGTAAAAPAAAAAAAAAAAAAAAAAAAAA-AAAAAATAGTCA (5'→3') cAtE2 TAGTCATTT-TTTTTTTTTTETTTTTTATCAGT (3'←5')	0.57	61.4
10 bp	AtP4 ATCAGTAAAAAPAAAAAAAAAAAAA-AAAAAATAGTCA (5'→3') cAtE2 TAGTCATTTT-TTTTTTTTTTETTTTTTATCAGT (3'←5')	0.66	60.9
9 bp	AtP5 ATCAGTAAAAAPAAAAAAAAAAAAA-AAAAAATAGTCA (5'→3') cAtE2 TAGTCATTTT-TTTTTTTTTTETTTTTTATCAGT (3'←5')	0.60	61.3
8 bp	AtP1 ATCAGTAPAAAAAAAAAAAAA-AAAAAAAAAATAGTCA (5'→3') cAtE3 TAGTCAT-TTTTTTTTETTTTTTTTTTATCAGT (3'←5')	0.46	58.6
7 bp	AtP2 ATCAGTAAAPAAAAAAAAAAAAA-AAAAAAAAAATAGTCA (5'→3') cAtE3 TAGTCATT-TTTTTTTTETTTTTTTTTTATCAGT (3'←5')	0.83	61.3
6 bp	AtP3 ATCAGTAAAAPAAAAAAA-AAAAAAAAAATAGTCA (5'→3') cAtE3 TAGTCATTT-TTTTTTETTTTTTTTTTATCAGT (3'←5')	0.94	61.2
5 bp	AtP4 ATCAGTAAAAAPAAAAA-AAAAAAAAAATAGTCA (5'→3') cAtE3 TAGTCATTTT-TTTTTTETTTTTTTTTTATCAGT (3'←5')	0.97	61.1
4 bp	AtP5 ATCAGTAAAAAPAAAAA-AAAAAAAAAATAGTCA (5'→3') cAtE3 TAGTCATTTT-TTTTETTTTTTTTTTATCAGT (3'←5')	0.96	62.2

^a Determined from a melting profile by monitoring absorbance at 260 nm.

Table S2-3. FRET efficiencies of nicked duplexes.

Distance	Sequence		Φ_T^a
19 nt (19 bp)	RnP1 Nt23/cRnE1s	ATCAGT P ATGTATGTATGTATTCACC-GTAGTCA TAGTCA-TACATACATACATAAGT G EGCATCAGT	(5' → 3') (3' ← 5') 0.017 ± 0.008
18 nt (18 bp)	RnP1 Nt22/cRnE2s	ATCAGT P ATGTATGTATGTATTCAC-CGTAGTCA TAGTCA-TACATACATACATAAGT G EGCATCAGT	(5' → 3') (3' ← 5') 0.046 ± 0.018
17 nt (17 bp)	RnP1 Nt21/cRnE3s	ATCAGT P ATGTATGTATGTATTCAC-CCGTAGTCA TAGTCA-TACATACATACATAAGT E GGCATCAGT	(5' → 3') (3' ← 5') 0.091 ± 0.019
16 nt (16 bp)	RnP1 Nt20/cRnE4s	ATCAGT P ATGTATGTATGTATTC-ACCGTAGTCA TAGTCA-TACATACATACATAAGT E GGCATCAGT	(5' → 3') (3' ← 5') 0.137 ± 0.006
15 nt (15 bp)	RnP2 Nt23/cRnE1s	ATCAGTATGT P ATGTATGTATTCACC-GTAGTCA TAGTCATACA-TACATACATAAGT G EGCATCAGT	(5' → 3') (3' ← 5') 0.110 ± 0.027
14 nt (14 bp)	RnP2 Nt22/cRnE2s	ATCAGTATGT P ATGTATGTATTCAC-CGTAGTCA TAGTCATACA-TACATACATAAGT G EGCATCAGT	(5' → 3') (3' ← 5') 0.068 ± 0.015
13 nt (13 bp)	RnP2 Nt21/cRnE3s	ATCAGTATGT P ATGTATGTATTCAC-CCGTAGTCA TAGTCATACA-TACATACATAAGT E GGCATCAGT	(5' → 3') (3' ← 5') 0.102 ± 0.014
12 nt (12 bp)	RnP2 Nt20/cRnE4s	ATCAGTATGT P ATGTATGTATTC-ACCGTAGTCA TAGTCATACA-TACATACATAAGT E GGCATCAGT	(5' → 3') (3' ← 5') 0.288 ± 0.013
11 nt (11 bp)	RnP3 Nt23/cRnE1s	ATCAGTATGTATGT P ATGTATTCACC-GTAGTCA TAGTCATACATACA-TACATAAGT G EGCATCAGT	(5' → 3') (3' ← 5') 0.475 ± 0.001
10 nt (10 bp)	RnP3 Nt22/cRnE2s	ATCAGTATGTATGT P ATGTATTCAC-CGTAGTCA TAGTCATACATACA-TACATAAGT G EGCATCAGT	(5' → 3') (3' ← 5') 0.533 ± 0.011
9 nt (9 bp)	RnP3 Nt21/cRnE3s	ATCAGTATGTATGT P ATGTATTCAC-CCGTAGTCA TAGTCATACATACA-TACATAAGT E GGCATCAGT	(5' → 3') (3' ← 5') 0.518 ± 0.006
8 nt (8 bp)	RnP3 Nt20/cRnE4s	ATCAGTATGTATGT P ATGTATTC-ACCGTAGTCA TAGTCATACATACA-TACATAAGT E GGCATCAGT	(5' → 3') (3' ← 5') 0.456 ± 0.004
7 nt (7 bp)	RnP4 Nt23/cRnE1s	ATCAGTATGTATGTATGT P ATTCACC-GTAGTCA TAGTCATACATACATACA-TAAGT G EGCATCAGT	(5' → 3') (3' ← 5') 0.757 ± 0.007
6 nt (6 bp)	RnP4 Nt22/cRnE2s	ATCAGTATGTATGTATGT P ATTCAC-CGTAGTCA TAGTCATACATACATACA-TAAGT G EGCATCAGT	(5' → 3') (3' ← 5') 0.888 ± 0.008
5 nt (5 bp)	RnP4 Nt21/cRnE3s	ATCAGTATGTATGTATGT P ATTCAC-CCGTAGTCA TAGTCATACATACATACA-TAAGT E GGCATCAGT	(5' → 3') (3' ← 5') 0.955 ± 0.001
4 nt (4 bp)	RnP4 Nt20/cRnE4s	ATCAGTATGTATGTATGT P ATTC-ACCGTAGTCA TAGTCATACATACATACA-TAAGT E GGCATCAGT	(5' → 3') (3' ← 5') 0.967 ± 0.001

^a Standard deviation was determined from three independent experiments.

Table S2-4. FRET efficiencies of 1-nt gapped duplexes.

Distance	Sequence		Φ_T^a
19 nt (18 bp+1Gap)	RnP1 Nt22/cRnE1s	ATCAGT P ATGTATGTATGTATTCACC-GTAGTCA (5' → 3') TAGTCA-TACATACATACATAAG G GE C ATCAGT (3' ← 5')	0.030 ± 0.017
18 nt (17 bp+1Gap)	RnP1 Nt21/cRnE2s	ATCAGT P ATGTATGTATGTATTCAC-CGTAGTCA (5' → 3') TAGTCA-TACATACATACATAA T GE G CATCAGT (3' ← 5')	0.054 ± 0.016
17 nt (16 bp+1Gap)	RnP1 Nt20/cRnE3s	ATCAGT P ATGTATGTATGTATTCAC-CCGTAGTCA (5' → 3') TAGTCA-TACATACATACATA G TE G GCATCAGT (3' ← 5')	0.109 ± 0.015
16 nt (15 bp+1Gap)	RnP1 Nt19/cRnE4s	ATCAGT P ATGTATGTATGTATTC-ACCGTAGTCA (5' → 3') TAGTCA-TACATACATACAT A GE T GGCATCAGT (3' ← 5')	0.118 ± 0.014
15 nt (14 bp+1Gap)	RnP2 Nt22/cRnE1s	ATCAGTATGT P ATGTATGTATTCACC-GTAGTCA (5' → 3') TAGTCATACA-TACATACATAAG G GE C ATCAGT (3' ← 5')	0.103 ± 0.023
14 nt (13 bp+1Gap)	RnP2 Nt21/cRnE2s	ATCAGTATGT P ATGTATGTATTCAC-CGTAGTCA (5' → 3') TAGTCATACA-TACATACATAA T GE G CATCAGT (3' ← 5')	0.117 ± 0.016
13 nt (12 bp+1Gap)	RnP2 Nt20/cRnE3s	ATCAGTATGT P ATGTATGTATTCAC-CCGTAGTCA (5' → 3') TAGTCATACA-TACATACATA G TE G GCATCAGT (3' ← 5')	0.225 ± 0.022
12 nt (11 bp+1Gap)	RnP2 Nt19/cRnE4s	ATCAGTATGT P ATGTATGTATTC-ACCGTAGTCA (5' → 3') TAGTCATACA-TACATACAT A GE T GGCATCAGT (3' ← 5')	0.352 ± 0.009
11 nt (10 bp+1Gap)	RnP3 Nt22/cRnE1s	ATCAGTATGTATGT P ATGTATTCACC-GTAGTCA (5' → 3') TAGTCATACATACA-TACATAAG G GE C ATCAGT (3' ← 5')	0.431 ± 0.003
10 nt (9 bp+1Gap)	RnP3 Nt21/cRnE2s	ATCAGTATGTATGT P ATGTATTCAC-CGTAGTCA (5' → 3') TAGTCATACATACA-TACATAA T GE G CATCAGT (3' ← 5')	0.386 ± 0.027
9 nt (8 bp+1Gap)	RnP3 Nt20/cRnE3s	ATCAGTATGTATGT P ATGTATTCAC-CCGTAGTCA (5' → 3') TAGTCATACATACA-TACATA G TE G GCATCAGT (3' ← 5')	0.477 ± 0.007
8 nt (7 bp+1Gap)	RnP3 Nt19/cRnE4s	ATCAGTATGTATGT P ATGTATTC-ACCGTAGTCA (5' → 3') TAGTCATACATACA-TACAT A GE T GGCATCAGT (3' ← 5')	0.643 ± 0.009
7 nt (6 bp+1Gap)	RnP4 Nt22/cRnE1s	ATCAGTATGTATGTATGT P ATTCACC-GTAGTCA (5' → 3') TAGTCATACATACATACA-TAAG G GE C ATCAGT (3' ← 5')	0.721 ± 0.008
6 nt (5 bp+1Gap)	RnP4 Nt21/cRnE2s	ATCAGTATGTATGTATGT P ATTCAC-CGTAGTCA (5' → 3') TAGTCATACATACATACA-TAA T GE G CATCAGT (3' ← 5')	0.690 ± 0.039
5 nt (4 bp+1Gap)	RnP4 Nt20/cRnE3s	ATCAGTATGTATGTATGT P ATTCAC-CCGTAGTCA (5' → 3') TAGTCATACATACATACA-TA G TE G GCATCAGT (3' ← 5')	0.914 ± 0.008

^a Standard deviation was determined from three independent experiments.

Table S2-5. FRET efficiencies of 2-nt gapped duplexes.

Distance	Sequence		Φ_T^a
19 nt (17 bp+2Gap)	RnP1 Nt21/cRnE1s	ATCAGT P ATGTATGTATGTATTCACC-GTAGTCA (5' → 3') TAGTCA-TACATACATACATAA G GE C ATCAGT (3' ← 5')	0.052 ± 0.015
18 nt (16 bp+2Gap)	RnP1 Nt20/cRnE2s	ATCAGT P ATGTATGTATGTATTCAC-CGTAGTCA (5' → 3') TAGTCA-TACATACATACATA T GE G CATCAGT (3' ← 5')	0.047 ± 0.002
17 nt (15 bp+2Gap)	RnP1 Nt19/cRnE3s	ATCAGT P ATGTATGTATGTATTCACC-CGTAGTCA (5' → 3') TAGTCA-TACATACATACAT G TE G GCATCAGT (3' ← 5')	0.076 ± 0.004
16 nt (14 bp+2Gap)	RnP1 Nt18/cRnE4s	ATCAGT P ATGTATGTATGTATTC-ACCGTAGTCA (5' → 3') TAGTCA-TACATACATACA A GE T GGCATCAGT (3' ← 5')	0.110 ± 0.013
15 nt (13 bp+2Gap)	RnP2 Nt21/cRnE1s	ATCAGTATGT P ATGTATGTATTCACC-GTAGTCA (5' → 3') TAGTCATACA-TACATACATAA G GE C ATCAGT (3' ← 5')	0.134 ± 0.018
14 nt (12 bp+2Gap)	RnP2 Nt20/cRnE2s	ATCAGTATGT P ATGTATGTATTCAC-CGTAGTCA (5' → 3') TAGTCATACA-TACATACATA T GE G CATCAGT (3' ← 5')	0.132 ± 0.017
13 nt (11 bp+2Gap)	RnP2 Nt19/cRnE3s	ATCAGTATGT P ATGTATGTATTCACC-CGTAGTCA (5' → 3') TAGTCATACA-TACATACAT G TE G GCATCAGT (3' ← 5')	0.210 ± 0.016
12 nt (10 bp+2Gap)	RnP2 Nt18/cRnE4s	ATCAGTATGT P ATGTATGTATTC-ACCGTAGTCA (5' → 3') TAGTCATACA-TACATACA A GE T GGCATCAGT (3' ← 5')	0.287 ± 0.012
11 nt (9 bp+2Gap)	RnP3 Nt21/cRnE1s	ATCAGTATGTATGT P ATGTATTCACC-GTAGTCA (5' → 3') TAGTCATACATACA-TACATAA G GE C ATCAGT (3' ← 5')	0.361 ± 0.011
10 nt (8 bp+2Gap)	RnP3 Nt20/cRnE2s	ATCAGTATGTATGT P ATGTATTCAC-CGTAGTCA (5' → 3') TAGTCATACATACA-TACATA T GE G CATCAGT (3' ← 5')	0.372 ± 0.013
9 nt (7 bp+2Gap)	RnP3 Nt19/cRnE3s	ATCAGTATGTATGT P ATGTATTCACC-CGTAGTCA (5' → 3') TAGTCATACATACA-TACAT G TE G GCATCAGT (3' ← 5')	0.504 ± 0.008
8 nt (6 bp+2Gap)	RnP3 Nt18/cRnE4s	ATCAGTATGTATGT P ATGTATTC-ACCGTAGTCA (5' → 3') TAGTCATACATACA-TACA A GE T GGCATCAGT (3' ← 5')	0.615 ± 0.008
7 nt (5 bp+2Gap)	RnP4 Nt21/cRnE1s	ATCAGTATGTATGTATGT P ATTCACC-GTAGTCA (5' → 3') TAGTCATACATACATACA-TAA G GE C ATCAGT (3' ← 5')	0.693 ± 0.006
6 nt (4 bp+2Gap)	RnP4 Nt20/cRnE2s	ATCAGTATGTATGTATGT P ATTCAC-CGTAGTCA (5' → 3') TAGTCATACATACATACA-TA T GE G CATCAGT (3' ← 5')	0.651 ± 0.026

^a Standard deviation was determined from three independent experiments.

Table S2-6. FRET efficiencies of 3-nt gapped duplexes.

Distance	Sequence		Φ_T^a
19 nt (16 bp+3Gap)	RnP1 Nt20/cRnE1s	ATCAGT P ATGTATGTATGTATTCACC-GTAGTCA TAGTCA-TACATACATACATA G G E C ATCAGT	(5' → 3') (3' ← 5') 0.043 ± 0.010
18 nt (15 bp+3Gap)	RnP1 Nt19/cRnE2s	ATCAGT P ATGTATGTATGTATTCAC-CGTAGTCA TAGTCA-TACATACATACAT T G E G CATCAGT	(5' → 3') (3' ← 5') 0.062 ± 0.010
17 nt (14 bp+3Gap)	RnP1 Nt18/cRnE3s	ATCAGT P ATGTATGTATGTATTC-CCGTAGTCA TAGTCA-TACATACATACA G T E G G C ATCAGT	(5' → 3') (3' ← 5') 0.076 ± 0.018
16 nt (13 bp+3Gap)	RnP1 Nt17/cRnE4s	ATCAGT P ATGTATGTATGTATTC-ACCGTAGTCA TAGTCA-TACATACATAC A G E T G G CATCAGT	(5' → 3') (3' ← 5') 0.104 ± 0.011
15 nt (12 bp+3Gap)	RnP2 Nt20/cRnE1s	ATCAGTATGT P ATGTATGTATTCACC-GTAGTCA TAGTCATACA-TACATACATA G G E C ATCAGT	(5' → 3') (3' ← 5') 0.139 ± 0.013
14 nt (11 bp+3Gap)	RnP2 Nt19/cRnE2s	ATCAGTATGT P ATGTATGTATTCAC-CGTAGTCA TAGTCATACA-TACATACAT T G E G CATCAGT	(5' → 3') (3' ← 5') 0.137 ± 0.021
13 nt (10 bp+3Gap)	RnP2 Nt18/cRnE3s	ATCAGTATGT P ATGTATGTATTC-CCGTAGTCA TAGTCATACA-TACATACA G T E G G C ATCAGT	(5' → 3') (3' ← 5') 0.214 ± 0.012
12 nt (9 bp+3Gap)	RnP2 Nt17/cRnE4s	ATCAGTATGT P ATGTATGTATTC-ACCGTAGTCA TAGTCATACA-TACATAC A G E T G G CATCAGT	(5' → 3') (3' ← 5') 0.262 ± 0.006
11 nt (8 bp+3Gap)	RnP3 Nt20/cRnE1s	ATCAGTATGTATGT P ATGTATTCACC-GTAGTCA TAGTCATACATACA-TACATA G G E C ATCAGT	(5' → 3') (3' ← 5') 0.367 ± 0.014
10 nt (7 bp+3Gap)	RnP3 Nt19/cRnE2s	ATCAGTATGTATGT P ATGTATTCAC-CGTAGTCA TAGTCATACATACA-TACAT T G E G CATCAGT	(5' → 3') (3' ← 5') 0.386 ± 0.015
9 nt (6 bp+3Gap)	RnP3 Nt18/cRnE3s	ATCAGTATGTATGT P ATGTATTC-CCGTAGTCA TAGTCATACATACA-TACA G T E G G C ATCAGT	(5' → 3') (3' ← 5') 0.576 ± 0.010
8 nt (5 bp+3Gap)	RnP3 Nt17/cRnE4s	ATCAGTATGTATGT P ATGTATTC-ACCGTAGTCA TAGTCATACATACA-TAC A G E T G G CATCAGT	(5' → 3') (3' ← 5') 0.717 ± 0.005
7 nt (4 bp+3Gap)	RnP4 Nt20/cRnE1s	ATCAGTATGTATGTATGT P ATTCACC-GTAGTCA TAGTCATACATACATACA-TA G G E C ATCAGT	(5' → 3') (3' ← 5') 0.697 ± 0.002

^a Standard deviation was determined from three independent experiments.

Table S2-7. Melting temperatures of nicked and gapped duplexes monitored by FRET.

Sequence		$T_m / ^\circ\text{C}^a$	
RnP3/cRnE1s nick	RnP3 Nt23/cRnE1s	ATCAGTATGTATGTPATGTATTCACC-GTAGTCA (5' → 3') TAGTCATACATACA-TACATAAGTGGECATCAGT (3' ← 5')	46.0
	RnP3 Nt22/cRnE1s	ATCAGTATGTATGTPATGTATTCACC-GTAGTCA (5' → 3') TAGTCATACATACA-TACATAAG GGGECATCAGT (3' ← 5')	36.1
2-base Gap	RnP3 Nt21/cRnE1s	ATCAGTATGTATGTPATGTATTCACC-GTAGTCA (5' → 3') TAGTCATACATACA-TACATAA GGGECATCAGT (3' ← 5')	35.5
	RnP3 Nt20/cRnE1s	ATCAGTATGTATGTPATGTATTCACC-GTAGTCA (5' → 3') TAGTCATACATACA-TACATA GGGECATCAGT (3' ← 5')	35.9
control	RnP3 cRnE1s	ATCAGTATGTATGTPATGTATTCACC-GTAGTCA (5' → 3') GGGECATCAGT (3' ← 5')	30.2
RnP3/cRnE2s nick	RnP3 Nt22/cRnE2s	ATCAGTATGTATGTPATGTATTCAC-CGTAGTCA (5' → 3') TAGTCATACATACA-TACATAAGTGGGCATCAGT (3' ← 5')	42.4
	RnP3 Nt21/cRnE2s	ATCAGTATGTATGTPATGTATTCAC-CGTAGTCA (5' → 3') TAGTCATACATACA-TACATAA TGGGCATCAGT (3' ← 5')	33.0
2-base Gap	RnP3 Nt20/cRnE2s	ATCAGTATGTATGTPATGTATTCAC-CGTAGTCA (5' → 3') TAGTCATACATACA-TACATA TGGGCATCAGT (3' ← 5')	33.7
	RnP3 Nt19/cRnE2s	ATCAGTATGTATGTPATGTATTCAC-CGTAGTCA (5' → 3') TAGTCATACATACA-TACAT TGGGCATCAGT (3' ← 5')	33.7
control	RnP3 cRnE2s	ATCAGTATGTATGTPATGTATTCAC-CGTAGTCA (5' → 3') TGGGCATCAGT (3' ← 5')	31.0
RnP3/cRnE3s nick	RnP3 Nt21/cRnE3s	ATCAGTATGTATGTPATGTATTCAC-CCGTAGTCA (5' → 3') TAGTCATACATACA-TACATAAGTGGGCATCAGT (3' ← 5')	49.1
	RnP3 Nt20/cRnE3s	ATCAGTATGTATGTPATGTATTCAC-CCGTAGTCA (5' → 3') TAGTCATACATACA-TACATA GTEGGGCATCAGT (3' ← 5')	41.6
2-base Gap	RnP3 Nt19/cRnE3s	ATCAGTATGTATGTPATGTATTCAC-CCGTAGTCA (5' → 3') TAGTCATACATACA-TACAT GTEGGGCATCAGT (3' ← 5')	39.3
	RnP3 Nt18/cRnE3s	ATCAGTATGTATGTPATGTATTCAC-CCGTAGTCA (5' → 3') TAGTCATACATACA-TACA GTEGGGCATCAGT (3' ← 5')	39.7
control	RnP3 cRnE3s	ATCAGTATGTATGTPATGTATTCAC-CCGTAGTCA (5' → 3') GTEGGGCATCAGT (3' ← 5')	36.4
RnP3/cRnE4s nick	RnP3 Nt20/cRnE4s	ATCAGTATGTATGTPATGTATTC-ACCGTAGTCA (5' → 3') TAGTCATACATACA-TACATAAGETGGGCATCAGT (3' ← 5')	52.3
	RnP3 Nt19/cRnE4s	ATCAGTATGTATGTPATGTATTC-ACCGTAGTCA (5' → 3') TAGTCATACATACA-TACAT AGETGGGCATCAGT (3' ← 5')	45.0
2-base Gap	RnP3 Nt18/cRnE4s	ATCAGTATGTATGTPATGTATTC-ACCGTAGTCA (5' → 3') TAGTCATACATACA-TACA AGETGGGCATCAGT (3' ← 5')	44.8
	RnP3 Nt17/cRnE4s	ATCAGTATGTATGTPATGTATTC-ACCGTAGTCA (5' → 3') TAGTCATACATACA-TAC AGETGGGCATCAGT (3' ← 5')	44.6
control	RnP3 cRnE4s	ATCAGTATGTATGTPATGTATTC-ACCGTAGTCA (5' → 3') AGETGGGCATCAGT (3' ← 5')	43.5

^a Determined from a melting profile by monitoring emission intensity at 500 nm with 345 nm excitation.

Chapter 3. Structural analysis of photoactive DNA by using Perylene-Cy3 FRET system

3-1 Abstract

In chapter 3, we describe a novel DNA-based FRET system for structural analyses by perylene and Cy3 as a donor and an acceptor. We introduced perylene and Cy3 at the termini of the DNA duplex via D-threoninol, and evaluated FRET efficiencies. Experimentally obtained FRET efficiencies were in good agreement with theoretical values calculated based on canonical B-form DNA model. This agreement showed that the FRET efficiency reflected the structure of the DNA duplex. Thus, the FRET efficiency between perylene and Cy3 can be used to obtain structural information of nucleic acids. Due to the relatively long Förster radius, this system can be used to analyze large DNA structures, and duplexes containing photo-reactive molecules can be analyzed since perylene can be excited with visible light. The system was used to analyze a DNA duplex containing stilbene, demonstrating that in the region of the stilbene cluster the duplex adopts a ladder-like structure rather than helical one. On the other hand, it was also suggested that another stilbene cluster is stacked in a right-handed helical manner. Upon photodimerization between stilbene residues, FRET efficiencies indicated the reaction

does not disturb DNA duplex. This FRET system will be useful for analysis of photoreactions of nucleobases as well as a wide range of nucleic acid structures.

3-2 Introduction

We developed an orientation-dependent FRET system by introducing dyes into DNA through D-threosinol.^[1] In chapter 2, differences in structures of nicked and gapped DNA duplexes were successfully revealed using this FRET system.^[2] In other report, binding of nucleosides to gapped DNA was also be analyzed.^[3] However, the FRET system using pyrene-perylene pair has two disadvantages. First, the Förster radius between pyrene and perylene is relatively short (33.8 Å, around 11 bp, when assuming random orientation). For example, DNA decoys, antisense oligonucleotides, and siRNAs, which are attracting attention as oligonucleotide therapeutics, are around 20 bp. Such larger structures cannot be analyzed. Second, excitation and emission wavelengths of pyrene are in UV region. It makes difficult to analyze DNA, which contains UV absorbing molecules, such as adducted nucleobases.^[4] Therefore, a FRET pair that works at longer wavelength is desirable.

We herein report a novel FRET system using perylene and Cy3 as a donor and an acceptor, respectively. Perylene emission has a large spectral overlap with Cy3 absorption

(Figure 3-1). The calculated Förster radius of perylene-Cy3 pair, assuming randomized orientation, is 56.8 Å (about 17 bp), which is much longer than that of pyrene-perylene pair.

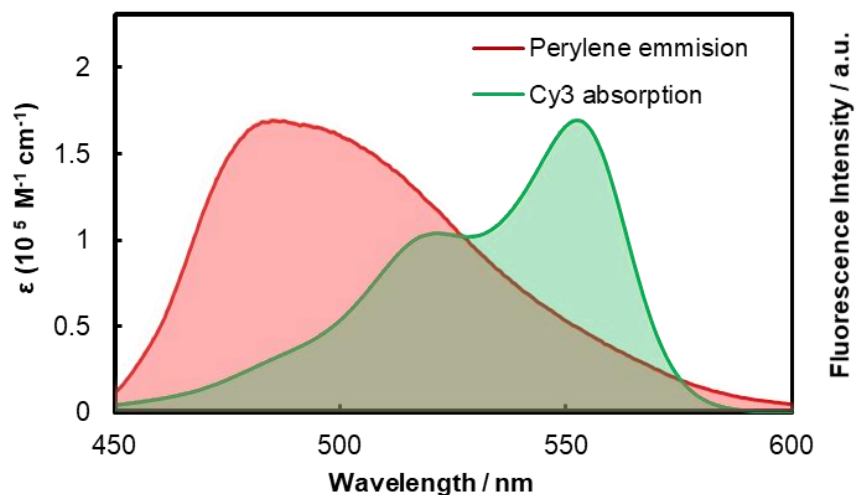


Figure 3-1.

Spectral overlap between perylene fluorescence and Cy3 absorption.

Moreover, the excitation wavelength of perylene is 425 nm. Owing to these properties, it should be possible to analyze structures containing UV absorbing molecules. In order to use this pair for detailed structural analyses of nucleic acids, orientation dependence as well as distance dependence of FRET must be observed. Therefore, we first investigated orientation dependence of the perylene-Cy3 pair using a native DNA duplex. We then used this FRET pair to analyze structures of DNA duplexes containing stilbene moieties.

Stilbene has unique photophysical properties and has been used as a photo-switch.^[5] Moreover, the stilbene cluster has recently been used in aggregation-induced emission materials.^[6] Stilbene has been incorporated into DNA for sensing, crosslinking, and stabilization.^[7] We also developed photo-switches by introducing clusters of stilbene derivatives into DNA.^[8] The structures of DNA containing stilbene clusters remain unclear, although clustered structures of dyes significantly affect their spectroscopic behaviors, as indicated by observed J- and H- aggregation.^[9] Herein, we investigated the structure of DNA containing a stilbene cluster using perylene-Cy3 FRET. It is noteworthy that the pyrene-erylene pair cannot be used in this case since photodimerization and/or photo-isomerization reactions between stilbene moieties occur upon UV light excitation of pyrene. We also evaluated the structural change that occurs upon photodimerization of stilbene moieties, which could be used to stabilize DNA duplexes and nano structures.

3-3 Results and discussions

3-3-1 Orientation dependence of FRET between perylene-Cy3 pair

DNA duplexes tethering perylene(**E**) and Cy3(**Y**) at opposite termini were first prepared to confirm the orientation dependence of FRET (**0aE/0bY** to **7aE/7bY** in Figure 3-2). Perylene and Cy3 were conjugated with D-threoninol via an amide bond, and these D-threoninol monomers were incorporated into DNA.^[10] D-Threoninol was used as a linker as it results in a defined dye orientation.^[11] The dyes were attached at termini of DNA due to relatively large size of Cy3 compared with pyrene. The number of base pairs (bps) between dyes was changed from 12 to 19 so that the orientation and distance between dyes varied periodically.

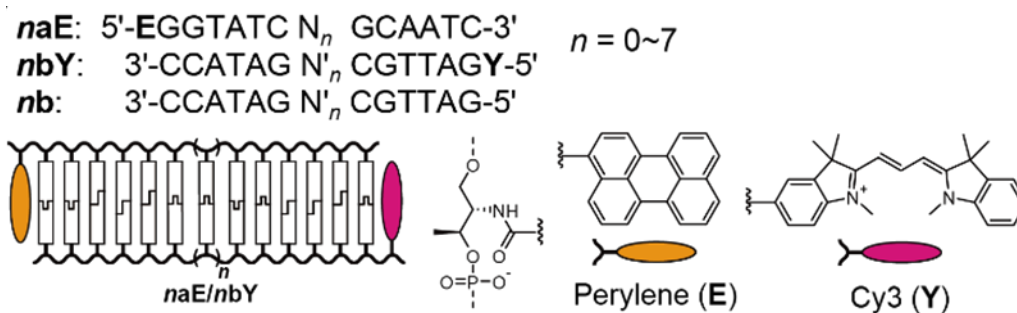


Figure 3-2.

Sequences used in this study of FRET between perylene (**E**)-Cy3 (**Y**) and schematics of analyzed duplexes. Chemical structures of dyes are also shown.

Fluorescent emission spectra of **naE/nb** duplexes were measured to calculate FRET

efficiencies. Spectra of duplexes containing only perylene (**naE/nb**) were also measured as controls (Figure S3-1 in Supporting Information). Representative data for duplexes containing 12 base pairs are shown in Figure 3-3a. Strong perylene emission was observed with **0aE/0b**, whereas the emission was substantially less in the duplex containing Cy3 (**0aE/0bY**). A peak of Cy3 emission at 570 nm was also observed with **0aE/0bY**. These results demonstrated efficient FRET from perylene to Cy3. Figure 3-3b shows the fluorescence spectra of **naE/nbY**, and intensities of perylene emission are summarized in Figure 3-3c. In general, fluorescence intensity of perylene decreased as the number of base pairs between the dyes increased. However, fluorescence intensity changed non-monotonously; emission intensity of the 14-bp duplex **2aE/2bY** was higher than intensities of the 13- and 15- bp duplexes **1aE/1bY** and **3aE/3bY**, respectively.

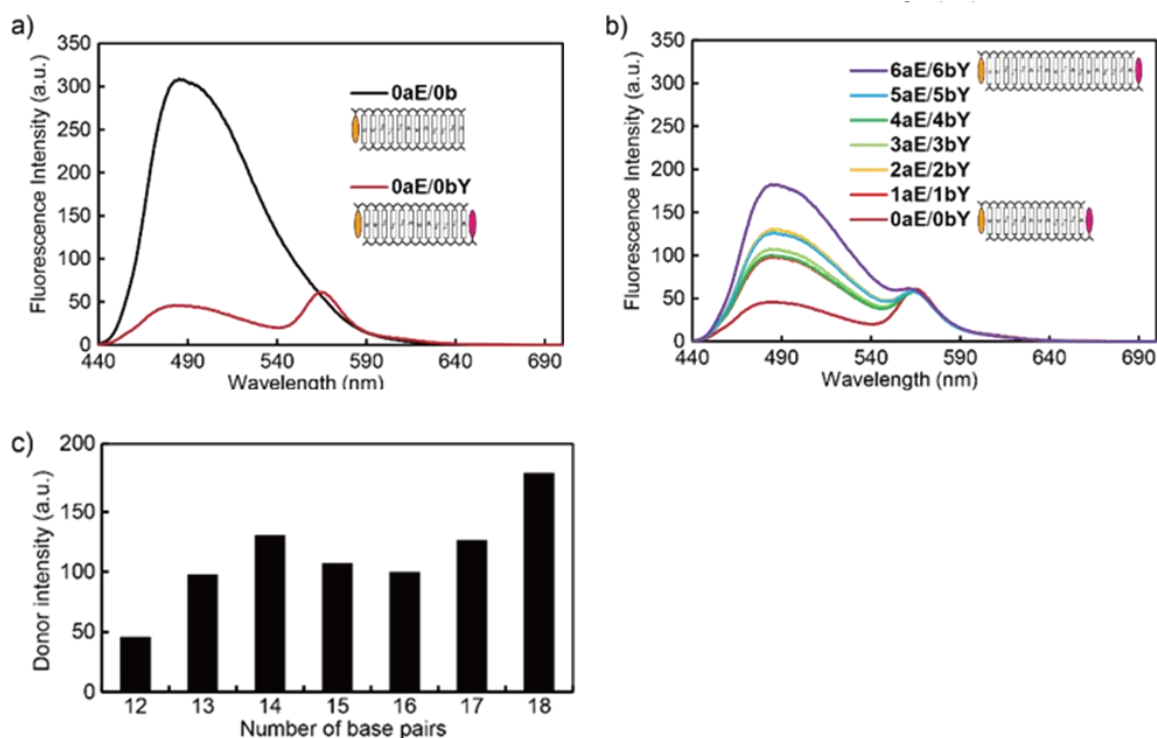


Figure 3-3.

a) Fluorescent emission spectra of DNA duplexes containing perylene and Cy3 (**0aE/0bY**) and only perylene (**0aE/0b**). b) Fluorescent emission spectra of DNA duplexes containing perylene and Cy3 (**naE/nbY**). c) The change in the fluorescence intensity of perylene as a function of the number of base pairs (**naE/nbY**).

FRET efficiencies were calculated from decreases in donor emission. Figure 3-4 shows FRET efficiencies of **naE/nbY** (circles). The FRET efficiency did not change monotonously as the number of base pairs between perylene and Cy3 increased. These results clearly showed that FRET depended not only on distance but also orientation. The experimentally determined efficiencies were compared with values calculated based on Förster theory for B-form DNA (rise: 3.2 Å/bp, rotation: 34°/bp; Figure 3-4, red line) or

for a random orientation (Figure 3-4, dotted line).

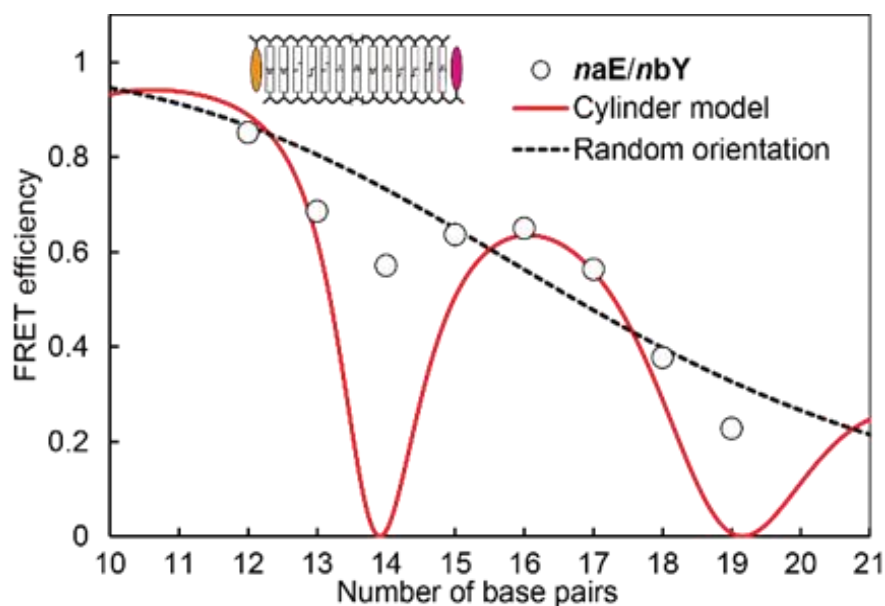


Figure 3-4.

FRET efficiencies of **naE/nbY** duplexes. Theoretical curves calculated based on the canonical B-form DNA cylinder model (red line) and the $\kappa^2=2/3$ model (dotted line) are also shown.

Since the persistence length of DNA duplex was reported as 50 nm,^[12] DNA duplex prepared in this study can be regarded as a rigid cylinder. The theoretical curve based on fixed orientation showed better agreement with experimental values than that based on random orientation. These agreements led us to conclude that each fluorophore was stacked with the neighboring base pair and that the dye orientation was fixed. Furthermore, the introduction of perylene and Cy3 into the DNA increased the melting temperature (T_m). The T_m of **0a/0b** was 47.7°C, whereas that of **0aE/0bY** was 57.3°C (Table 3-1).

Table 3-1. FRET efficiencies and melting temperatures of duplexes tethering dyes.

Sequence			Φ_T	T_m (°C)
0aE	EGGTATCGCAATC	(5'→3')	0.854	57.3
0bY	CCATAGCGTTAGY	(3'←5')		
0a	GGTATCGCAATC	(5'→3')	-	47.7
0b	CCATAGCGTTAG	(3'←5')		
1aE	EGGTATCAGCAATC	(5'→3')	0.660	-
1bY	CCATAGTCGTTAGY	(3'←5')		
1b	CCATAGTCGTTAG	(3'←5')	-	-
2aE	EGGTATCCAGCAATC	(5'→3')	0.508	-
2bY	CCATAGGTCGTTAGY	(3'←5')		
2b	CCATAGGTCGTTAG	(3'←5')	-	-
3aE	EGGTATCTCAGCAATC	(5'→3')	0.622	-
3bY	CCATAGAGTCGTTAGY	(3'←5')		
3b	CCATAGAGTCGTTAG	(3'←5')	-	-
4aE	EGGTATCGTCAGCAATC	(5'→3')	0.643	-
4bY	CCATAGCAGTCGTTAGY	(3'←5')		
4b	CCATAGCAGTCGTTAG	(3'←5')	-	-
5aE	EGGTATCCGTCAGCAATC	(5'→3')	0.534	-
5bY	CCATAGGCAGTCGTTAGY	(3'←5')		
5b	CCATAGGCAGTCGTTAG	(3'←5')	-	-
6aE	EGGTATCTCGTCAGCAATC	(5'→3')	0.336	-
6bY	CCATAGAGCAGTCGTTAGY	(3'←5')		
6b	CCATAGAGCAGTCGTTAG	(3'←5')	-	-
7aE	EGGTATCTTCGTCAGCAATC	(5'→3')	0.227	-
7bY	CCATAGAAGCAGTCGTTAGY	(3'←5')		
7b	CCATAGAAGCAGTCGTTAG	(3'←5')	-	-

This result supported the hypothesis that the dyes stack with the terminal base pairs.

On the other hand, larger discrepancy was observed with 14- and 19-bp duplexes. We also calculated theoretical values by assuming that 50% of chromophores in random orientation and 50% in fixed orientation (Figure 3-5). Although large discrepancy was still observed, calculated values showed better agreement with experimental values, suggesting some portion of chromophores is in stacked-unstacked equilibrium.

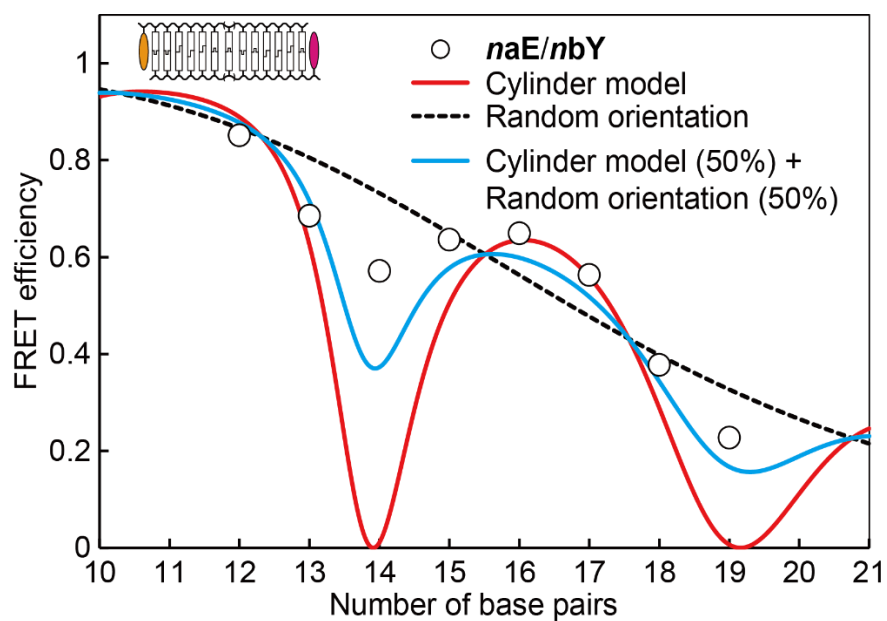


Figure 3-5.

FRET efficiencies of *naE/nbY* duplexes. Theoretical curves calculated based on cylinder model (red line) and random orientation (dotted line) are shown. Blue line was calculated by assuming an equilibrium between fixed (50%) and random orientation (50%).

Lifetimes of perylene in 19-bp duplexes (*7aE/7b* and *7aE/7bY*) were also determined via time-resolved fluorescence measurements (Figure 3-6 and Table 3-2).

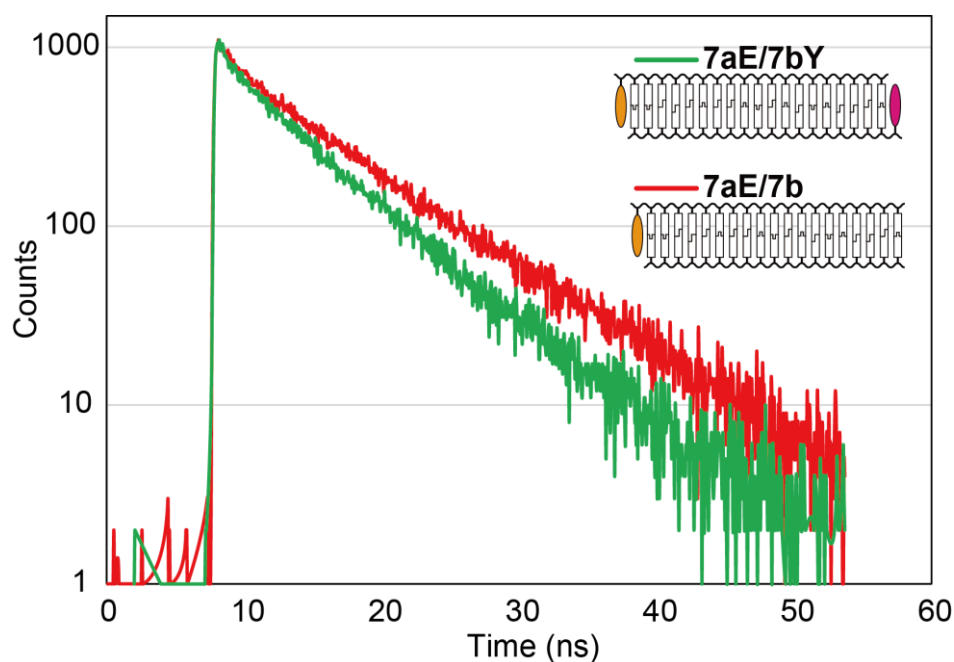


Figure 3-6.

Fluorescence decay profiles of perylene emission in **7aE/7bY** and **7aE/7b** duplexes.

Table 3-2. FRET efficiencies and melting temperatures of duplexes tethering dyes.

Sequence	τ_1 (ns)	τ_2 (ns)	α_1	α_2	χ^2	$\langle\tau\rangle$ (ns)	$\Phi_{T, \langle\tau\rangle}$ [a]	Φ_{T, τ_2} [b]	Φ_T [c]
7aE/7bY	0.936	6.52	0.38	0.62	1.09	6.08	0.230	0.226	0.227
7aE/7b	1.10	8.43	0.37	0.63	1.18	7.90	-	-	-

[a] FRET efficiency calculated by using mean lifetimes ($\langle\tau\rangle$).

[b] FRET efficiency calculated by using longer lifetimes (τ_2).

[c] FRET efficiency determined from static measurements.

Both duplexes showed two lifetimes. The longer lifetimes are consistent with values reported previously.^[13] The shorter lifetimes could be attributable to quenching via intermolecular interaction since perylene residues are attached at termini of DNA

duplexes. Such intermolecular interaction between aromatic compounds at DNA termini has also been reported in previous reports^[14] The FRET efficiency of 19-bp duplex determined from longer lifetimes was 0.226, which agreed with that from steady-state measurements (0.227). FRET efficiency using mean lifetimes also showed almost the same value (0.230), indicating the effects of the minor species on FRET efficiency are marginal. In addition, acceptor lifetimes increased by introducing a donor (Figure S3-2 and Table S1). These data confirmed that the perylene-Cy3 pair can be used to obtain nucleic acid structural information.

3-3-2 Structural analysis of stilbene modified DNA by using FRET system

Next, we analyzed the structure of DNA containing a stilbene cluster using the perylene-Cy3 FRET pair. We first evaluate the properties of DNA duplexes tethering stilbene residues but not perylene and Cy3 (**Xma/Xnb** in Figure 3-7).

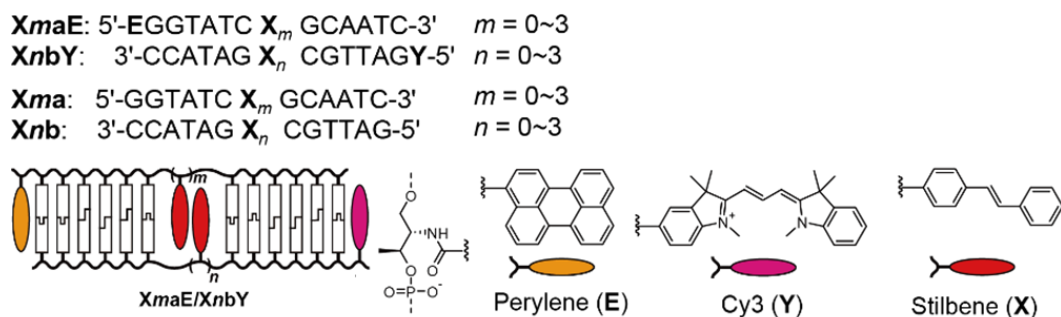


Figure 3-7.

Sequences used in this study of structural analysis of stilbene modified DNA and schematics of analyzed duplexes. Chemical structures of dyes are also shown.

Stilbene (**X**) residues were incorporated into DNA by using stilbene phosphoramidite monomer as we reported previously.^[8b] **X** residues were introduced into the counter position with each other so that they form a dye cluster.^[15] The T_m increased as the number of stilbene residues increased, suggesting that stacking interactions between dyes was stabilizing (Table 3-3). In addition, a hypsochromic shift was observed as the number of stilbene residues increased (Figure S3-3.), showing that stilbene moieties form H aggregates.^[9]

Table 3-3. FRET efficiencies and melting temperatures of duplexes containing stilbene (X) residues.

Sequence			Φ_T	T_m (°C)
X1aE	EGGTATC X GCAATC	(5'→3')	0.808	57.9
0bY	CCATAG CGTTAG Y	(3'←5')		
X1a	GGTATC X GCAATC	(5'→3')	-	49.5
0b	CCATAG CGTTAG	(3'←5')		
X1aE	EGGTATC X GCAATC	(5'→3')	0.766	54.0
X1bY	CCATAG X CGTTAG Y	(3'←5')		
X1a	GGTATC X GCAATC	(5'→3')	-	48.5
X1b	CCATAG X CGTTAG	(3'←5')		
X2aE	EGGTATC XX GCAATC	(5'→3')	0.721	55.6
X1bY	CCATAG X CGTTAG Y	(3'←5')		
X2a	GGTATC XX GCAATC	(5'→3')	-	50.7
X1b	CCATAG X CGTTAG	(3'←5')		
X2aE	EGGTATC XX GCAATC	(5'→3')	0.642	57.2
X2bY	CCATAG XX CGTTAG Y	(3'←5')		
X2a	GGTATC XX GCAATC	(5'→3')	-	54.1
X2b	CCATAG XX CGTTAG	(3'←5')		
X3aE	EGGTATC XXX GCAATC	(5'→3')	0.606	58.0
X2bY	CCATAG XX CGTTAG Y	(3'←5')		
X3a	GGTATC XXX GCAATC	(5'→3')	-	55.9
X2b	CCATAG XX CGTTAG	(3'←5')		
X3aE	EGGTATC XXX GCAATC	(5'→3')	0.558	58.4
X3bY	CCATAG XXX CGTTAG Y	(3'←5')		
X3a	GGTATC XXX GCAATC	(5'→3')	-	57.4
X3b	CCATAG XXX CGTTAG	(3'←5')		

Next, we studied DNA duplexes with perylene and Cy3 attached at the termini and also containing one to six stilbene moieties (**XmaE/XnbY**). Duplexes containing perylene but not Cy3 (**XmaE/Xnb**) were prepared as controls. Decreased donor emission and increased acceptor emission were observed upon the introduction of the acceptor as representatively shown in Figure 3-8a. Emission spectra of **XmaE/XnbY** duplexes are shown in Figure. 3-8b, and their emission intensities are summarized in Figure 3-8c.

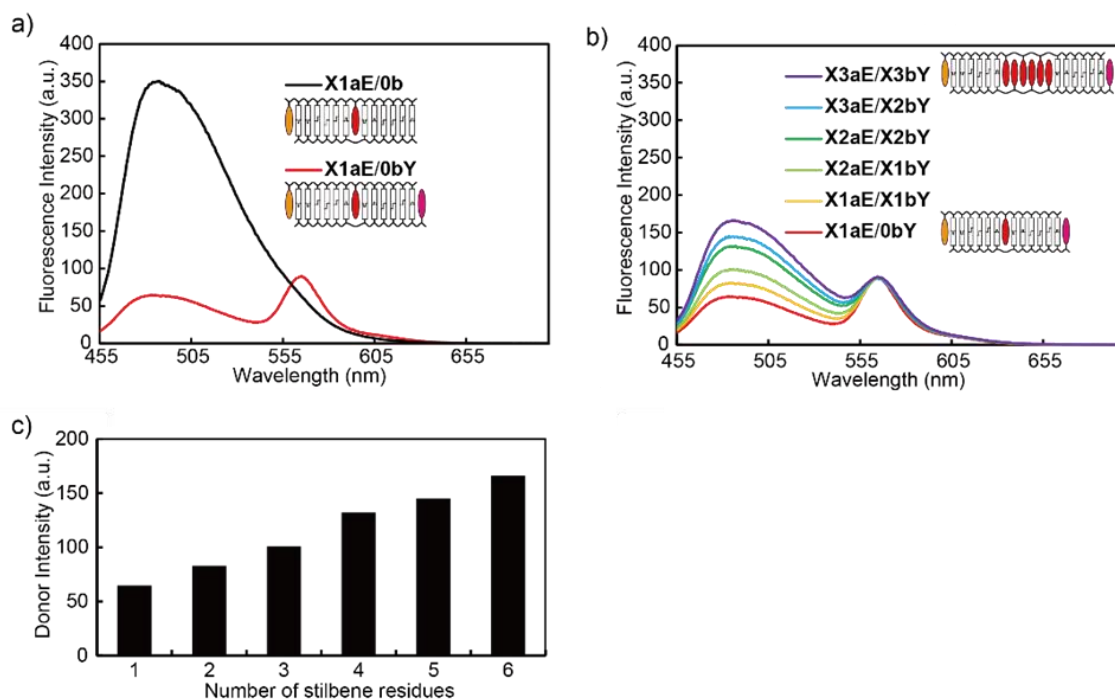


Figure 3-8.

a) Fluorescent emission spectra of DNA duplexes containing one stilbene residue. X1aE/0bY has both the donor and acceptor, whereas X1aE/0b has only donor. b) Fluorescent emission spectra of DNA duplexes containing various number of stilbene residues (**XmaE/XnbY**). c) Effects of the number of stilbene residue on the donor emission intensity Sequences used in this study of structural analysis of stilbene modified DNA and schematics of analyzed duplexes.

Interestingly, the emission spectra of **XmaE/XnbY** changed monotonously as the number of stilbene moieties increased; stronger perylene emission was observed for longer duplexes. This behavior is in striking contrast to that observed with natural base pairs (compare with Figure 3-3). This indicates that upon addition of stilbene pairs, the relative orientation between the donor and acceptor did not change.

FRET efficiencies were calculated by comparing these spectra with those of **XmaE/Xnb** (Figure S3-4). FRET efficiencies also showed monotonous change as the number of stilbene moieties in the DNA duplex were increased (Figure 3-9, circles). The change in efficiency was distinct from that expected assuming a helical model using parameters of B-form DNA duplex (Figure 3-9, dotted line). The experimental data showed much better agreement with a theoretical curve assuming that stilbene moieties form a non-helical ladder-like cluster (Figure 3-9, red line). These results suggest that stilbene moieties are stacked in non-helical manner consistent with previous studies of azobenzene derivatives incorporated within DNA duplexes.^[15b]

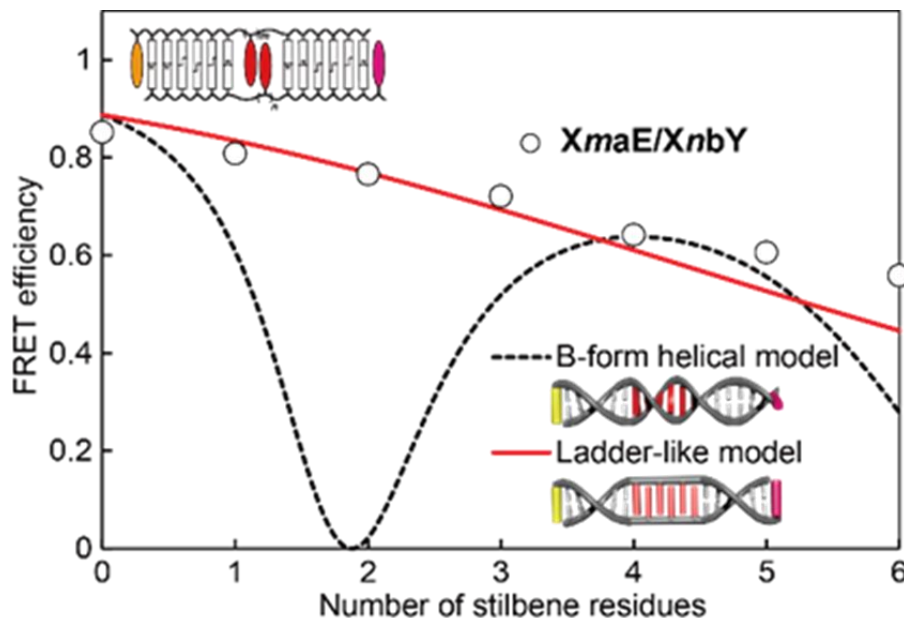


Figure 3-9.

FRET efficiencies of **XmaE/XnbY** duplexes. Theoretical curves calculated based on the B-form helical model (dotted line) and the ladder-like model (red line) are also shown.

3-3-3 Structural changes upon photodimerization between stilbene residues

We analyzed structural changes upon photodimerization between stilbene residues using the perylene-Cy3 FRET system. We previously reported that [2 + 2] photodimerization between stilbene residues occurs in DNA duplex (Figure 3-10a).^[8b] However, the structure changes induced by photodimerization were not characterized. **X1aE/X1bY** was irradiated with 340 nm UV light, and the reaction was monitored via absorption spectrometry (Figure S3-5a). There was a decrease in intensity of π - π^* absorption bands due to [2+2] photocycloaddition with a plateau after 90 seconds. As shown by HPLC analyses (Figure S3-5b), only the expected photocrosslinked product was observed after UV irradiation, demonstrating that the reaction proceeded without any side reactions. The fluorescent emission spectra of **X1aE/X1bY** with and without UV irradiation are shown in Figure 3-10b. Quite interestingly, almost no change in fluorescent emission was observed upon UV irradiation; FRET efficiency after irradiation was 75.8%, whereas that before irradiation was 76.6%. These results clearly demonstrate that photodimerized stilbene can be accommodated within a DNA duplex, indicating that stilbene residues could be used to stabilize DNA nano-structures, such as DNA origami, without structural disturbance.

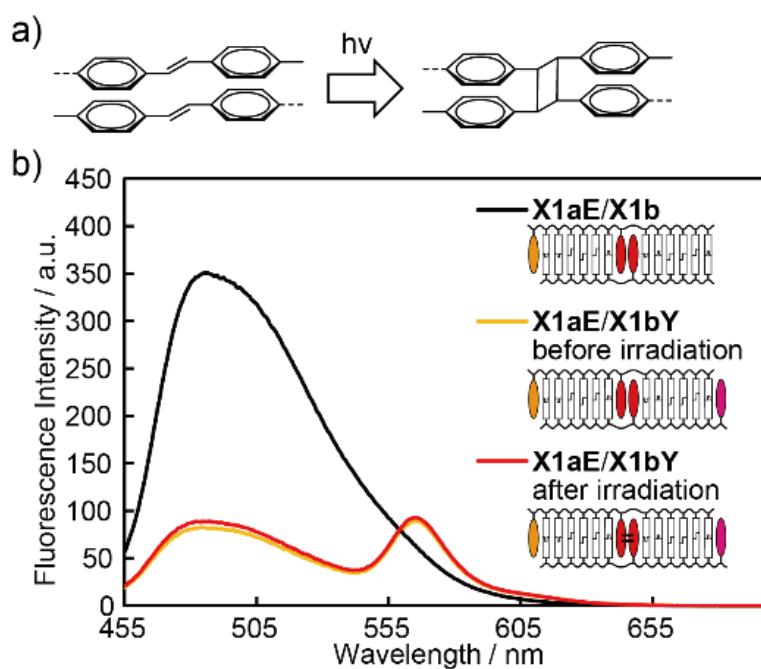


Figure 3-10.

a) [2+2] Photocycloaddition reaction between stilbene moieties. b) Fluorescent emission spectra of **X1aE/X1bY** before (orange) and after (red) UV irradiation (90 sec). Spectrum of **X1aE/X1b** is shown as a control (black).

3-3-4 Structural analysis of stilbene with spacers (1,3-propanediol) modified

DNA by using FRET system

We have previously reported two different dye clusters with and without spacers (**S**, 1,3-propanediol) in DNA duplexes.^[15a] Although they have different physical properties, structural information of dye clusters with spacers has not been revealed in detail. Finally, we analyzed different stilbene clusters with spacers (1,3-propanediol) using the perylene-Cy3 FRET pair. (**XSma/XSmb** in Figure 3-11)

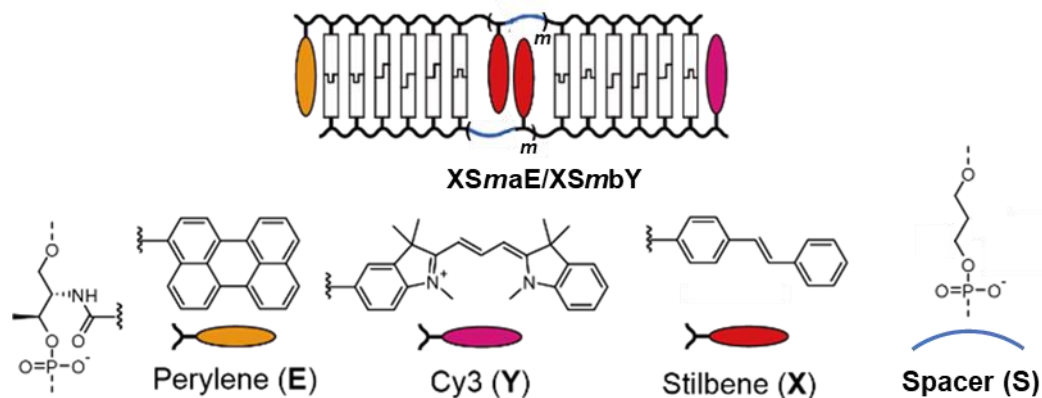
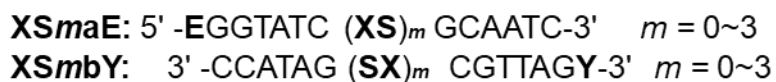


Figure 3-11.

Sequences used in this study of structural analysis of stilbene modified DNA and schematics of analyzed duplexes. Chemical structures of dyes are also shown.

X and S were introduced into the counter position with each other so that they form a dye cluster. The melting temperatures (T_m) of all duplexes had higher than 40 °C (Table 3-4.), however, lower than that of **0a/0b** (without stilbene and spacer). This was different from the result of **Xma/Xnb**. The introduction of spacers may have weakened the stacking interaction. On the other hand, a hypsochromic shift was also observed as the number of stilbene and spacer increased (Figure S3-6.), showing that stilbene moieties form H aggregates.

Table 3-4. FRET efficiencies and melting temperatures of duplexes containing stilbene (**X**) and spacer (**S**).

Sequence			Φ_T	T_m (°C)
X1aE	EGGTATCXGCAATC	(5'→3')	0.742	53.2
S1bY	CCATAGSCGTTAGY	(3'←5')		
X1a	GGTATCXGCAATC	(5'→3')	-	45.5
S1b	CCATAGSCGTTAG	(3'←5')		
XS1aE	EGGTATCXSGCAATC	(5'→3')	0.562	48.8
XS1bY	CCATAGSXCGTTAGY	(3'←5')		
XS1a	GGTATCXSGCAATC	(5'→3')	-	42.6
XS1b	CCATAGSXCGTTAG	(3'←5')		
XS2aE	EGGTATCXXSXGCAATC	(5'→3')	0.652	45.5
XS2bY	CCATAGSXXSXCGTTAGY	(3'←5')		
XS2a	GGTATCXXSXGCAATC	(5'→3')	-	43.4
XS2b	CCATAGSXXSXCGTTAG	(3'←5')		
XS3aE	EGGTATCXXSXSXGCAATC	(5'→3')	0.655	44.5
XS3bY	CCATAGSXXSXSXCGTTAGY	(3'←5')		
XS3a	GGTATCXXSXSXGCAATC	(5'→3')	-	44.4
XS3b	CCATAGSXXSXSXCGTTAG	(3'←5')		

Next, we analyzed the structure of **X** clusters with spacers (**XSmaE/XSmbY**, respectively). Each duplex was labeled with **E** and **Y** at its 5'-termini. Duplexes containing perylene but not Cy3 (**XSmaE/XSmb**) were prepared as controls. As an example, Figure 3-12a shows a difference of fluorescent emission spectra with and without Cy3 (**XS1aE/XS1bY** and **XS1aE/XS1b**). Fluorescent Emission spectra of **XSmaE/XSmbY** duplexes are shown in Figure 3-12b, and their emission intensities are summarized in Figure 3-12c.

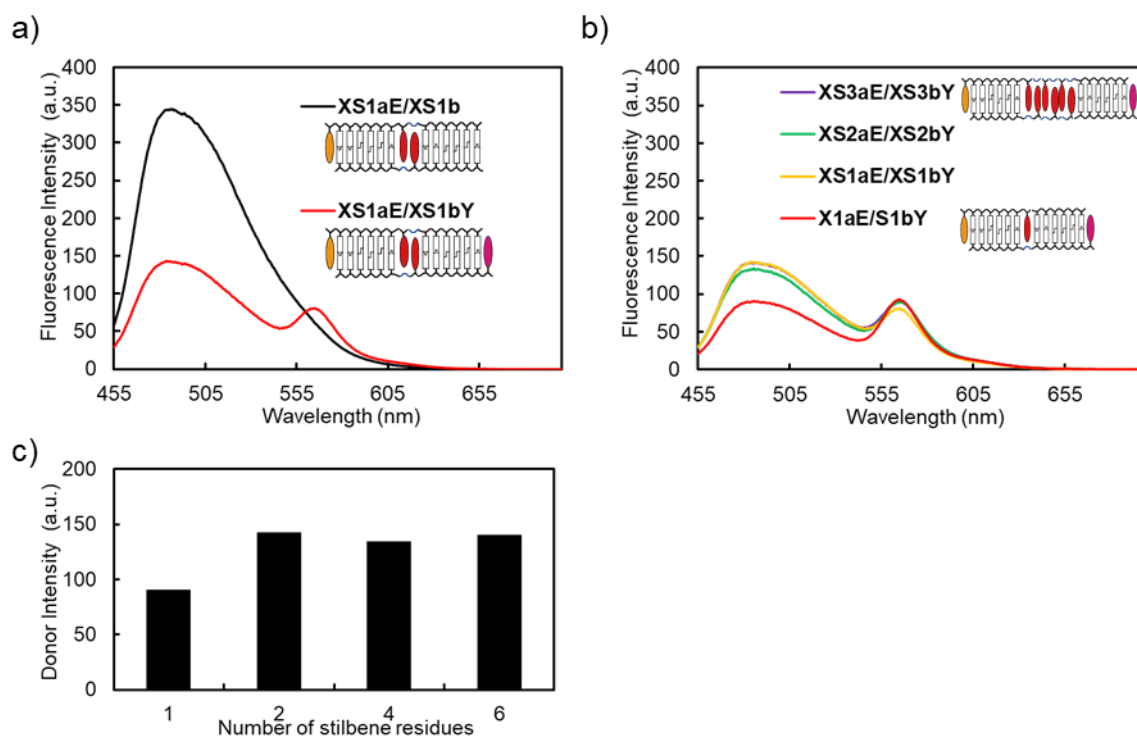


Figure 3-12.

a) Fluorescent emission spectra of DNA duplexes containing one stilbene residue. **XS1aE/XS1bY** has both the donor and acceptor, whereas **XS1aE/XS1b** has only donor. b) Fluorescent emission spectra of DNA duplexes containing various number of stilbene residues (**XS m aE/XS m bY**). c) Effects of the number of stilbene residue on the donor emission intensity Sequences used in this study of structural analysis of stilbene modified DNA and schematics of analyzed duplexes.

In contrast to the stilbene clusters without spacers, the fluorescence intensity of the donor did not change monotonically (compare with Figure 3-8). It is clear from Figure 3-12c that not only distance but also orientation dependence was observed. This result suggested that the structure is different with and without the spacers. To discuss this structure in more detail, we compared the measured FRET efficiency with the theoretical

curve.

FRET efficiencies were calculated by comparing these spectra with those of **XSmaE/XSmb** (Figure S3-7). Figure 3-13 depicts the FRET efficiencies of stilbene clusters with spacers (**XSmaE/XSmbY**). Theoretical curves calculated based on B-form helical model (dotted line) and the ladder-like model (red line) are also shown. The right-handed helical model was considered to be based on canonical B-form DNA (Rise: 3.2 Å / bp, Rotation: 34°), which corresponded to one stilbene per one base pair. FRET efficiency plots of **XSmaE/XSmbY** did not match the theoretical curves based on the ladder-like model. It is hard to say that it matches the B-form model. However, the orientation dependence of FRET efficiency suggested that stilbene residues are stacked in a helical manner. This result leads to the conclusion that structural differences of stilbene clusters are successfully analyzed by using FRET system of perylene and Cy3.

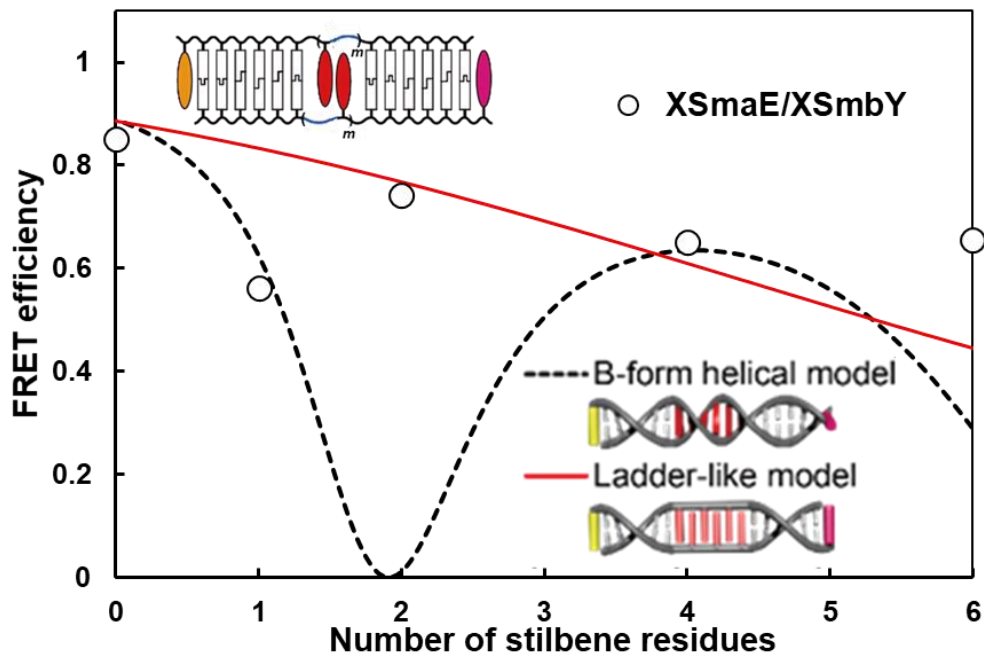


Figure 3-13.

FRET efficiencies of **XSmaE/XSmbY** duplexes. Theoretical curves calculated based on the B-form helical model (dotted line) and the ladder-like model (red line) are also shown.

3-4 Conclusions

In conclusion, we have developed a new FRET system using perylene as a donor and Cy3 as an acceptor. Perylene and Cy3 were attached to the termini of native DNA duplexes via D-threoinol, and FRET efficiencies were determined. Orientation dependence of FRET was observed as the number of base pairs in the duplex was increased. Therefore, the perylene-Cy3 pair can be used to obtain structural parameters of nucleic acids.

The structural effects of a stilbene cluster within a DNA duplex were also analyzed using this FRET pair. FRET efficiencies changed monotonously as the number of stilbene residues was increased. This indicated that within the DNA duplex scaffold, the stilbene pairs form a ladder-like cluster. Since perylene can be excited with visible light, we were able to use the perylene-Cy3 FRET pairs to analyze the structural changes that result from upon [2+2] photodimerization. Photodimerization did not distort the structure.

The perylene-Cy3 pair characterized here has a larger Förster radius. Therefore, this system can be used to analyze larger complexes whereas the previous pyrene-perylene pair is more suitable to investigate the small local conformational changes. Moreover, perylene-Cy3 pair could also be utilized to analyze structural change caused by photochemical damage of DNA. For example, natural pyrimidine bases form cyclobutane

pyrimidine dimers upon UV irradiation, yielding several stereoisomeric products.^[16] The present FRET system will be able to detect such photolesions because its efficiency is highly dependent on relative distance and orientation. The present results also demonstrated that orientation can be precisely controlled by attaching dyes at the termini of a DNA duplex via D-threoninol. Other FRET pairs could be incorporated into DNA through D-threoninol.

3-5 Experimental section

Oligonucleotide synthesis

All conventional phosphoramidite monomers, CPG columns, reagents for DNA synthesis, and Poly-Pak II cartridges were purchased from Glen Research. Other reagents for the synthesis of phosphoramidite monomers were purchased from Tokyo Chemical Industry, Wako, and Aldrich. Native oligodeoxyribonucleotides (ODNs) were purchased from Integrated DNA Technologies or Hokkaido System Science Co., Ltd. Phosphoramidite monomers tethering perylene^[11a], Cy3^[11b] or stilbene^[9b] were synthesized according to our previous reports. Modified ODNs were synthesized by employing these phosphoramidite monomers and standard DNA monomers on an automated DNA synthesizer (H-8-SE, Nihon Techno Service). ODNs were purified by reversed-phase HPLC and characterized by MALDI-TOF MS (Autoflex II, Bruker Daltonics) and HPLC.

Fluorescence measurements

Fluorescence spectra were measured on JASCO models FP-6500 or FP-8500. The excitation wavelength was 425 nm for **naE/nbY** and 450 nm for **XmaE/XnbY** and

XSmaE/XSnbY. Band widths were 3 nm (FP-6500) or 2.5 nm (FP-8500) for excitation and emission. Before measurements, sample solutions containing DNA duplex were heated at 80 °C, then slowly cooled down to 20 °C at a rate of 4 °C min⁻¹. Fluorescence spectra were measured at 80 to 20 °C at 10 °C intervals after 4 min incubations. Emission spectra were measured at 20 °C. Sample solutions contained 100 mM NaCl, 10 mM phosphate buffer, pH 7.0. Concentrations of ODNs were 1.0 μM for ODNs tethering perylene (**naE**, **XmaE**, **XSmaE**) and 2.0 μM for those tethering Cy3 (**nbY**, **nb**, **XnbY**, **Xnb**, **XSnbY** and **XSnb**). We used two-fold excess amount of acceptor strand to reduce the effects of emission from single-stranded donor strand.

Fluorescence lifetime measurements

Decay profiles of donor fluorescence at 500 nm and acceptor fluorescence at 650 nm were monitored with 445 nm excitation at room temperature by a time-correlated single-photon counting apparatus (Hamamatsu, Quantaaurus-Tau). Before measurements, sample solutions containing DNA duplex were heated at 80 °C, then slowly cooled down to 20 °C. Lifetimes were measured at 20 °C. Sample solutions contained 100 mM NaCl, 10 mM phosphate buffer, pH 7.0.

Measurement of absorption spectra and melting temperatures

Absorption spectra were measured on a JASCO model V-530, V-550, or V-560. The sample solutions contained 100 mM NaCl, 10 mM phosphate buffer, pH 7.0, 5.0 μ M each strand. Absorption spectra were measured at 20 °C. The melting curves were measured with a UV-1800 (Shimadzu) by monitoring 260 nm absorbance versus temperature. The T_m was determined from the maximum in the first derivative of the melting curve. Both the heating and the cooling curves were measured, and the calculated T_m agreed to within 1.0 °C. The temperature ramp was 0.5 °C min⁻¹. The sample solutions contained 100 mM NaCl, 10 mM phosphate buffer, pH 7.0, 5.0 μ M each strand.

UV irradiation

A xenon light source (MAX-301, Asahi Spectra) equipped with interference filters centered at 340 nm (half bandwidth 10 nm, power density 0.15 mW cm⁻²) was used for photoreaction. The sample solution was added to a cuvette, and the temperature of light irradiation was controlled using a programmable temperature controller. Photo-irradiation was conducted at 20 °C.

HPLC analyses

A Merck LiChrospher 100 RP-18(e) column heated to 50 °C was used for HPLC analyses. The flow rate was 0.5 mL min⁻¹. A solution of 50 mM ammonium formate (solution A) and a solution of 50 mM ammonium formate and acetonitrile (50/50, v/v; solution B) were used as mobile phases. A linear gradient of 5-35% solution B over 30 min was employed. HPLC chromatograms were monitored at 260 nm.

Calculation of FRET efficiency

FRET efficiency (Φ_T) was experimentally determined from the decrease in donor emission:

$$\Phi_T = 1 - I_{DA}/I_D \quad (1)$$

where I_{DA} is maximum emission intensity of a duplex containing a donor and an acceptor (about 485 nm), and I_D is that of donor-only duplex. Emission intensities were measured at 20 °C. In order to eliminate the effects of concentration errors, each emission intensity was normalized by the intensity at 80 °C, at which all duplexes dissociate into single strands.

FRET efficiency from lifetime measurements ($\Phi_{T,\tau}$) was determined from the following equation:

$$\Phi_{T,\tau} = 1 - \tau_{DA}/\tau_D \quad (2)$$

where τ_{DA} is the lifetime of perylene in a duplex containing a donor and an acceptor (**7aE/7bY**), and τ_D is that in a donor-only duplex (**7aE/7b**).

Calculation of theoretical curves

FRET efficiency (Φ_T) was calculated from the following equations:

$$\Phi_T = \frac{1}{1 + (R/R_0)^6} \quad (3)$$

$$R_0 = 0.2108[J(\lambda)\kappa^2 n^{-4}\Phi_D]^{1/6} \quad (4)$$

$$\kappa^2 = \cos^2\theta_T \quad (5)$$

where R is the distance between donor and acceptor, and R_0 is a Förster radius (the distance where $\Phi_T = 0.5$). $J(\lambda)$ is integral of spectral overlap between donor emission and acceptor absorption at λ nm. n is a refractive index, which is typically assumed to be 1.4 for biomolecules, and Φ_D is a donor quantum yield. The orientation factor, κ^2 , was

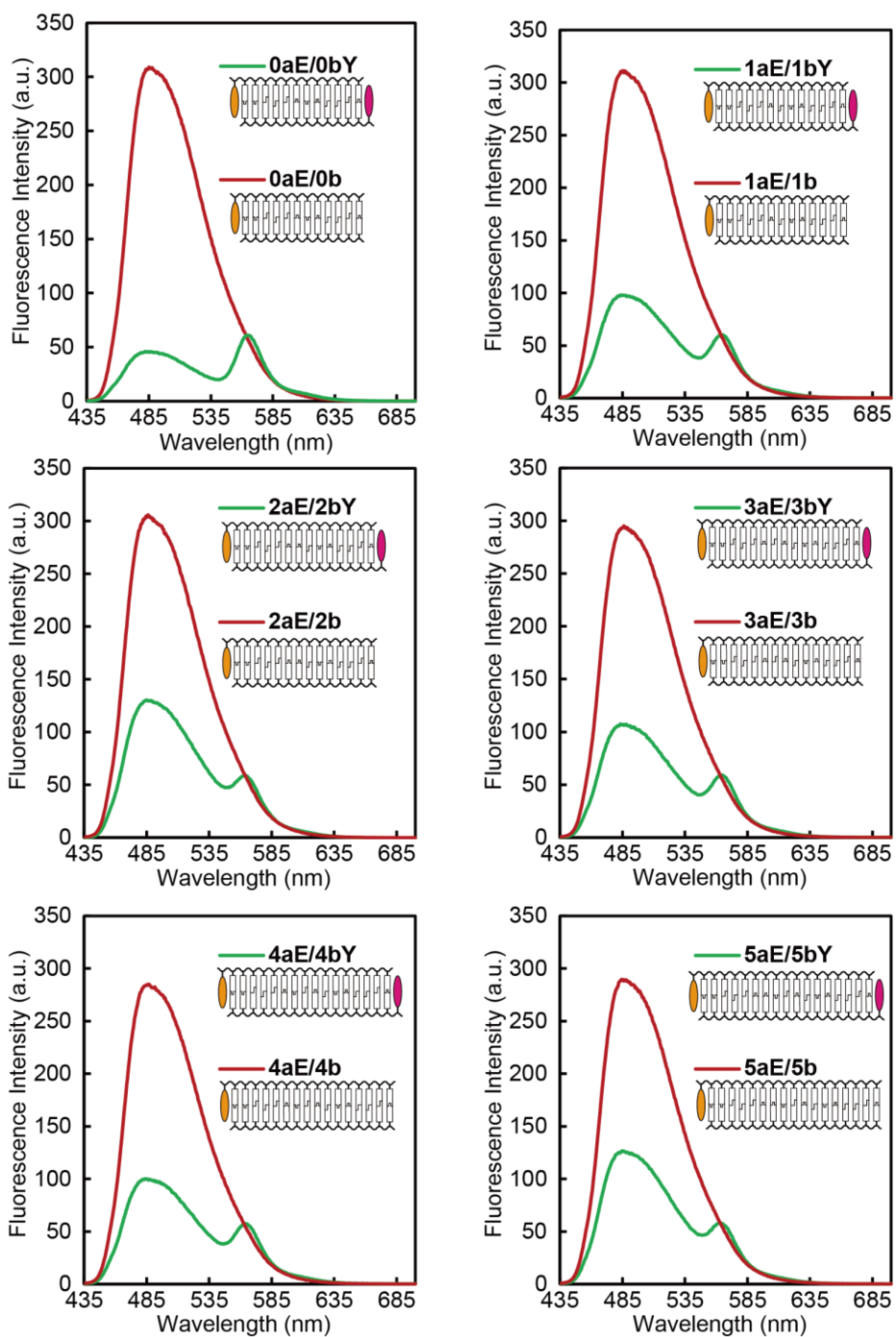
calculated from the above equation, where θ_T is the angle between transition dipoles of donor and acceptor.

By using these equations, FRET efficiency was calculated from the distance (R) and the angle (θ_T) between dyes. We used typical parameters of B-form DNA duplex; rise per base pair (3.2 Å), angle per base pair (34°). The angle between dyes and flanking base pairs was determined to be 9° by fitting calculated FRET efficiencies with experimentally obtained efficiencies. The orientation factor (κ^2) of 2/3 was used to calculate the theoretical curve assuming averaged orientation. For the structural analyses of duplex containing stilbene residues, the distance between stilbene residues was set to 3.2 Å, which is the same as the distance between base pairs in a B-form duplex. The angle between stilbene residues was set to 0° in the ladder-like model, whereas 34° was used for the B-form helical model.

3-6 References

- [1] T. Kato, H. Kashida, H. Kishida, H. Yada, H. Okamoto, H. Asanuma, *J. Am. Chem. Soc.*, **2013**, *135*, 741–750.
- [2] H. Kashida, A. Kurihara, H. Kawai, H. Asanuma, *Nucleic Acids Res.*, **2017**, *45*, e105.
- [3] H. Kashida, Y. Kokubo, K. Makino, H. Asanuma, *Org. Biomol. Chem.*, **2019**, *17*, 6786–6789.
- [4] B. Hwa Yun, J. Guo, M. Bellamri, R. J. Turesky, *Mass Spectrom. Rev.*, **2020**, *39*, 55–82.
- [5] D. H. Waldeck, *Chem. Rev.*, **1991**, *91*, 415–436.
- [6] Chi, X. Zhang, B. Xu, X. Zhou, C. Ma, Y. Zhang, S. Liu, J. Xu, *Chem. Soc. Rev.*, **2012**, *41*, 3878–3896.
- [7] a) F. D. Lewis, T. Wu, E. L. Burch, D. M. Bassani, J.-S. Yang, S. Schneider, W. Jaeger, R. L. Letsinger, *J. Am. Chem. Soc.*, **1995**, *117*, 8785–8792. b) Z. Dogan, R. Paulini, J. A. Rojas Stütz, S. Narayanan, C. Richert, *J. Am. Chem. Soc.*, **2004**, *126*, 4762–4763. c) Y. Higuchi, K. Furukawa, T. Miyazawa, N. Minakawa, *Bioconjugate Chem.*, **2014**, *25*, 1360–1369. d) F. D. Lewis, L. Zhang, X. Liu, X. Zuo, D. M. Tiede, H. Long, G. C. Schatz, *J. Am. Chem. Soc.*, **2005**, *127*, 14445–14453.
- [8] a) H. Kashida, T. Doi, T. Sakakibara, T. Hayashi, H. Asanuma, *J. Am. Chem. Soc.*, **2013**, *135*, 7960–7966, b) T. Doi, H. Kashida, H. Asanuma, *Org. Biomol. Chem.*, **2015**, *13*, 4430–4437, c) T. Doi, H. Kawai, K. Murayama, H. Kashida, H. Asanuma, *Chem. Eur. J.*, **2016**, *22*, 10533–10538.
- [9] E. G. McRae, M. Kasha, *J. Chem. Phys.*, **1958**, *28*, 721–722.
- [10] a) H. Asanuma, M. Akahane, N. Kondo, T. Osawa, T. Kato, H. Kashida, *Chem.*

- Sci.*, **2012**, *3*, 3165–3169. b) H. Kashida, T. Osawa, K. Morimoto, Y. Kamiya, H. Asanuma, *Bioorg. Med. Chem.*, **2015**, *23*, 1758–1762.
- [11] H. Asanuma, K. Murayama, Y. Kamiya, H. Kashida, *Bull. Chem. Soc. Jpn.*, **2018**, *91*, 1739–1748.
- [12] a) C. Bustamante, J. Marko, E. Siggia, S. Smith, *Science*, **1994**, *265*, 1599–1600; b) J. F. Marko, E. D. Siggia, *Macromolecules*, **1995**, *28*, 8759–8770.
- [13] H. Kashida, H. Kawai, R. Maruyama, Y. Kokubo, Y. Araki, T. Wada, H. Asanuma, *Commun. Chem.*, **2018**, *1*, 91.
- [14] a) D. Baumstark, H. A. Wagenknecht, *Angew. Chem. Int. Ed.*, **2008**, *47*, 2612–2614. b) M. Hariharan, Y. Zheng, H. Long, T. A. Zeidan, G. C. Schatz, J. Vura-Weis, M. R. Wasielewski, X. Zuo, D. M. Tiede, F. D. Lewis, *J. Am. Chem. Soc.*, **2009**, *131*, 5920–5929.
- [15] a) H. Kashida, T. Fujii, H. Asanuma, *Org. Biomol. Chem.*, **2008**, *6*, 2892–2899. b) T. Fujii, H. Kashida, H. Asanuma, *Chem. Eur. J.*, **2009**, *15*, 10092–10102. c) H. Asanuma, K. Murayama, Y. Kamiya, H. Kashida, *Polym. J.*, **2017**, *49*, 279–289.
- [16] a) M. Lukin, C. de los Santos, *Chem. Rev.*, **2006**, *106*, 607–686. b) K. Heil, D. Pearson, T. Carell, *Chem. Soc. Rev.*, **2011**, *40*, 4271–4278.



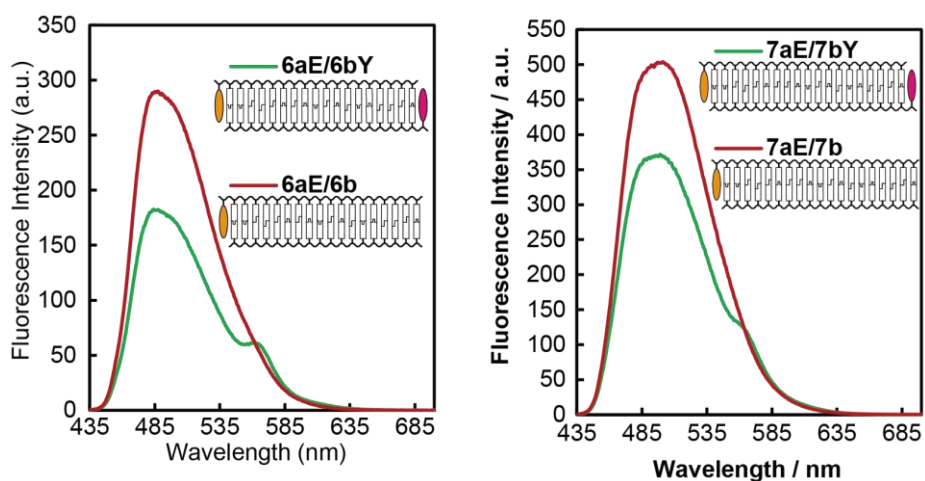


Figure S3-1. Fluorescent emission spectra of DNA duplexes containing perylene and Cy3 (*naE/nbY*) or only perylene (*naE/nb*). Intensities of *7aE/7bY* and *7aE/7b* were much different from those of other duplexes since these spectra were measured with different apparatus.

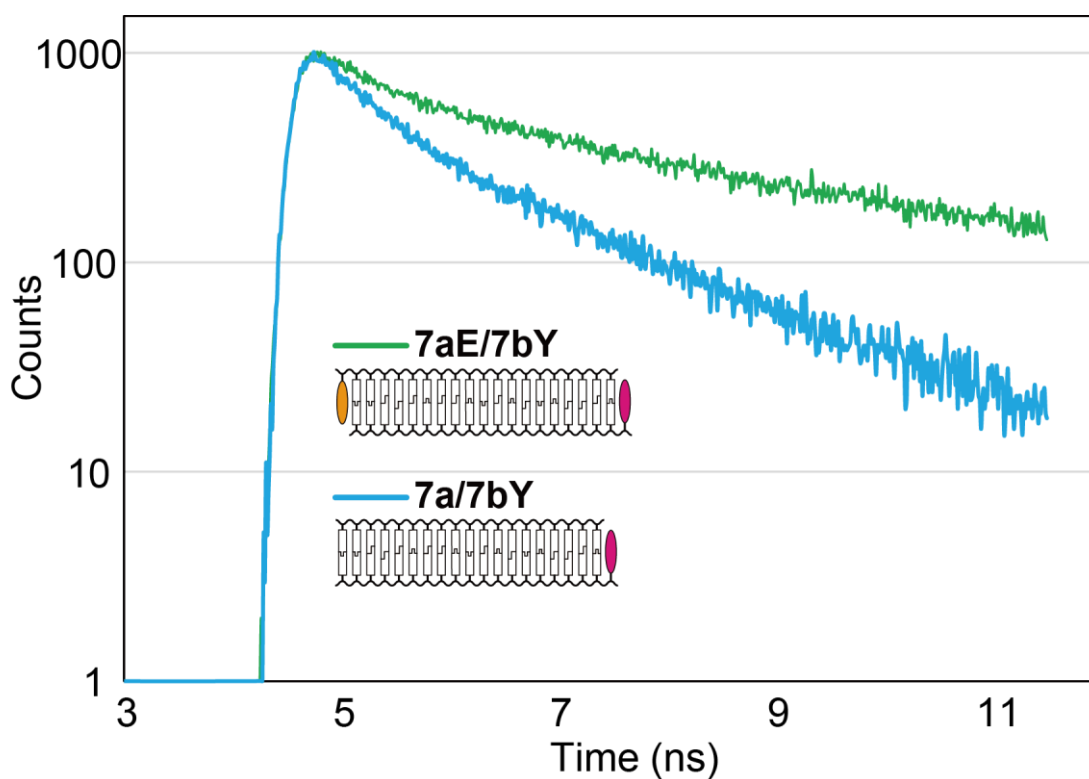


Figure S3-2. Fluorescence decay profiles of Cy3 emission in *7aE/7bY* and *7a/7bY* duplexes.

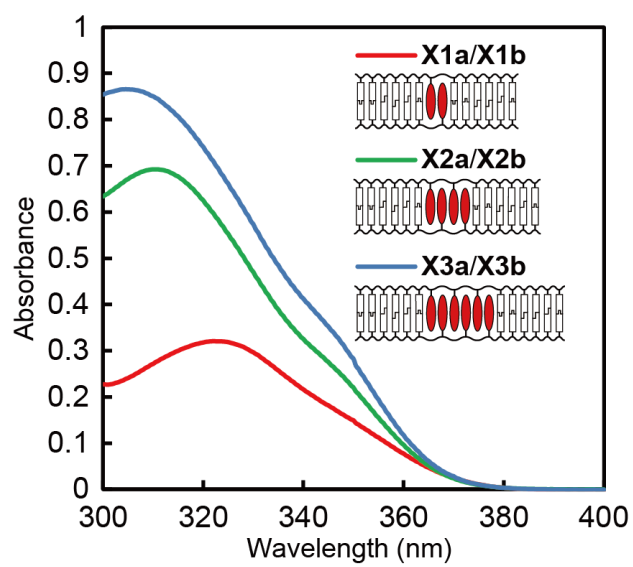


Figure S3-3. UV-Vis spectra of X1a/X1b, X2a/X2b, and X3a/X3b.

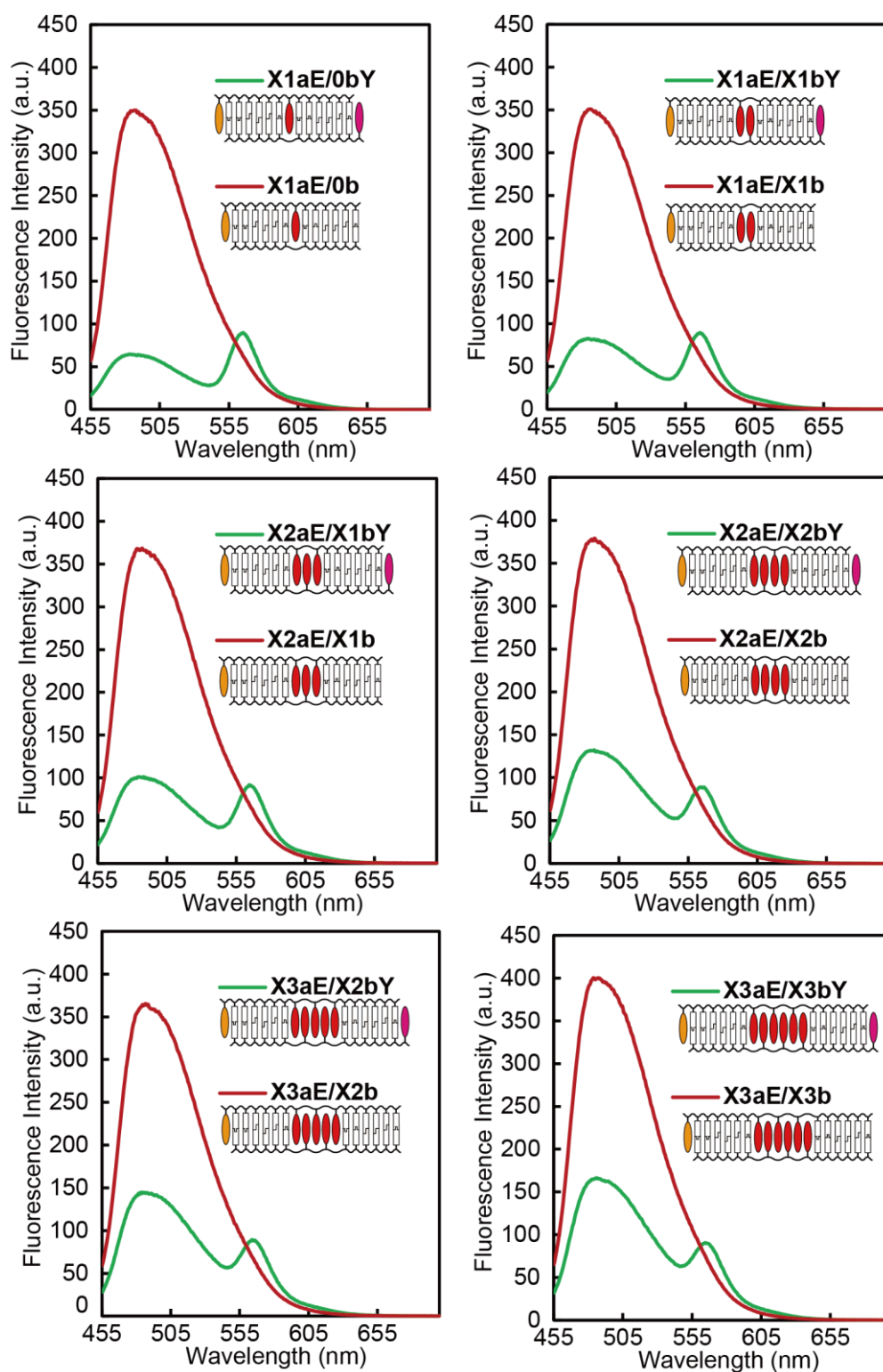


Figure S3-4. Fluorescent emission spectra of stilbene clusters containing perylene and Cy3 ($XmaE/XnbY$) or only perylene ($XmaE/Xnb$).

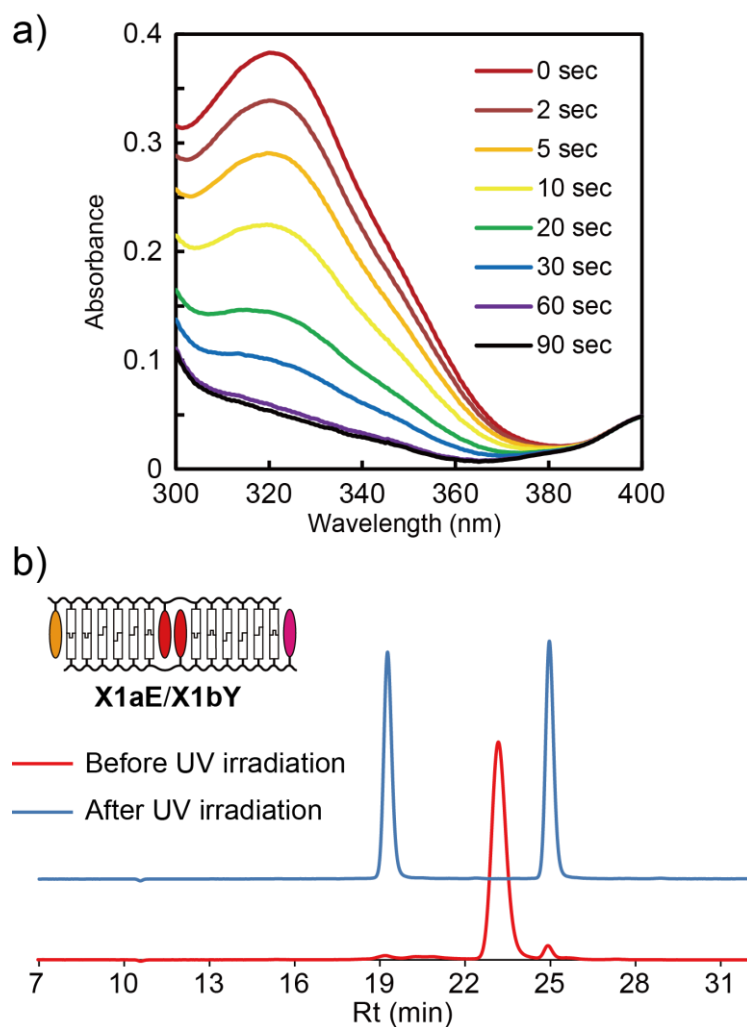


Figure S3-5. (a) UV-Vis spectra of **X1aE/X1bY** with UV irradiation for the indicated times. (b) HPLC chromatograms of **X1aE/X1bY** before and after UV irradiation for 90 seconds (A:B=95:5→65:35, linear gradient 30 min). A solution of 50 mM ammonium formate (solution A) and a solution of 50 mM ammonium formate and acetonitrile (50/50, v/v; solution B) were used as mobile phases.

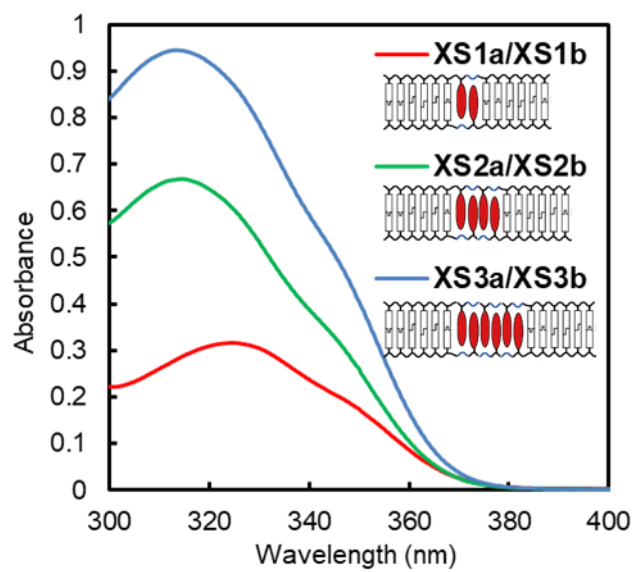


Figure S3-6. UV-Vis spectra of XS1a/XS1b, XS2a/XS2b, and XS3a/XS3b.

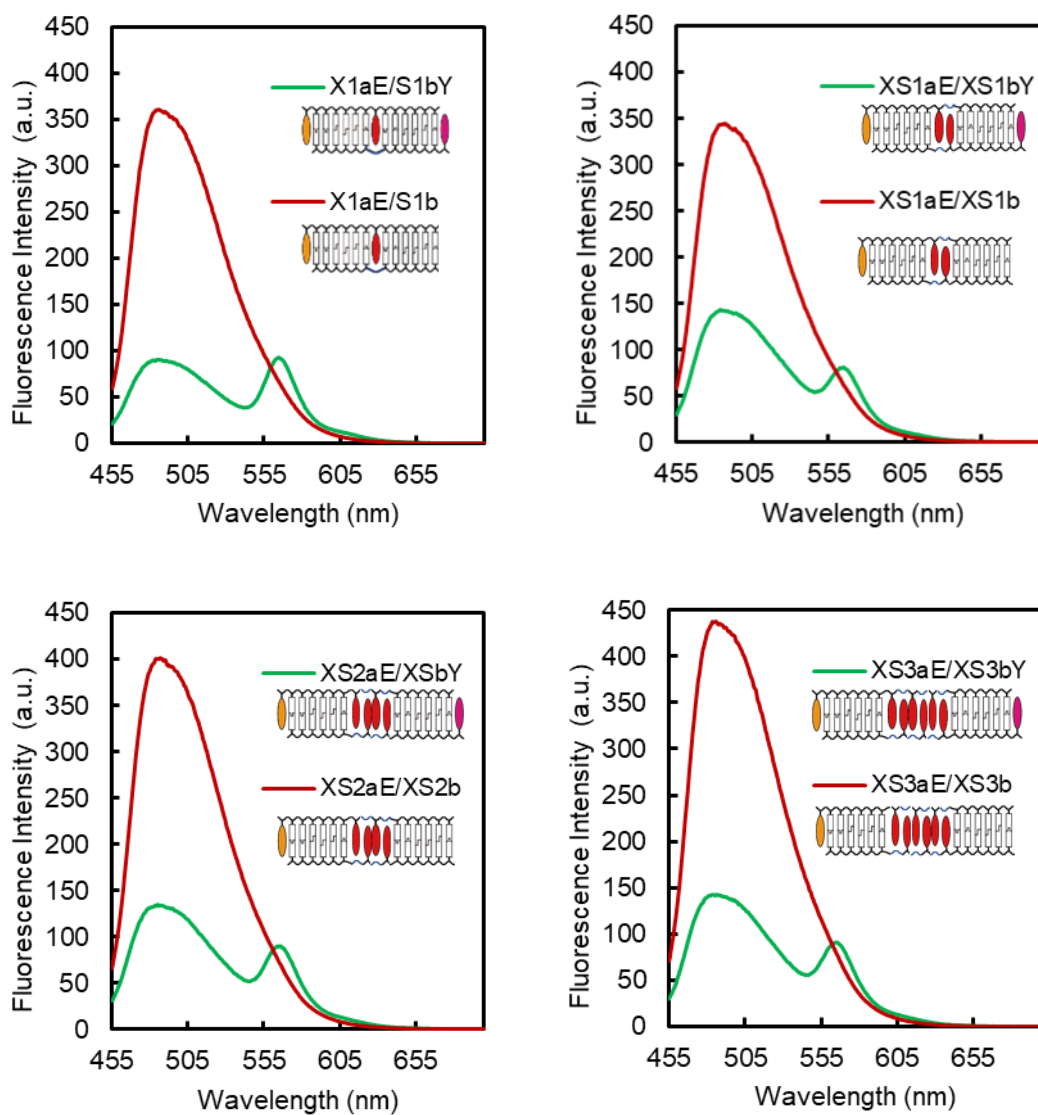


Figure S3-7. Fluorescent emission spectra of stilbene clusters containing perylene and Cy3 (**XSmaE/XSmbY**) or only perylene (**XSmaE/XSmb**).

Table S3-1. Acceptor lifetimes and FRET efficiencies for 19-bp duplexes.

Sequence	τ_1 (ns)	τ_2 (ns)	α_1	α_2	χ^2	$\langle\tau\rangle$ (ns)
7aE/7bY	0.592	4.74	0.59	0.41	1.12	4.11
7a/7bY	0.477	2.06	0.71	0.29	0.99	1.49

Chapter 4. Study of energy migration between the identical chromophores by using a DNA scaffold

4-1 Abstract

In chapter 4, we report energy migration between the identical chromophores (perylene) enabled by breaking symmetry. Energy migration is a necessary process in both natural and artificial photosynthesis. However, the distance and orientation dependence of energy migration have not been experimentally investigated in detail. Here we propose a method to investigate energy migration by using DNA scaffold. Two fluorophores are introduced into a DNA duplex and one quencher is placed next to one of the fluorophores. This design enables asymmetrization of identical fluorophores and allows one fluorophore to behave as an acceptor. The emission intensities and lifetimes decrease depending on the efficiency of energy migration. Distance and orientation dependence are successfully observed and the measured excitation energy transfer efficiencies are in excellent agreement with those calculated based on the Förster theory. We also demonstrate that multi-step energy migration among four fluorophores can be estimated from the theory. These results may provide a basis for design and preparation of efficient light-harvesting photonic devices and chemical probes.

4-2 Introduction

In chapter 2 and 3, we developed an orientation-dependent FRET system and analyzed structure of various DNA duplexes including DNA containing stilbene moieties. Fluorophores introduction via D-threoninol enabled this analysis by controlling dye orientation.

Excitation energy migration (EM) or homo Förster resonance energy transfer (homo-FRET) indicates energy transfer between the identical fluorophores. This type of transfer is a key process in natural photosynthesis. However, distance and orientation dependences of EM have not been elucidated because EM occurs among the identical chromophores, and each chromophore can function both as a donor and an acceptor. In chapter 4, we describe a system for analysis of EM using a DNA scaffold in which the symmetry between the identical fluorophores is broken. Our design is depicted in Figure 4-1. Two identical fluorophores are introduced into the DNA duplex. The distance between the two fluorophores is controlled by changing the number of intervening base pairs. A quencher is located next to one of two fluorophores in the DNA duplex, which makes that particular fluorophore non-emissive so that the quenched fluorophore functions not as a donor but as an acceptor. Since absorbed energy on this fluorophore is no longer transferred, EM efficiency can be quantified by measuring the decrease of emission intensity and lifetime

as hetero FRET. In this chapter, we elucidate distance and orientation dependence of energy migration by using this system. Multi-step energy migration among four fluorophores is also analyzed. To our knowledge, this is the first study to experimentally reveal the distance and orientation dependence of energy migration among identical chromophores.

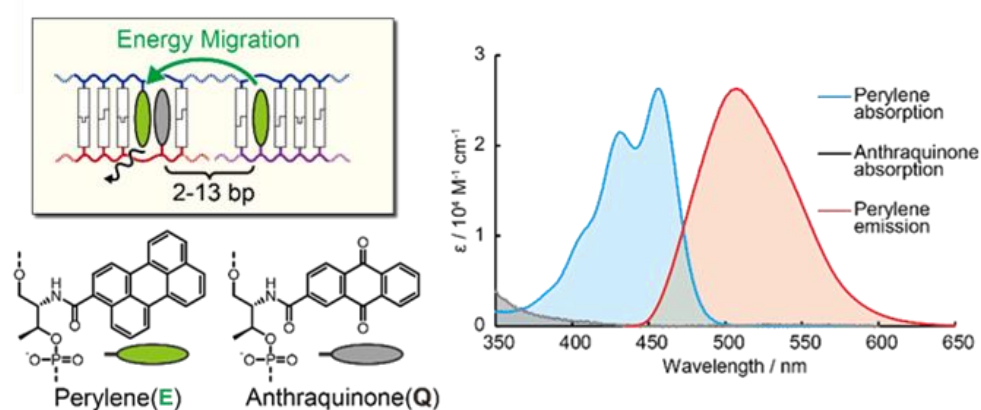


Figure 4-1.

Schematic illustration of **EQ** duplex and chemical structures of **E** and **Q** residues. Absorption and emission spectra of perylene and anthraquinone are also shown.

4-3 Results and discussions

4-3-1 Sequence design in this study

Perylene(**E**) and anthraquinone(**Q**) (Figure 4-1) were selected as the fluorophore and the quencher, respectively, for these experiments for three reasons. First, anthraquinone quenches perylene emission very efficiently as we reported previously^[1]. Therefore, back

energy transfer from the quenched fluorophore that is next to the quencher to the emissive fluorophore can be neglected. Second, anthraquinone absorption has almost no overlap with perylene emission (Figure 4-1) so that hetero energy transfer from perylene to anthraquinone, which disturbs the quantitative analyses of energy migration, does not occur. Third, these molecules have planar structures, and therefore stack with natural base pairs. For the introduction of these chromophores, D-threoninol is one of the best linkers to facilitate intercalation of these molecules into DNA duplex ^[2].

Sequence design to investigate orientation and distance dependence of EM is schematically illustrated in Figure 4-2, and the actual sequences are listed in Table S4-1. We introduced one perylene residue into a 32-mer DNA (strands **E1-E4**). One perylene or one anthraquinone residue was introduced into split complementary strands (**cE1s-cE3s** or **cQE1-cQE4**, respectively). By hybridizing three strands, nicked duplexes with two perylenes, one of which is located in opposite anthraquinone, were prepared (duplex **EQ-E**). The number of base pairs between perylene and anthraquinone were varied from 2 to 13 (see Table S4-1 for details). Control duplexes with one perylene residue or one perylene-anthraquinone pair (duplexes **E** and **EQ**, respectively) were prepared by using native strands (**NE**, **cNE** or **cNEs**). We previously showed that incorporation of planar molecules via D-threoninol does not distort the double helical structure ^[2,3] and that dyes

are stacked with a base pair at 5' side when they are introduced into the base-pairing position^[3]. Accordingly, in our design, anthraquinone is located between two perylenes in the EQ-E duplex, and the distance between anthraquinone and perylene is the same in EQ-E and Q-E duplexes (see Figure 4-2).

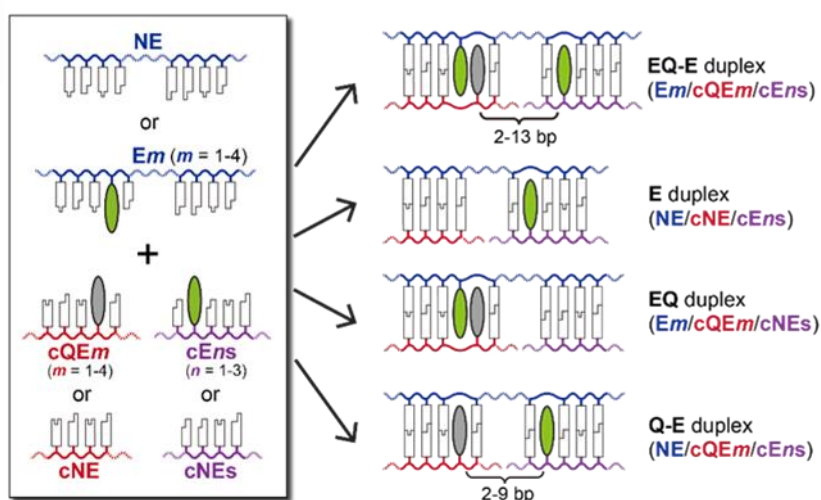


Figure 4-2.

Illustration of EQ-E, E, EQ and Q-E duplexes. These duplexes can be prepared by changing the combination of the three strands.

4-3-2 Investigation of perylene separated from anthraquinone

First, we evaluated the effects between perylene and anthraquinone prior to the study of energy transfer between perylene. As we described in chapter 4-3-1, the absorption of anthraquinone has almost no overlap with perylene emission, and it is considered that hetero energy transfer from perylene to anthraquinone does not occur. To demonstrate this

idea, we measured the steady-state emission spectra (Figure 4-3) and the absorption spectra (Figure 4-4) of **Q-E** duplexes.

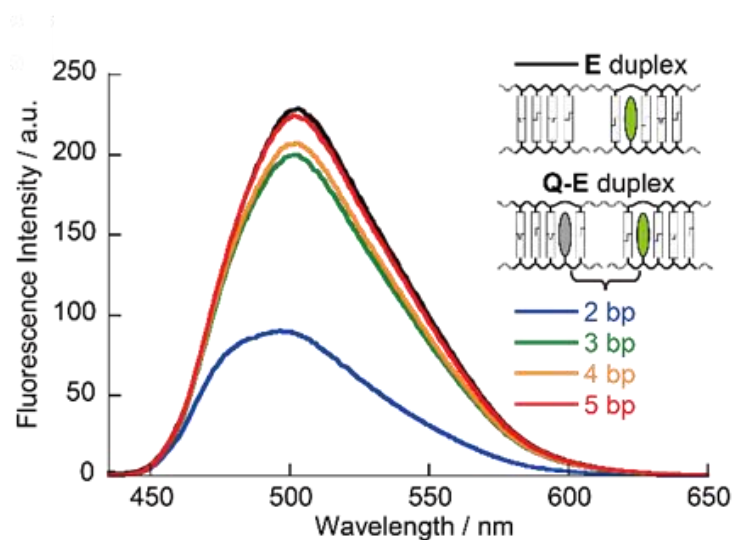


Figure 4-3.

Fluorescent emission spectra of **Q-E** duplex (2~5bp) and **E** duplex. Effects of quenching of perylene emission by anthraquinone with 2 to 5 bp separation is shown.

Emission intensity of **Q-E** duplex with a 2-base-pair separation was much lower than that of control **E** duplex, whereas quenching was not detectable when residues were separated by 3 or more base pairs. Anthraquinone quenches the perylene fluorescence through not FRET but electron transfer. Thus, separation of perylene and anthraquinone with more than two base-pairs no longer reduces the perylene emission.

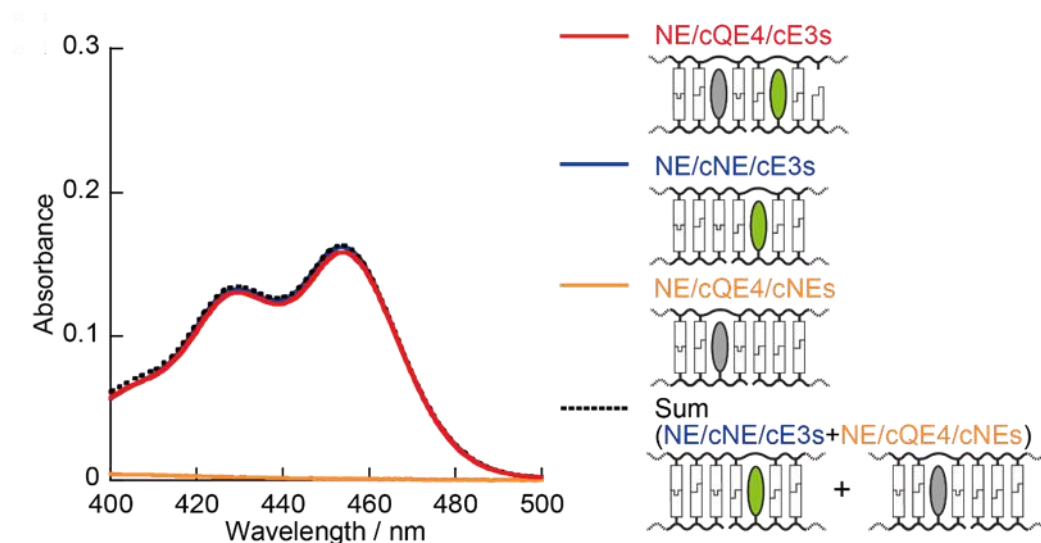


Figure 4-4.

Absorption spectra of several duplex (2bp). Effects of excitonic interaction between perylene and anthraquinone in the case of 2bp separation is shown.

We also measured the absorption spectra in the case of 2bp separation between perylene and anthraquinone. The results are shown in Figure 4-4. Absorption spectra of Q-E duplex (red line) showed completely agreement with the summed spectra (dotted line) of duplex with a perylene moiety (blue line) and duplex with an anthraquinone moiety (yellow line). This data indicated no effects of excitonic interaction between perylene and anthraquinone in the case of 2bp separation. These results have prompted us to conclude that quenching by anthraquinone can be neglected when the distance between perylene and anthraquinone is more than 2bp.

4-3-3 Investigation of perylene next to anthraquinone

We also investigate effects of perylene next to anthraquinone. The absorption spectra are shown in Figure 4-5. Absorption spectra of **Q-E** duplex (red line) did not show agreement with the summed spectra (dotted line) of duplex with a perylene moiety (blue line) and duplex with an anthraquinone moiety (yellow line), slight hypsochromism was observed. This is interpreted as being derived from the excitonic interaction^[3].

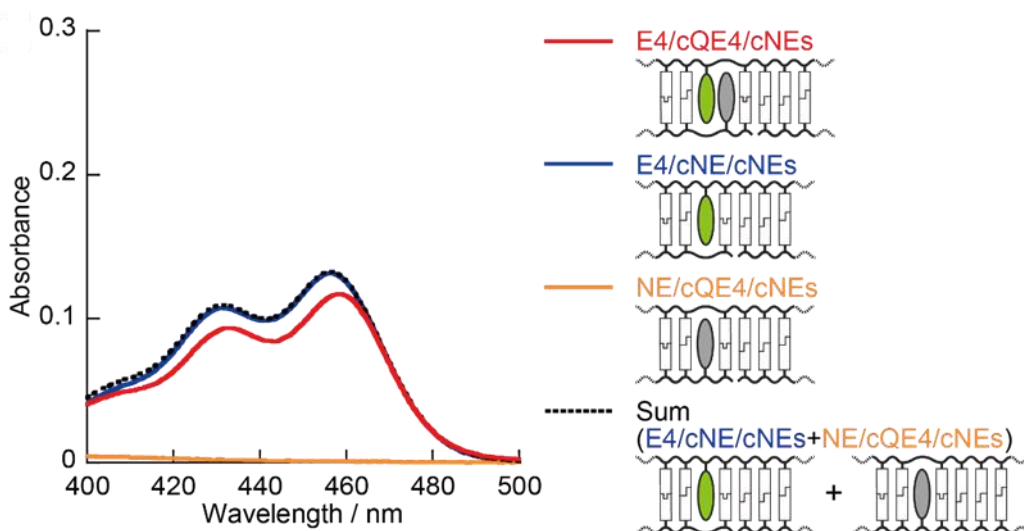


Figure 4-5.

Absorption spectra of several duplex. Effects of excitonic interaction between perylene and anthraquinone in the case of cluster is shown. This small hypochromicity is derived from the excitonic interaction.

In order to investigate the effects of this change on energy migration between two

perylene, we calculated the spectral overlap.

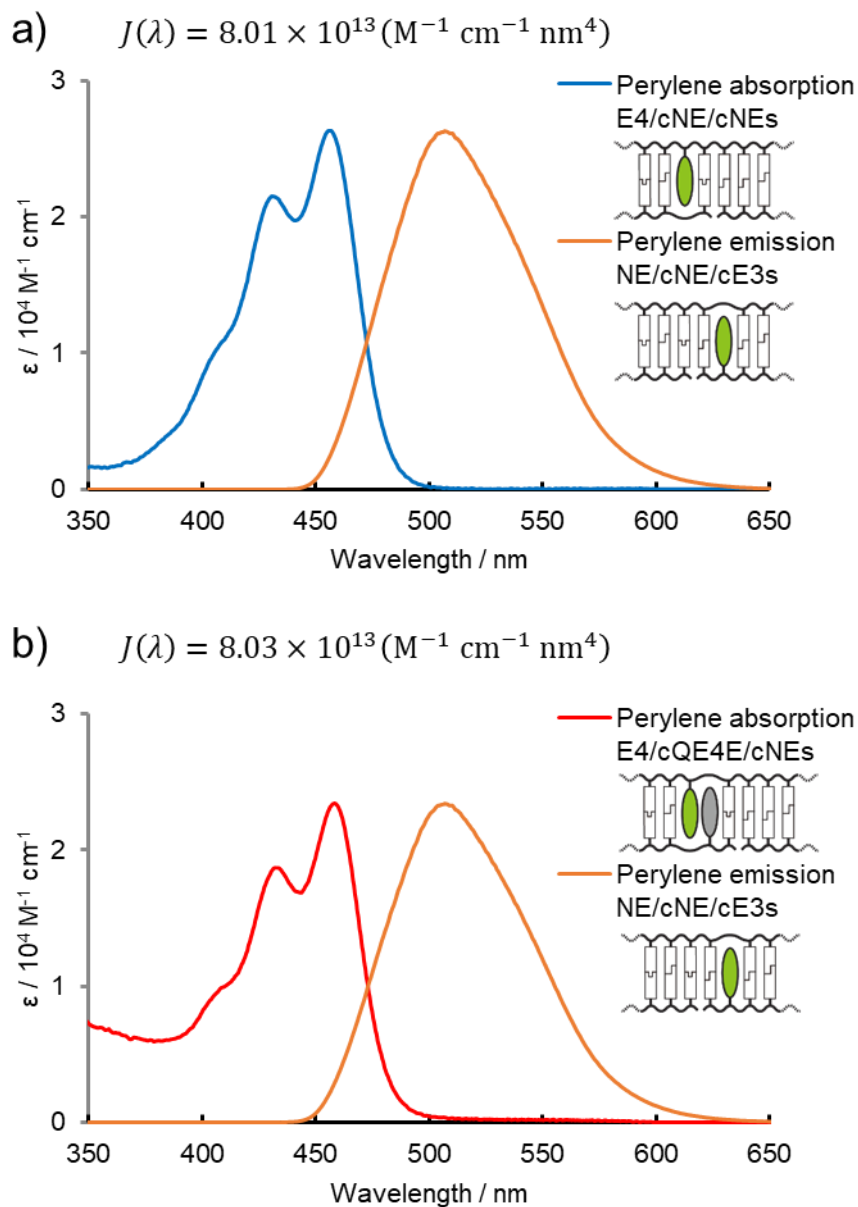


Figure 4-6.

Absorption and normalized fluorescent emission spectra of perylene and anthraquinone in the case of (a) energy transfer from perylene to perylene and (b) energy transfer from perylene to perylene next to anthraquinone.

Slight hypsochromism was observed in the absorption spectrum of **Q-E** duplex, however, its effect on spectral overlap was <1%. Therefore, we concluded that optical property of quenched perylene is virtually identical to that of the unquenched on.

4-3-4 Melting temperatures (T_m s) of duplexes

We measured melting temperatures (T_m s) of duplexes and confirmed that duplexes were stable below 20 °C (Table 4-1). Incorporation of perylene and/or anthraquinone residues resulted in duplexes more stable than the appropriate control duplexes, indicating that there are stacking interactions of perylene and anthraquinone with neighbouring natural base pairs.

Table 4-1. Effects of incorporation of perylene onto the duplex stability.

Sequence		$T_m / ^\circ\text{C}$
E1 cQE1	TGACTAC E GGTGAATACATACATACTGAT ACTGATG Q CCAC	(5'→3') (3'←5') 60.3
E2 cQE2	TGACTAC E GTGAATACATACATACTGAT ACTGATGC Q CAC	(5'→3') (3'←5') 54.1
E3 cQE3	TGACTAC G GTGAATACATACATACTGAT ACTGATGCC Q AC	(5'→3') (3'←5') 52.7
E4 cQE4	TGACTAC G TEGAATACATACATACTGAT ACTGATGCCA Q C	(5'→3') (3'←5') 56.5
E1 cNE	TGACTAC E GGTGAATACATACATACTGAT ACTGATG CCAC	(5'→3') (3'←5') 53.0
E2 cNE	TGACTAC E GTGAATACATACATACTGAT ACTGATGC CAC	(5'→3') (3'←5') 48.7
E3 cNE	TGACTAC G GTGAATACATACATACTGAT ACTGATGCC AC	(5'→3') (3'←5') 45.4

E4 cNE	TGACTACGGT E GAATACATACATACTGAT ACTGATGCCA C	(5'→3') (3'←5')	50.8
NE cQE1	TGACTAC GGTGAATACATACATACTGAT ACTGATG Q CCAC	(5'→3') (3'←5')	54.3
NE cQE2	TGACTACG GTGAATACATACATACTGAT ACTGATGC Q CAC	(5'→3') (3'←5')	49.6
NE cQE3	TGACTACGG TGAATACATACATACTGAT ACTGATGCC Q AC	(5'→3') (3'←5')	48.7
NE cQE4	TGACTACGGT GAATACATACATACTGAT ACTGATGCCA Q C	(5'→3') (3'←5')	48.7
NE cNE	TGACTACGGTGAATACATACATACTGAT ACTGATGCCAC	(5'→3') (3'←5')	45.4
NE cE1s	TGACTACGGTGAATACATAC ATACATACTGAT TTATGTATG E TATGTATGACTA	(5'→3') (3'←5')	60.7
NE cE2s	TGACTACGGTGAATAC ATACATACTGAT TTATG E TATGTATGTATGACTA	(5'→3') (3'←5')	60.6
NE cE3s	TGACTACGGTGA ATACATACTGAT T E TATGTATGTATGTATGACTA	(5'→3') (3'←5')	59.5
NE cNEs	TGACTACGGTGAATACATACATACTGAT TTATGTATGTATGTATGACTA	(5'→3') (3'←5')	54.3

4-3-5 Quantitative analysis of energy migration between two perylenes

From the results in chapters 4-3-2 to 4-3-4, we conclude that this sequence design is suitable for studying energy migration between the identical chromophores from the following points.

-When perylene and anthraquinone are separated by 3 bases or more, the effect of quenching can be ignored.

-The optical properties of perylene in contact with anthraquinone are substantially identical to that of the unquenched on.

-At 20 °C, all chains form a stable duplex.

We compared emission spectra of **E**, **EQ** and **EQ-E** duplexes. In the **EQ-E** duplexes the perylene and the anthraquinone are separated by from 2 to 13 base pairs. The **E** duplex had a strong emission (Figure. 4-7a), whereas virtually no emission was observed with the **EQ** duplex (Figure. 4-7b), demonstrating the efficient quenching of perylene by anthraquinone. The duplexes in the **EQ-E** series had much lower emission than the **E** duplex (Figure. 4-7c).

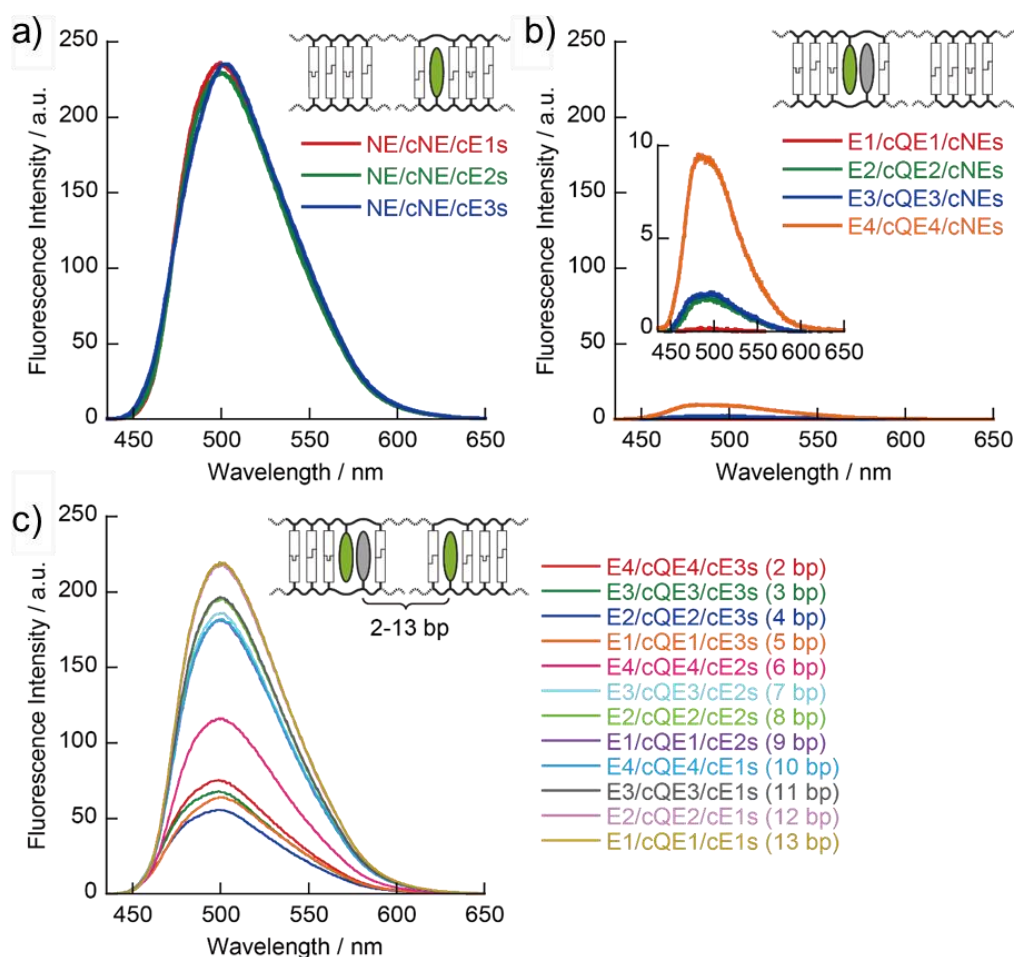


Figure 4-7.

Emission spectra of (a) **E** duplexes, (b) **EQ** duplexes and (c) **EQ-E** duplexes.

A representative result for the duplex with a 5-base-pair separation between fluorophores is shown in Figure 4-8a. This quenching clearly demonstrated the occurrence of energy migration between two perylenes. Similar quenching was observed with all the other **EQ-E** duplexes (Figure S4-1), and their emission intensities are summarized in Figure 4-8b.

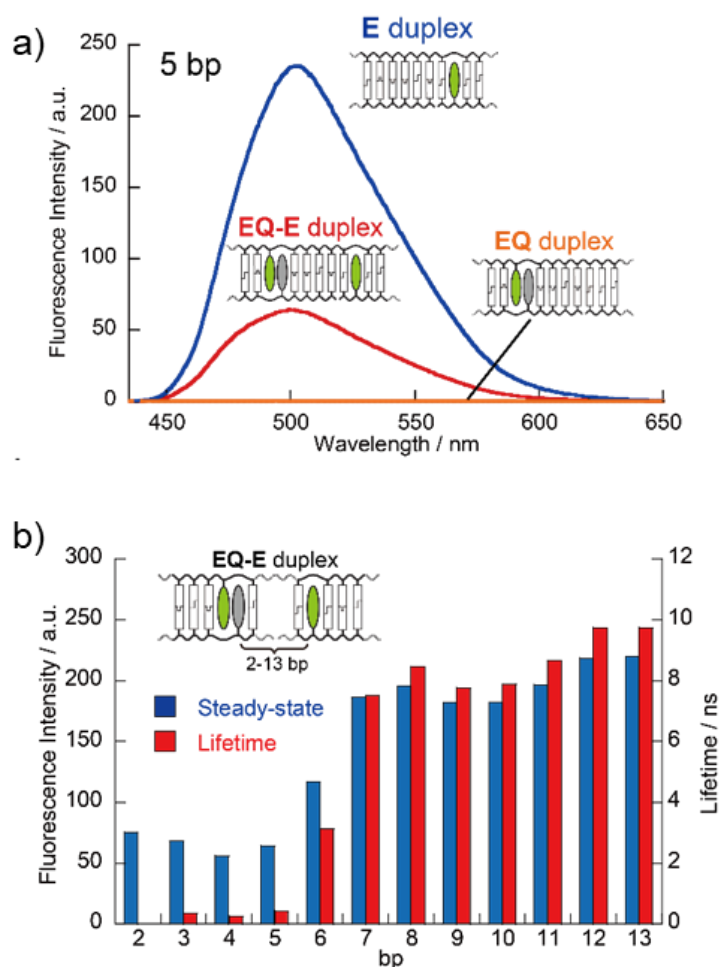


Figure 4-8.

a) Fluorescence emission spectra of **EQ-E**, **E** and **EQ** duplexes with 5-base-pair separation. b) Fluorescence emission intensities and lifetimes of **EQ-E** duplexes.

Generally, emission intensity increased as the number of base pairs increased; however, maxima of emission intensity were observed when 8 and 13 base pairs separated the fluorophores. A 5-base-pair cycle of similar emission intensity was observed with hetero FRET from pyrene to perylene that corresponds to a half turn of the B-form DNA duplex^[4,5]. Our result indicated that energy migration between identical chromophores also exhibits orientation dependence.

We also performed time-resolved fluorescence measurements and representative results of the duplex with 5-base-pair spacing are shown in Figure 4-9 (see Figure S4-2 for decay curves of other duplexes).

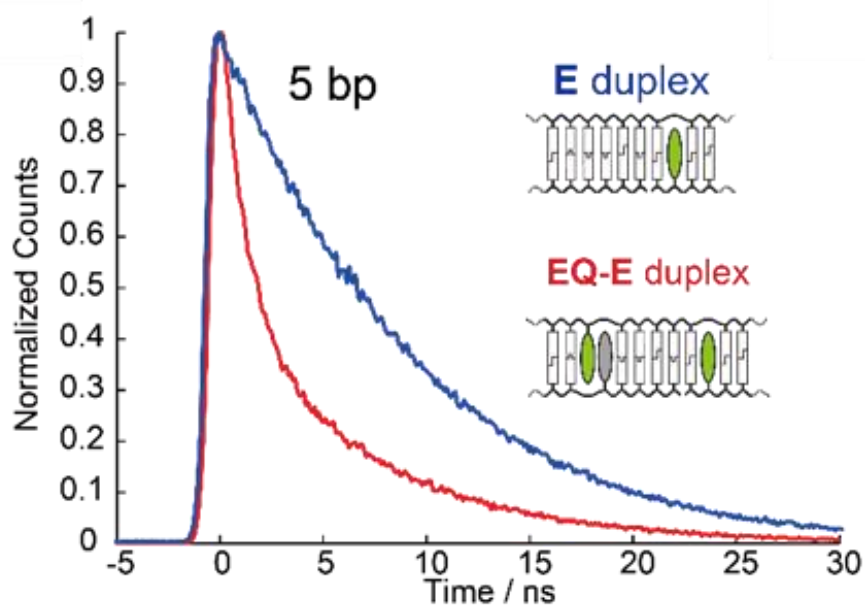


Figure 4-9.

Fluorescence lifetime measurements of **EQ-E** and **E** duplexes with 5-base-pair separation.

The **EQ-E** duplex showed much faster decay than the **E** duplex, indicative of quenching due to energy migration. We also monitored decay of **EQ** duplexes; however, lifetimes could not be determined as decay was too rapid. Lifetimes of **EQ-E** duplexes are shown in Table 4-2 and Figure 4-8b (lifetimes of control duplexes are listed in Table S4-2).

Table 4-2. Lifetimes and EM efficiencies of EQ-E duplexes.

bp	τ_1 (ns)	τ_2 (ns)	α_1	α_2	χ^2	Φ_{T1}	Φ_{T2}
2	-*	-*	-	-	-	0.82	-
3	0.36	7.51	0.67	0.33	1.22	0.71	0.96
4	0.25	7.63	0.58	0.42	1.08	0.76	0.97
5	0.43	7.27	0.56	0.44	1.08	0.72	0.95
6	3.12	7.45	0.64	0.36	1.20	0.57	0.66
7	7.51	-	1	-	1.10	0.22	0.19
8	8.46	-	1	-	1.31	0.18	0.09
9	7.76	-	1	-	1.20	0.22	0.17
10	7.88	-	1	-	1.22	0.25	0.19
11	8.66	-	1	-	1.22	0.15	0.11
12	9.74	-	1	-	1.18	0.03	0.00
13	9.74	-	1	-	1.18	0.00	0.00

*Lifetimes cannot be determined due to fast decay.

Although two lifetimes were observed when fluorophores were 3 to 6 base pairs apart, the longer lifetimes are attributed to emission from perylene in residual single strands. We used the shorter lifetimes for calculation of energy migration efficiencies. We calculated EM efficiencies from the decrease of emission intensities and lifetimes (Φ_{T1} and Φ_{T2} in Table 4-2, respectively). Φ_{T1} and Φ_{T2} generally decreased as the distance between two perylenes increased. The lifetimes exhibited similar trends as emission intensities with the longest lifetimes observed at intervals of about 5 base pairs, also demonstrating the orientation dependence of energy migration. The difference between Φ_{T1} and Φ_{T2} at short distances is relatively large; Φ_{T2} values are above 0.95 with 3 to 5 base pairs between fluorophores, whereas Φ_{T1} values are about 0.7. We hypothesized that these differences are due to the emission from excess perylene strands. Although perylene strands (**Em** and **cEns** in Figure 4-2) of the same concentration were used for measurements, emission from perylene in the excess single strands lowered the apparent Φ_{T1} . In contrast, lifetime measurements can discriminate emission of excess single strands from that of **EQ-E** duplex.

4-3-6 Comparison with Förster theory

These experimentally determined efficiencies were compared with values calculated from Förster theory. Distance, orientation factor, and spectral overlap were determined and used for the calculation of migration efficiency. Regarding spectral overlap, we ignored the effects of anthraquinones, as shown in chapter 4-3-3. Molecular modelling of **EQ-E** duplexes indicated that perylene and anthraquinone are stacked between base pairs without disturbing double helical structure (Figure 4-10a). The angle between perylene and the neighbouring base pairs were estimated from curve fitting and molecular modelling (Figure 4-10b). We used a cylinder model where the distance increased by 3.3 Å per base pair and the angle by 33° per base pair (Figure 4-10c). The increment of distance due to anthraquinone was assumed to be the same as for a natural base pair (3.3 Å). The theoretically calculated EM efficiencies are shown in Figure 4-11. The theoretical curve showed the same tendency as experimental values. Especially, Φ_{T2} values showed excellent agreement. We also measured Φ_{T1} at various temperatures (Figure S4-3), and values were almost the same irrespective of temperature. The insensitivity to temperature indicated that effects of dynamics and disorder are marginal under the conditions employed. These results clearly demonstrated that the energy migration between two perylenes strictly obeys Förster theory. Thus, these results provided the first experimental

validation of Förster theory for the calculation of efficiencies and rate constants of energy migration.

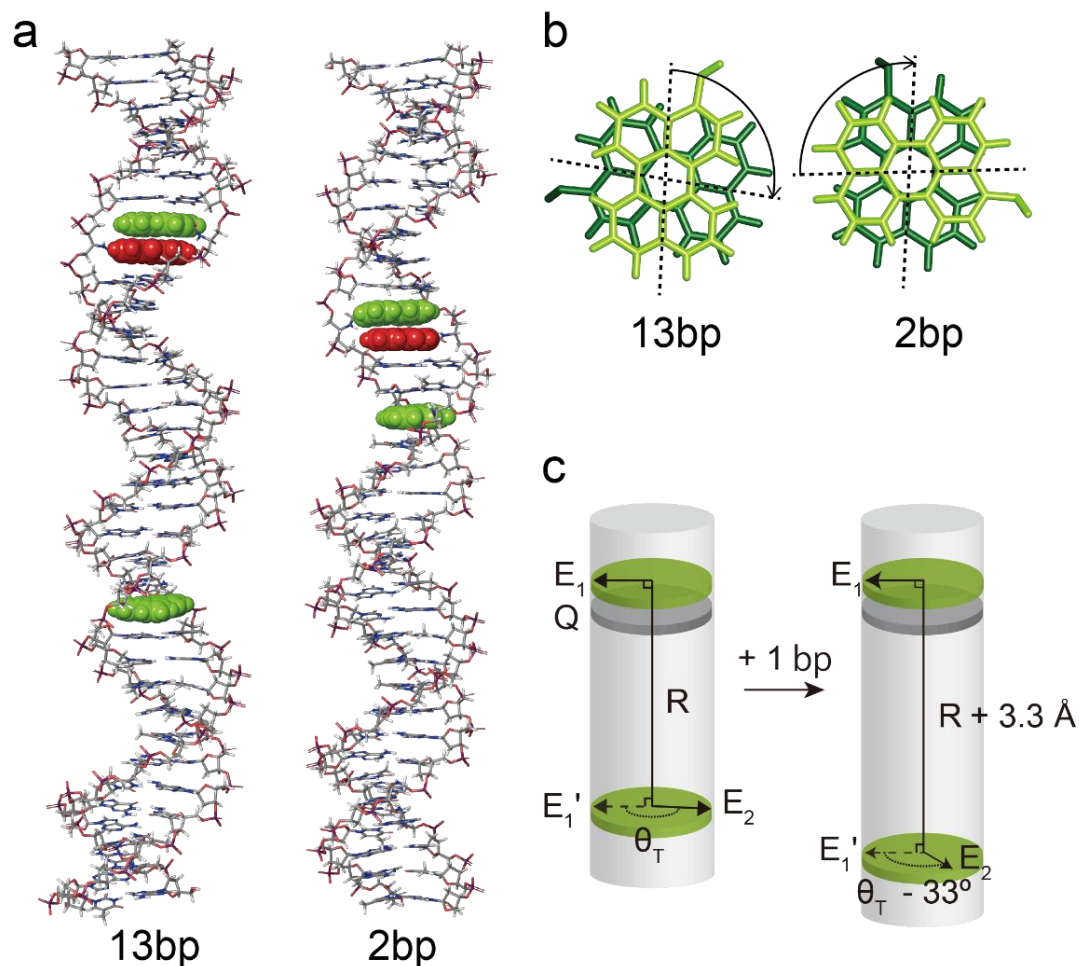


Figure 4-10.

Molecular modelling and cylinder model of EQ-E duplexes. a) Molecular modelling of EQ-E duplexes with 13- and 2-base-pair separations. Perylene and anthraquinone moieties are shown in CPK model and colored in green and red, respectively. b) Relative orientations of two perylene moieties in EQ-E duplexes. Angles between perylene moieties and neighbouring base pairs are 97° and 95° for 13-base-pair and 2-base-pair separations, respectively. c) Cylinder model of DNA duplex for theoretical calculation of EM efficiencies. Distance and angle increase by 3.3 \AA and 33° per base pair in this model, respectively. Fluorescence lifetime measurements of EQ-E and E duplexes with 5-base-pair separation.

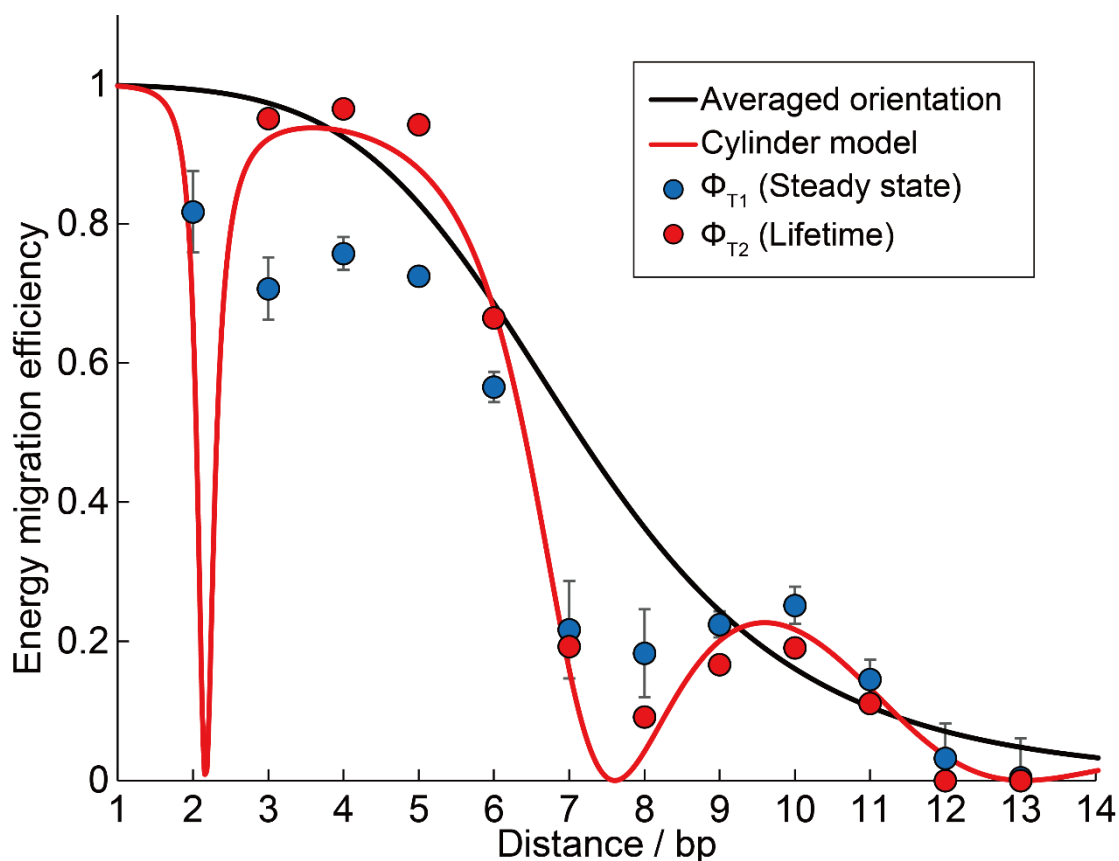


Figure 4-11.

Dependence of EM efficiency on the number of base pairs between two perylene moieties. Experimentally obtained efficiencies from emission intensities and lifetimes are shown in blue and red circles, respectively. Theoretically calculated values assuming random or fixed orientations are shown in black and red lines, respectively. Error bars of Φ_{T1} show standard deviation of three independent fluorescence measurements.

4-3-7 Analysis of energy migration among four perylenes

We then used a similar system to investigate multi-step energy migration among four perylenes. A schematic of the experimental design is illustrated in Figure 4-12 (see Table S4-3 for DNA sequences).

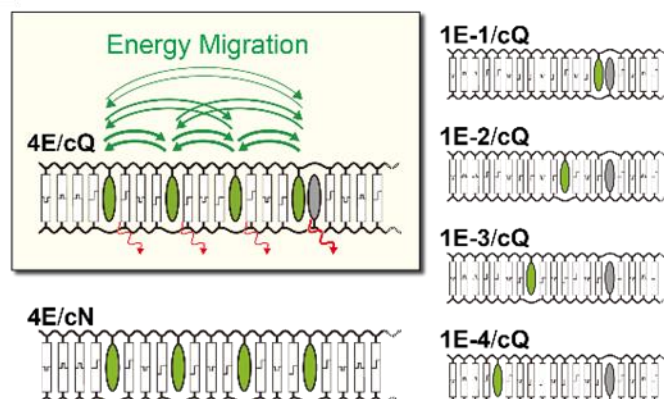


Figure 4-12.

Sequence design to investigate multi-step energy migration.

Four perylenes were introduced into DNA at 3- nucleotide intervals in strand **4E**. The complementary strand, **cQ**, has one anthraquinone opposite the terminal perylene of **4E**. When **4E** is hybridized with **cQ**, emission from the three perylenes located distant from the anthraquinone should be quenched through multi-step energy migration. Therefore, energy migration among four perylenes can be monitored by analysis of emission intensity and lifetime. We also synthesized DNA strands tethering perylene residues at different positions (**1E-1** to **1E-4**) as controls. The controls showed similar emission intensities when each was hybridized with a complementary strand without a quencher (**cN**) as shown in Figure 4-13. **4E/cN** showed almost identical intensity to the sum of intensities of **1E-1/cN**, **1E-2/cN**, **1E-3/cN** and **1E-4/cN**.

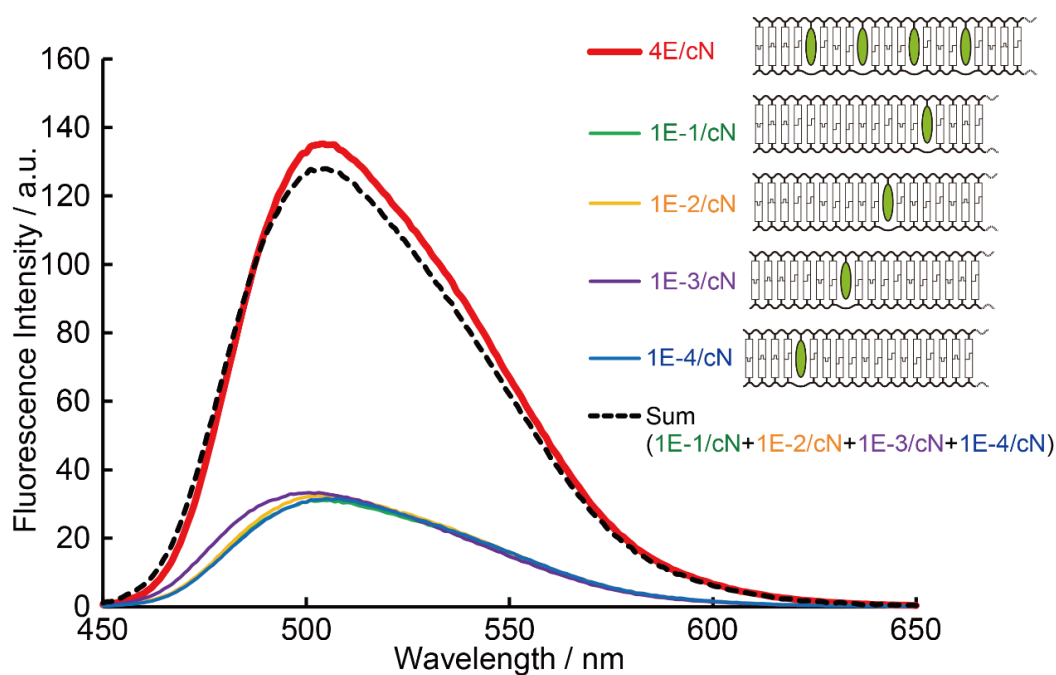


Figure 4-13.

Emission spectra of **4E/cN**, **1E-1/cN**, **1E-2/cN**, **1E-3/cN**, **1E-4/cN** duplexes, which contain no quenchers. Sum of the spectra of **1E-1/cN**, **1E-2/cN**, **1E-3/cN** and **1E-4/cN** are also shown.

The emission intensity of **1E-1/ cQ** was almost nil, whereas other combinations were the same as **1E** duplex without Q (Figure 4-14). The **4E/cQ** duplex with four fluorophores had much lower emission than the sum of the emission from each perylene (Figure 4-14, compare red line with dotted line). This large difference between **4E/cQ** and the sum is clear evidence of multi-step energy migration among four perylenes.

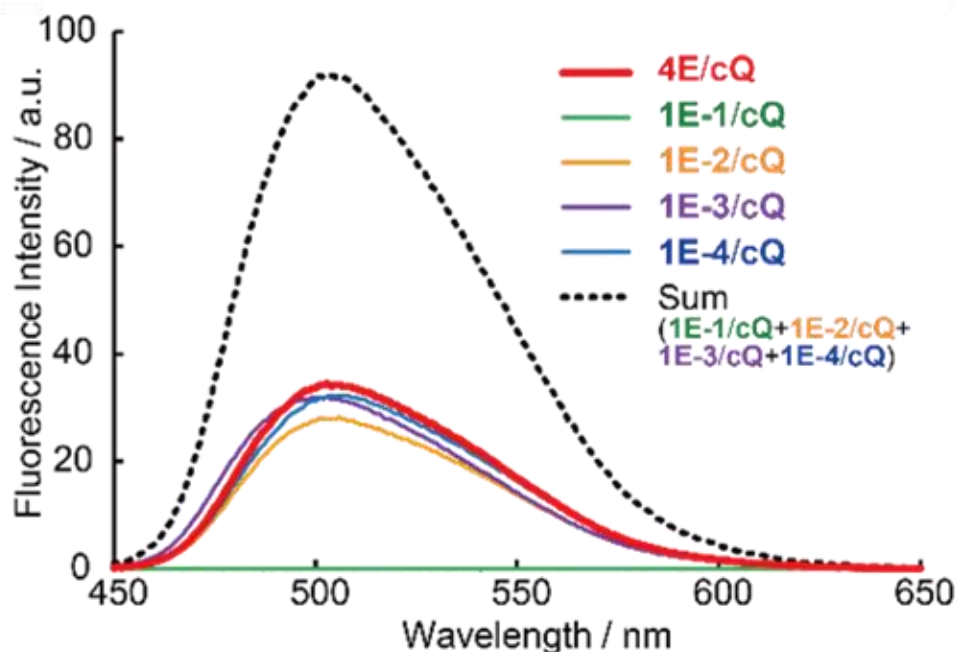


Figure 4-14.

Fluorescence emission spectra of **4E/cQ**, **1E-1/cQ**, **1E-2/cQ**, **1E-3/cQ** and **1E-4/cQ**. Sum of spectra of **1E-1/cQ**, **1E-2/cQ**, **1E-3/cQ** and **1E-4/cQ** is also shown.

The higher T_m of **4E/cQ** than those of control duplexes (**1E-1/cQ** to **1E-4/cQ**) indicated that base pairing of natural base pairs is not severely disturbed upon the introduction of non-natural residues (Table S4-4). We also performed time-resolved fluorescence measurements, and decay curves of **4E/cQ** and **4E/cN** are shown in Figure 4-15. **4E/cN** showed a mono exponential decay with a lifetime of 8.40 ns (Table 4-3). In contrast, biexponential decay with lifetimes of 1.19 ns and 3.80 ns was observed for **4E/cQ**. The decrease in lifetime associated with the incorporation of anthraquinone clearly demonstrates the efficient energy migration among four perylenes.

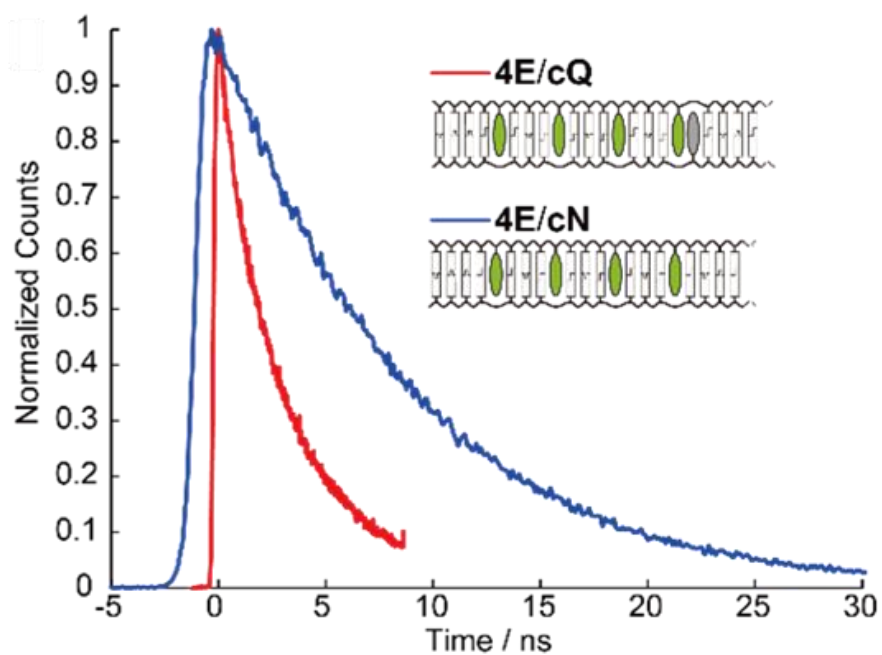


Figure 4-15.

Fluorescence lifetime measurements of **4E/cQ** and **4E/cN** duplexes.

Table 4-3. Lifetimes and EM efficiencies of EQ-E duplexes.

	τ_1 (ns)	τ_2 (ns)	α_1	α_2	χ^2
4E/cQ (Observed)	1.19	3.80	0.27	0.73	1.06
4E/cQ (Simulated)	0.05	1.42	0.30	0.70	-
4E/cN	8.40	-	1	-	1.23
1E-1/cQ	-*	-	-	-	-
1E-2/cQ	8.06	-	1	-	1.03
1E-3/cQ	9.74	-	1	-	1.23
1E-4/cQ	9.22	-	1	-	1.28

*Lifetimes cannot be determined due to fast decay.

We simulated the fluorescence decay of **4E/cQ** from the non-coherent energy hopping mechanism based on Förster theory [6-8]. The decay curve of each perylene can be simulated by solving differential equations using migration and decay rate constants. Rate constants of intrinsic decays of each perylene were determined from lifetimes; the exception was the decay rate of the perylene adjacent to anthraquinone, which was estimated from emission intensity. Energy migration rate constants were calculated using decay rates and migration efficiencies (Table S4-5). Migration efficiencies were calculated from Förster theory by using the distances and orientation factors between perylenes, which were determined from molecular modelling (Figure 4-16b). Simulated decay curves of the four perylenes are shown in Figure 4-16a. The resultant decay curve of each perylene depended on its position. The perylene located far from anthraquinone had the slowest decay, whereas the perylene located to the 5' side of anthraquinone had the fastest (Figure 4-16a). Interestingly, the average curve of four perylenes, which corresponds to the overall decay curve of **4E/cQ**, could be fitted with a biexponential curve with lifetimes of 0.05 and 1.42 ns (Table 4-3 and Figure S4-4). A 0.05-ns lifetime is too short to be detected by our apparatus. In contrast, observed lifetime of 1.19 ns is in good agreement with the simulated lifetime (1.42 ns). The longer lifetime (3.80 ns) might be due to excess single strand or to structural disorder; either would result in incomplete

migration. These results indicated that even efficiency and rate constants of multi-step energy migration can be estimated using Förster theory.

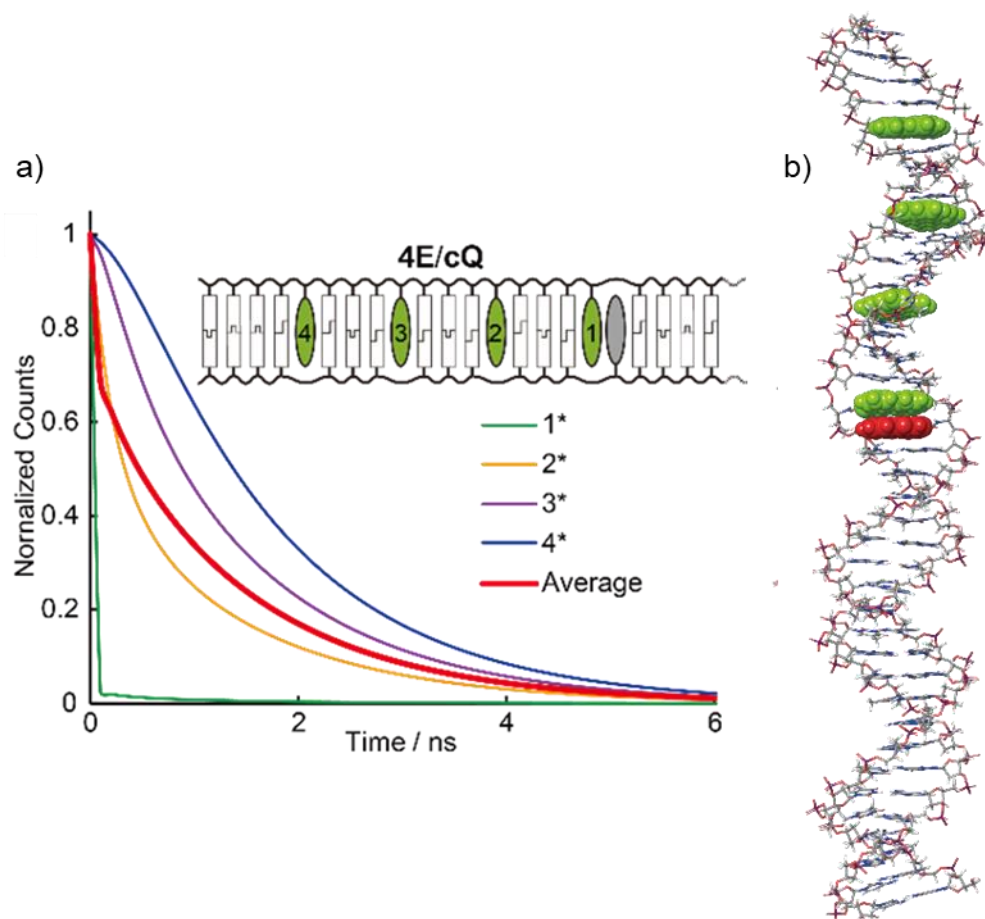


Figure 4-16.

- a) Simulated decay curve of **4E/cQ**. Time evolution of excited population of each perylene is also shown. Numbering of perylenes is schematically illustrated in the inset.
- b) Molecular modelling of **4E/cQ** duplex. Perylene and anthraquinone moieties are shown in CPK model and are coloured in green and red, respectively.

4-4 Conclusions

Here we clarified the distance and orientation dependence of energy migration in detail. We demonstrated that energy migration between identical chromophores strictly obeys Förster's theory. Our system can be used to determine and predict efficiencies and rate constants of energy migration steps of various chromophoric arrays. Recent studies have revealed that coherent coupling plays important roles in efficient energy transport in natural photosynthesis ^[9,10]. Since our system is simple but robust, it could be used to analyse other fluorophores such as Cy3 or thiazole orange ^[11]. Furthermore, it could be used to investigate energy migration processes in strongly coupling regimes. We also demonstrated that multi-step migration can also be estimated from the theory. Energy migration is used in many applications such as light-harvesting antennae, logic gates, chemical sensing, and photon energy conversion ^[12]. In order to achieve the best performance of these devices, it is necessary to tune rate constants of each energy transport step precisely. The present results may provide a framework for design and preparation of photonic devices, circuits, and sensors with desirable properties.

4-5 Experimental section

Oligonucleotide synthesis

All conventional phosphoramidite monomers, CPG columns, reagents for DNA synthesis, and Poly-Pak II cartridges were purchased from Glen Research. Other reagents for the synthesis of phosphoramidite monomers were purchased from Tokyo Chemical Industry, Wako, and Aldrich. Native oligodeoxyribonucleotides (ODNs) were purchased from Integrated DNA Technologies or Hokkaido System Science Co., Ltd. ODNs tethering perylene or anthraquinone were synthesized on an automated DNA synthesizer (H-8-SE, Gene World) as we reported previously. ODNs were purified by reversed-phase HPLC and characterized by MALDI-TOF MS (Autoflex II, Bruker Daltonics) and HPLC.

The MALDI-TOF MS data for the modified DNA were as follows: **E1**: Obsd. 10257 (Calcd. for [**E1**+H⁺]: 10257). **E2**: Obsd. 10257 (Calcd. for [**E2**+ H⁺]: 10257). **E3**: Obsd. 10257 (Calcd. for [**E3**+ H⁺]: 10257). **E4**: Obsd. 10256 (Calcd. for [**E4**+ H⁺]:10257). **cQE1**: Obsd. 3703 (Calcd. for [**cQE1**+ H⁺]: 3702). **cQE2**: Obsd. 3703 (Calcd. for [**cQE2**+H⁺]: 3702). **cQE3**: Obsd. 3703 (Calcd. for [**cQE3**+ H⁺]: 3702). **cQE4**: Obsd. 3703 (Calcd. for [**cQE4**+H⁺]: 3702). **cE1s**: Obsd. 6905 (Calcd. for [**cE1s**+H⁺]: 6908). **cE2s**: Obsd. 6908 (Calcd. for [**cE2s**+H⁺]: 6908). **cE3s**: Obsd. 6908 (Calcd. For [**cE3s**+H⁺]: 6908).

H⁺): 6908). **4E**: Obsd. 12227 (Calcd. for [**4E**+H⁺]: 12233). **1E-1**: Obsd. 10897 (Calcd. for [**1E-1**+H⁺]: 10898). **1E-2**: Obsd. 10895 (Calcd. for [**1E-2**+H⁺]: 10898). **1E-3**: Obsd. 10892 (Calcd. for [**1E-3**+H⁺]: 10898). **1E-4**: Obsd. 10896 (Calcd. For [**1E-4**+H⁺]: 10898). **cQ**: Obsd. 10822 (Calcd. for [**cQ**+H⁺]: 10823)

Fluorescence measurements

Fluorescence spectra were measured on JASCO models FP-6500 or FP-8500. The excitation wavelength was 427 nm Band widths were 3 nm (FP-6500) or 2.5 nm (FP-8500) for excitation and emission. Before measurements, sample solutions containing DNA duplex were heated at 80 °C, then slowly cooled down to 0 °C at a rate of 4 °C min⁻¹. Fluorescence spectra were measured at 80 to 0 °C at 10 °C intervals after 4 min incubations. Emission spectra were measured at 0 °C. Sample solutions contained 100 mM NaCl, 10 mM phosphate buffer, pH 7.0. Concentrations of oligonucleotides were 1.0 μM for those tethering perylene (**E1** to **E4**, **cE1s** to **cE3s**, **4E**, **1E-1** to **1E-4**) and 1.5 μM quencher strands (**cQE1** to **cQE4**, **cQ**). For control measurements, concentrations of native strands were 1.0 μM for **NE** and **cNEs** and 1.5 μM for **cNE** and **cN**. We used excess amount of quencher strands to reduce the effects of emission from single-stranded donor strand.

Fluorescence lifetime measurements

A pulse at 780 nm was generated by a Ti: sapphire laser system (Spectra-Physics, Tsunami; 3950-L2S, fwhm 150 fs, 82 MHz). The repetition rate was reduced to 4 MHz by a pulse selector (Spectra-Physics Model 3980). The exciting source was a laser with wavelength converted to 390 nm by passage through SHG crystals. Fluorescence emission was captured by a streak camera (Hamamatsu C4334) operating in photon counting mode. Measurements were performed at room temperature.

Measurement of absorption spectra and melting temperatures

Absorption spectra were measured on a JASCO model V-530, V-550, or V-560. The sample solutions contained 100 mM NaCl, 10 mM phosphate buffer, pH 7.0, 5.0 μ M each strand. Absorption spectra were measured at 0 °C. The melting curves were measured with a UV-1800 (Shimadzu) by monitoring 260 nm absorbance versus temperature. The T_m was determined from the maximum in the first derivative of the melting curve. Both the heating and the cooling curves were measured, and the calculated T_m agreed to within 1.0 °C. The temperature ramp was 0.5 °C min⁻¹. The sample solutions contained 100 mM

NaCl, 10 mM phosphate buffer, pH 7.0, 1.0 μM (for data shown in Table 4-1) or 2.0 μM (for data shown in Table S4-4) each strand.

Calculation of FRET efficiency

Energy transfer efficiency was calculated from steady-state fluorescence (Φ_{T1}) or fluorescent lifetimes (Φ_{T2}). Φ_{T1} was calculated from the following equation:

$$\Phi_{T1} = \frac{I_D + I_Q - I}{I_D - I_Q} \quad (1)$$

where I , I_Q and I_D are emission intensities of **EQ-E** duplex, **EQ** duplex and **E** duplex, respectively. When energy transfer between two perylenes does not occur, I should be equal to I_D plus I_Q so that Φ_{T1} becomes zero. In contrast, when excitation energy of perylene at distant position perfectly transfers to perylene next to anthraquinone, the intensity of the perylene should be the same as that of the quenched one. Therefore, I should be equal to $2 I_Q$. In this case, Φ_{T1} becomes unity (Figure S4-5).

The energy migration efficiency, Φ_{T2} , was determined from fluorescence lifetime measurements. For duplexes containing one fluorophore with no quencher (**E** duplex), the fluorescent lifetime (τ_D) can be represented as follows:

$$\frac{1}{\tau_D} = k_f + k_{d1} \quad (2)$$

where k_f and k_{d1} are an emissive rate constant and a non-radiative decay rate, respectively (Figure S4-6). τ , which is a lifetime of **EQ-E** duplex, can be represented by using the energy migration rate constant (k_t):

$$\frac{1}{\tau} = k_t + k_f + k_{d1} \quad (3)$$

Lifetimes of **EQ** duplexes could not be determined in time-resolved fluorescence measurements with our apparatus. Besides, emission intensity of **EQ** duplexes was much lower than those of **E** duplexes, indicating quenching by anthraquinone occurs very rapidly. Therefore, we ignored the decay rate of quenched perylene (k_{d2}) because it is much larger than other rate constants. By using equations (2) and (3), energy transfer efficiency from fluorescent lifetimes (Φ_{T1}) can be simply calculated as follows:

$$\Phi_{T2} = \frac{k_t}{k_t + k_f + k_{d1}} = 1 - \frac{\tau}{\tau_D} \quad (4)$$

Energy minimization based on molecular mechanics.

The energy minimization for the molecular structure model of DNA duplexes tethering perylene and anthraquinone was carried out using MacroModel (MacroModel, version 11.6; Schrödinger) applying the AMBER force field. Duplexes were constructed from

canonical B-form DNA duplex by using a graphical programme. The water solvent effects were simulated using the analytical Generalized-Born/Surface-Area (GB/SA) model. Convergence threshold was set to 0.05 kJ Å⁻¹ mol⁻¹.

Theoretical calculation of energy transfer efficiencies based on Förster theory

Energy transfer efficiency was calculated from the following equations:

$$\Phi_T = \frac{1}{1 + (R/R_0)^6} \quad (5)$$

$$R_0 = 0.2108[J(\lambda)\kappa^2n^{-4}\Phi_D]^{1/6} \quad (6)$$

$$\kappa^2 = \cos^2\theta_T \quad (7)$$

where R is the distance between donor and acceptor, and R_0 is a Förster radius (the distance where $\Phi_T = 0.5$). $J(\lambda)$ is integral of spectral overlap between donor emission and acceptor absorption at λ nm. n is a refractive index, which is typically assumed to be 1.4 for biomolecules, and Φ_D is a donor quantum yield. The orientation factor, κ^2 , was calculated from the above equation, where θ_T is the angle between transition dipoles of donor and acceptor.

Theoretical transfer efficiency can be calculated from the distance and angle between two chromophores. Rise and typical twist angle of B-form duplex, 3.3 Å per base pair and 33° per base pair, respectively, were used to calculate the distance and the angle between dyes. These parameters were determined by fitting theoretically calculated efficiencies with experimental data, and the resultant values are consistent with reported parameters^[13,14]. In our design, anthraquinone is located between two perylenes. Therefore, we hypothesized that the distance between perylenes and anthraquinone was also 3.3 Å. We assumed an angle of 52° between dyes angles based on an estimate from molecular modelling and curve fitting. When anthraquinone was introduced into the counter position of perylene, slight hypochromic effect was observed in UV-vis spectrum (Figure 4-5), which were used to calculate spectral overlap integral (Figure 4-6).

Simulation of multi-step energy migration

Energy migration among four perylenes was simulated by solving the following differential equations.

$$\frac{dP_1}{dt} = -(k_{12} + k_{13} + k_{14} + k_{d1})P_1 + k_{21}P_2 + k_{31}P_3 + k_{41}P_4 \quad (8)$$

$$\frac{dP_2}{dt} = -(k_{21} + k_{23} + k_{24} + k_{d2})P_2 + k_{12}P_1 + k_{32}P_3 + k_{42}P_4 \quad (9)$$

$$\frac{dP_3}{dt} = -(k_{31} + k_{32} + k_{34} + k_{d3})P_3 + k_{13}P_1 + k_{23}P_2 + k_{43}P_4 \quad (10)$$

$$\frac{dP_4}{dt} = -(k_{41} + k_{42} + k_{43} + k_{d4})P_4 + k_{14}P_1 + k_{24}P_2 + k_{34}P_3 \quad (11)$$

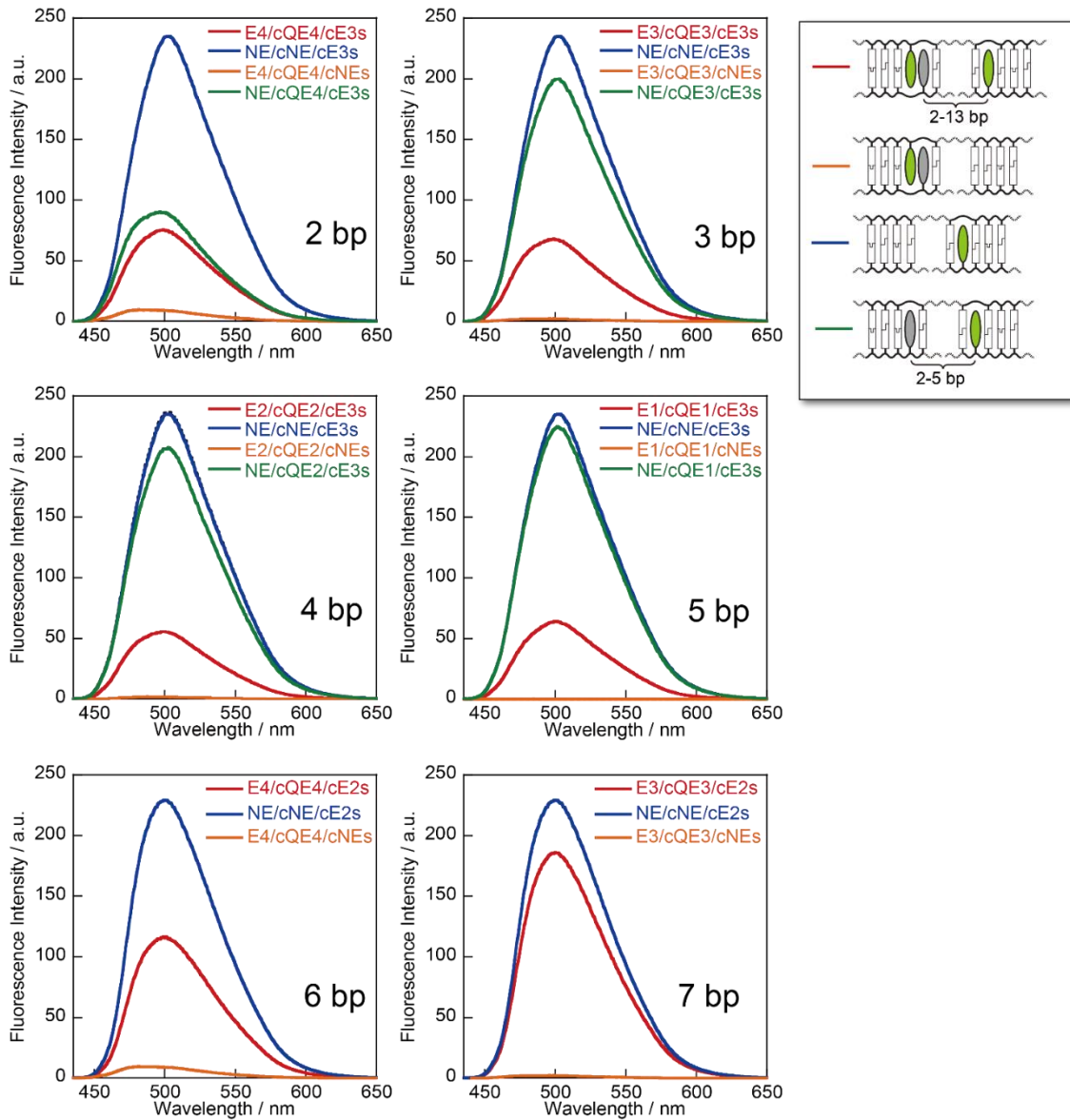
where P_n is probability of n th perylene being excited, k_{mn} is rate constant of energy transfer from m th perylene to n th perylene (see Figure 4-16a for the number of perylenes), and k_{dn} is rate constant of intrinsic decay of n th perylene. k_{nm} s were calculated from equations (5) to (7). Distances and orientation factors were calculated based on molecular modelling shown in Figure 4-16b. For simplicity, it was assumed that constants of forward transfers were equal to those of reverse transfer (i.e., $k_{mn} = k_{nm}$). k_{d2} , k_{d3} and k_{d4} were calculated from fluorescence lifetimes of **1E-2/cQ**, **1E-3/cQ** and **1E-4/cQ**, respectively. Since k_{d1} cannot be determined directly due to fast decay of **1E-1/cQ**, we estimated k_{d1} from its fluorescence intensity (Figure 4-14, green line). Since intensity of **1E-1/cQ** is about one thousand times lower than that of **1E-1/cN**, we used $1.00 \times 10^{11} \text{ s}^{-1}$ as k_{d1} . We also confirmed that small difference of k_{d1} does not significantly affect the results of the simulation. Rate constants used for the simulation are listed in Table S4-5. Differential equations were solved by using `lsode` function in GNU Octave 4.2.1. The simulated fluorescence lifetime of **4E/cQ** was calculated by fitting the biexponential curve to the averaged decay curve (Figure S4-4).

2-6 References

- [39] H. Kashida, T. Takatsu, T. Fujii, K. Sekiguchi, X. Liang, K. Niwa, T. Takase, Y. Yoshida, H. Asanuma, *Angew. Chem. Int. Ed.*, **2009**, *48*, 7044–7047.
- [40] H. Asanuma, K. Murayama, Y. Kamiya, H. Kashida, *Polym. J.*, **2016**, *49*, 279–289.
- [41] T. Fujii, H. Kashida, H. Asanuma, *Chem. Eur. J.*, **2009**, *15*, 10092–10102.
- [42] T. Kato, H. Kashida, H. Kishida, H. Yada, H. Okamoto, H. Asanuma, *J. Am. Chem. Soc.*, **2013**, *135*, 741–750.
- [43] H. Kashida, A. Kurihara, H. Kawai, H. Asanuma, *Nucleic Acids Res.* 2017, *45*, e105.
- [44] K. Pan, Et. Boulais, L. Yang, M. Bathe, *Nucleic Acids Res*, **2014**, *42*, 2159–2170 .
- [45] J. S. Melinger, A. Khachatryan, M. G. Ancona, S. B.-White, E. R. Goldman, C. M. Spillmann, I. L. Medintz, P. D. Cunningham, *ACS Photonics*, **2016**, *3*, 659–669.
- [46] H. S. Cho, H. Rhee, J. K. Song, C.K. Min, M. Takase, N. Aratani, S. Cho, A. Osuka, T. Joo, D. Kim, *J. Am. Chem. Soc.*, **2003**, *125*, 5849–5860.
- [47] É. Boulais, N. P. D. Sawaya, R. Venezian, A. Andreoni, J. L. Banal, T. Kondo, S. Mandal, S. Lin, G. S. Schlau-Cohe, N. W. Woodbury, H. Yan, A. Aspuru-Guzik, M. Bathe, *Nat. Mater.*, **2017**, *17*, 159–166.
- [48] A. Chenu, G. D. Scholes, *Annu. Rev. Phys. Chem.*, **2015**, *66*, 69–96.
- [49] H. Kashida, K. Morimoto, H. Asanuma, *Sci. Technol. Adv. Mater.*, **2016**, *17*, 267–273.
- [50] H.-Q. Peng, L.-Y. Niu, Y.-Z. Chen, L.-Z. Wu, C.-H. Tung, Q.-Z. Yang, *Chem. Rev.*, **2015**, *115*, 7502–7542.
- [51] R. E. Dickerson, H. R. Drew, *J. Mol. Biol.*, **1981**, *149*, 761–786.
- [52] R. E. Dickerson, H. R. Drew, B. N. Conner, R. M. Wing, A. V. Fratini, M. L. Kopka.

Science, **1982**, 216, 475–485.

4-7 Appendixes



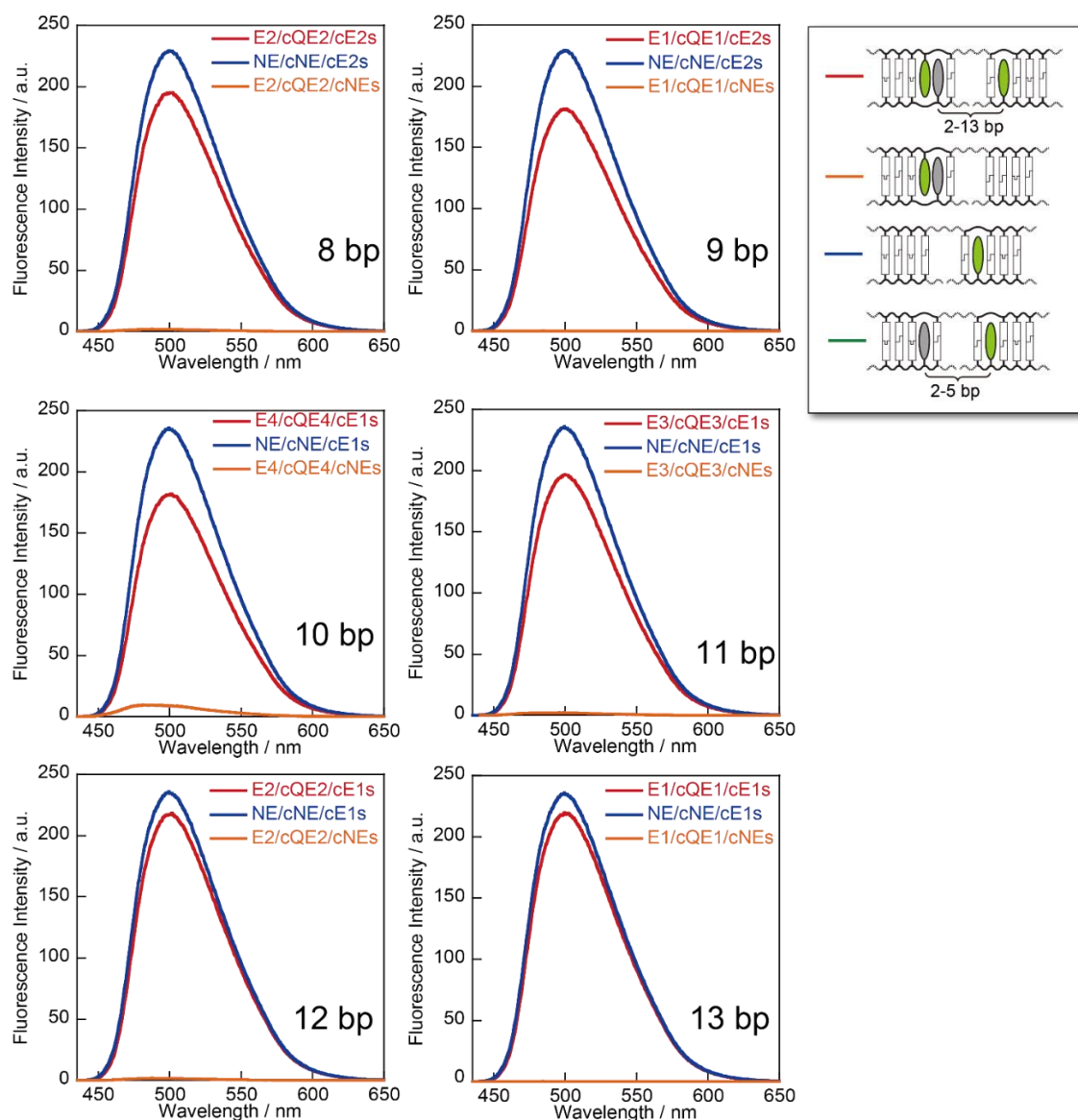
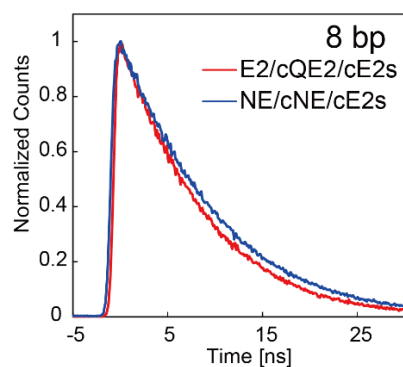
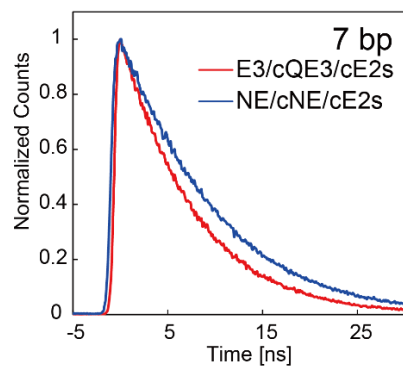
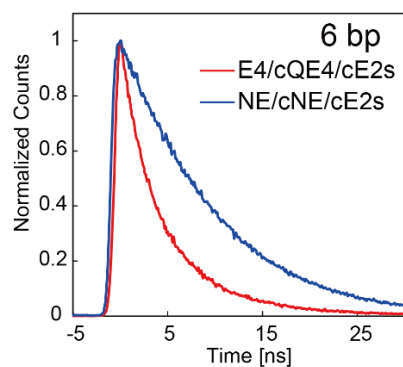
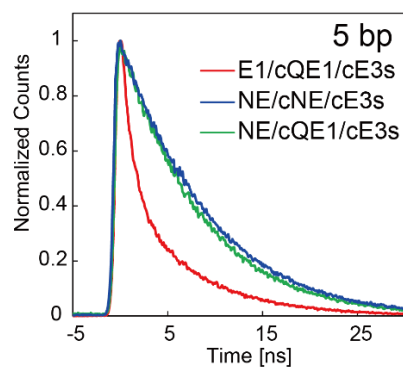
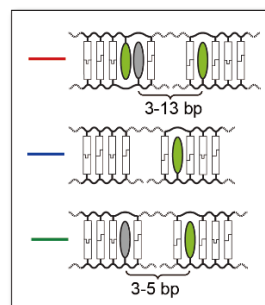
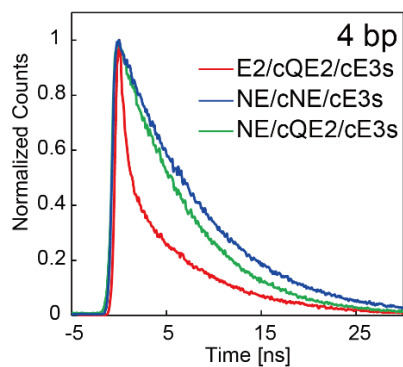
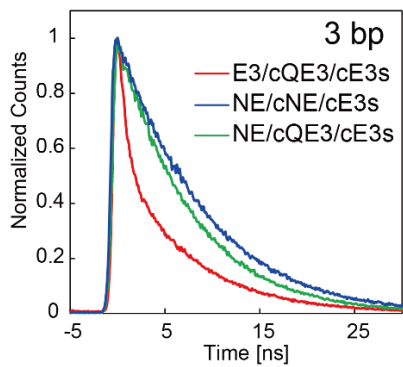


Figure S4-1. Comparison of emission spectra of EQ-E (red lines), E (blue lines), EQ (orange lines) and Q-E duplexes (green lines) at each distance.



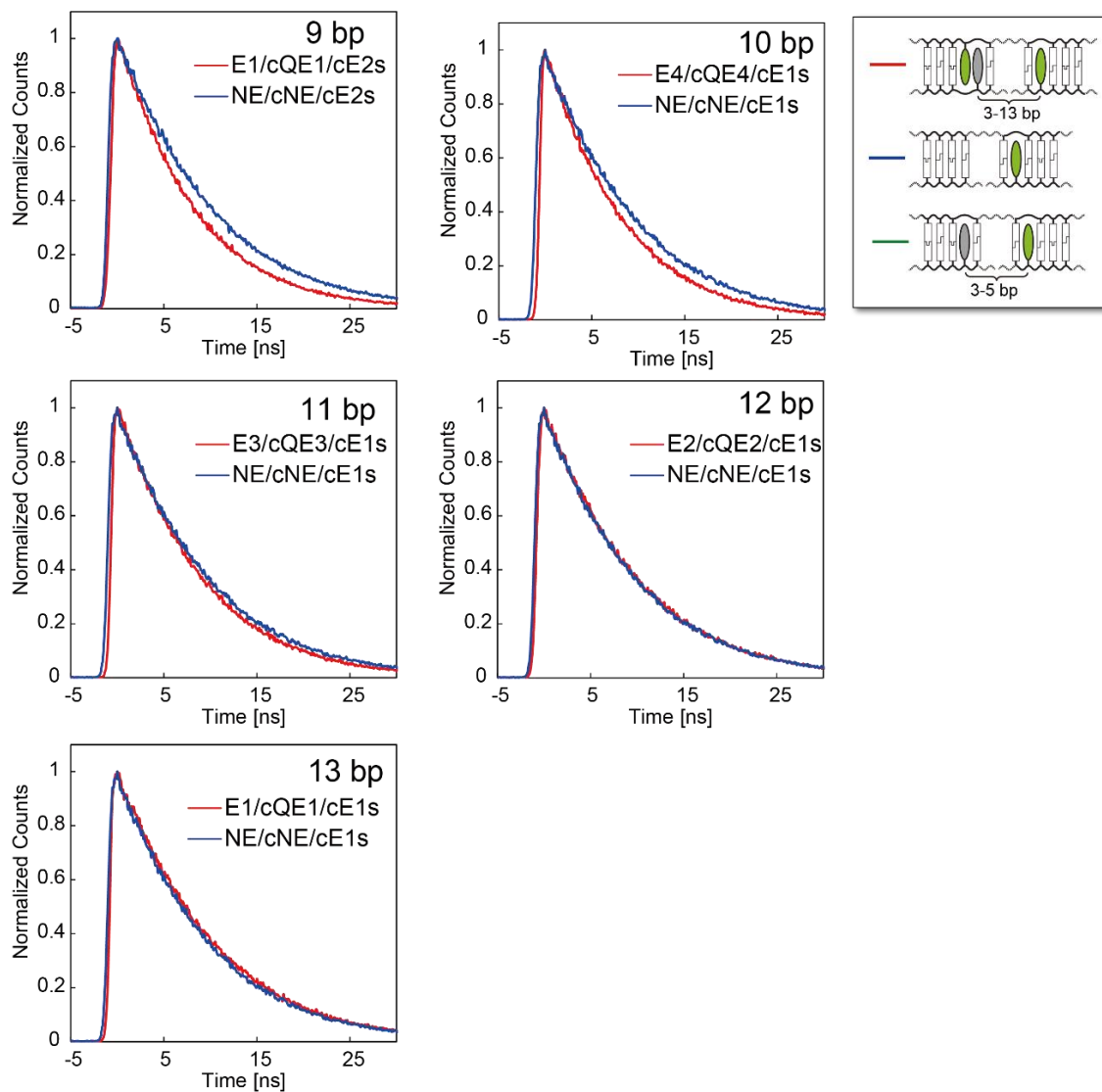


Figure S4-2. Fluorescence lifetime measurements of EQ-E (red lines), E (blue lines) and Q-E duplexes (green lines) at each distance.

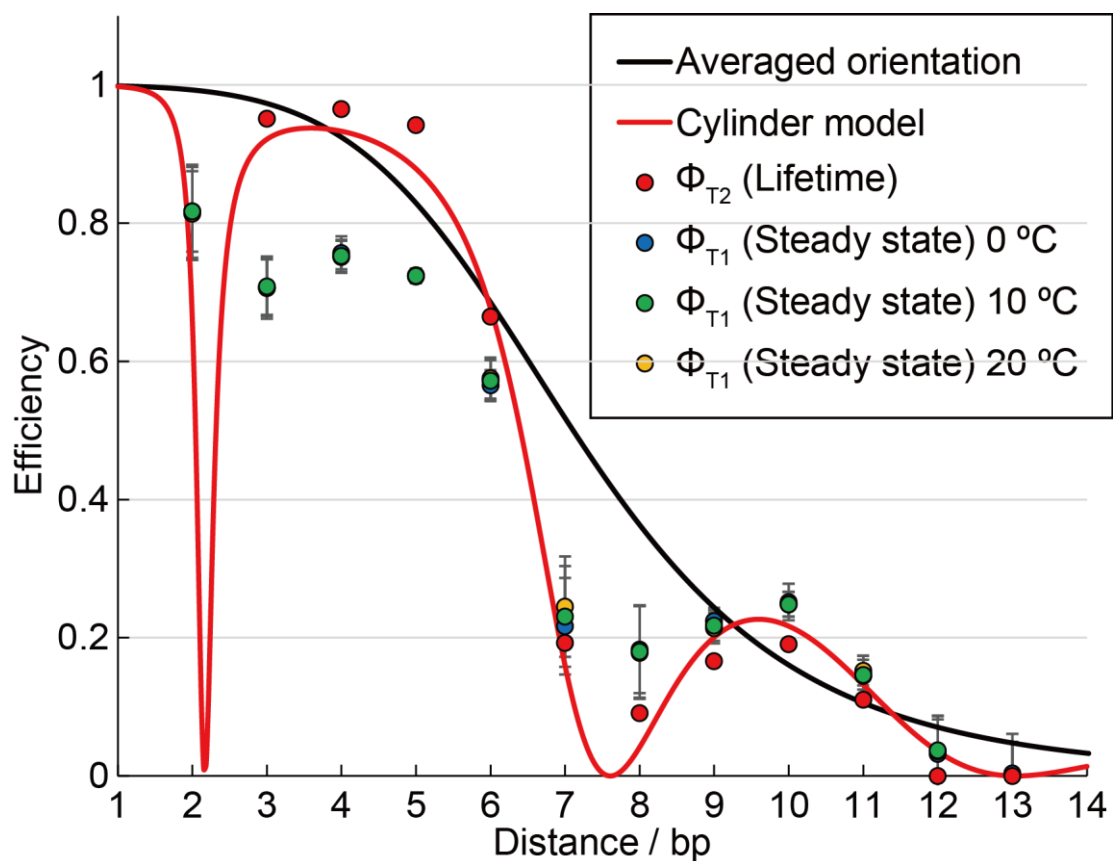


Figure S4-3. Effects of temperature on EM efficiency of perylene determined from steady-state fluorescence measurements.

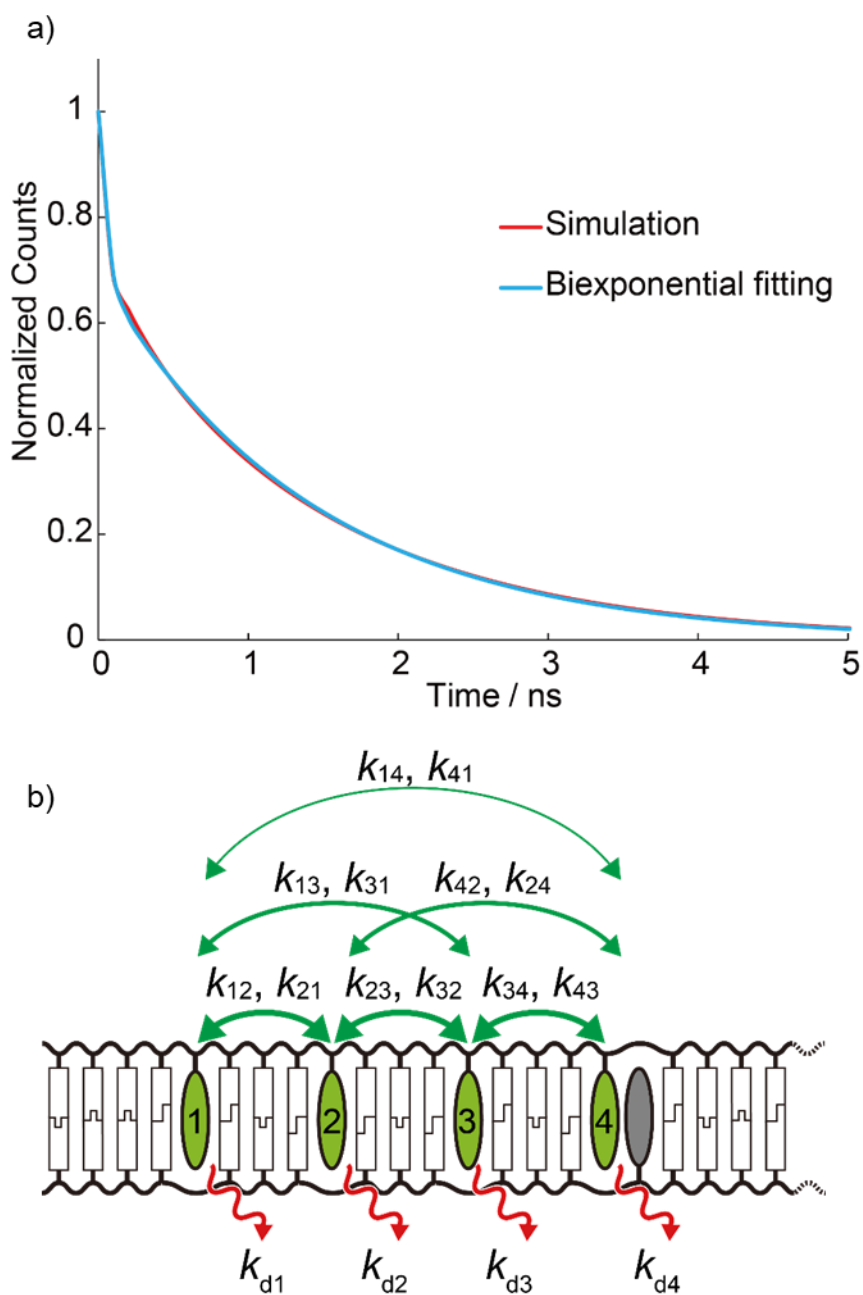


Figure S4-4. a) Comparison of the simulated decay curve of **4E/cQ** and a curve fit to the biexponential function. b) Illustration of **4E/cQ** and the rate constants of perylenes.

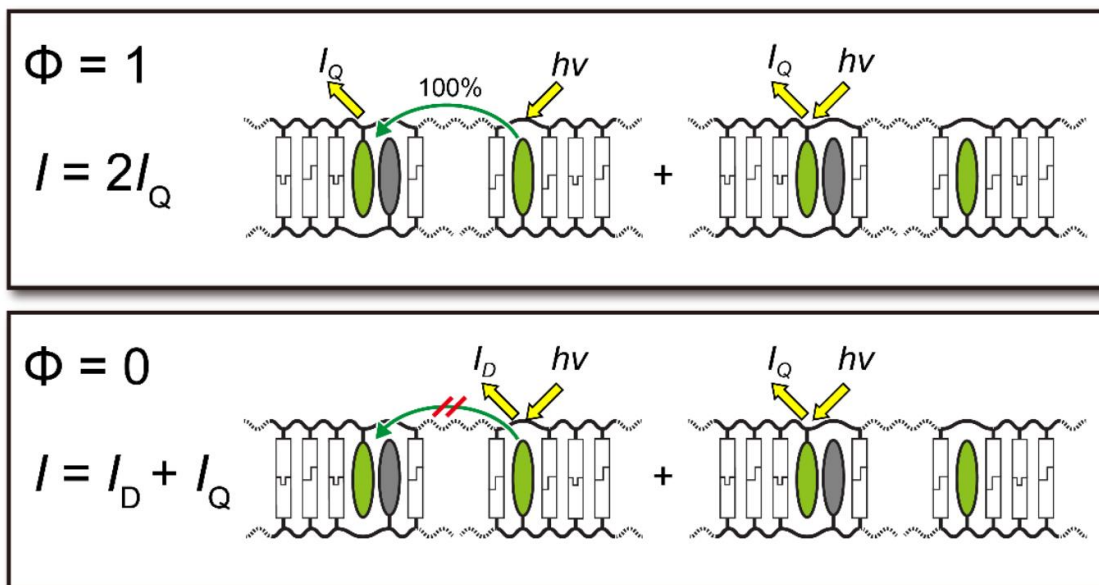


Figure S4-5. Schematic illustration of total emission observed from EQ-E duplex.

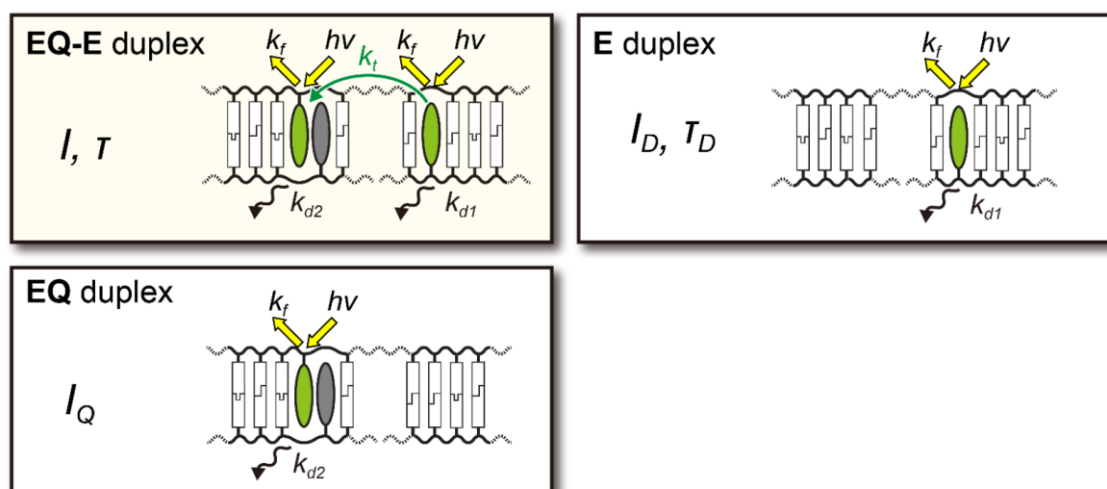
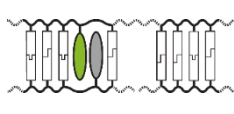


Figure S4-6. Schematic illustration of definition of rate constants.

Table S4-1. Sequences of EQ-E, E, EQ, Q-E duplexes prepared in this study.

	bp	Sequence	
 <p>EQ-E duplex</p>	2	E4 TGACTACGGTEGA ATACATACATACATACTGAT (5'→3')	
		cQE4/cE3s ACTGATGCCAQC TE TATGTATGTATGTATGACTA (3'←5')	
	3	E3 TGACTACGGETGA ATACATACATACATACTGAT (5'→3')	
		cQE3/cE3s ACTGATGCCQ ACTE TATGTATGTATGTATGACTA (3'←5')	
	4	E2 TGACTACGEGTGA ATACATACATACATACTGAT (5'→3')	
		cQE2/cE3s ACTGATGC QCACTE TATGTATGTATGTATGACTA (3'←5')	
	5	E1 TGACTACEGGTGA ATACATACATACATACTGAT (5'→3')	
		cQE1/cE3s ACTGATG QCCACTE TATGTATGTATGTATGACTA (3'←5')	
	6	E4 TGACTACGGTEGAATAC ATACATACATACTGAT (5'→3')	
		cQE4/cE2s ACTGATGCCA QCTT ATG ET ATGTATGTATGACTA (3'←5')	
	7	E3 TGACTACGGETGAATAC ATACATACATACTGAT (5'→3')	
		cQE3/cE2s ACTGATGCC QACTT ATG ET ATGTATGTATGACTA (3'←5')	
	8	E2 TGACTACGEGTGAATAC ATACATACATACTGAT (5'→3')	
	cQE2/cE2s ACTGATGC QCACTT ATG ET ATGTATGTATGACTA (3'←5')		
9	E1 TGACTACEGGTGAATAC ATACATACATACTGAT (5'→3')		
	cQE1/cE2s ACTGATG QCCACTT ATG ET ATGTATGTATGACTA (3'←5')		
10	E4 TGACTACGGTEGAATACATAC ATACATACTGAT (5'→3')		
	cQE4/cE1s ACTGATGCCA QCTT ATGTATG ET ATGTATGACTA (3'←5')		
11	E3 TGACTACGGETGAATACATAC ATACATACTGAT (5'→3')		
	cQE3/cE1s ACTGATGCC QACTT ATGTATG ET ATGTATGACTA (3'←5')		
12	E2 TGACTACGEGTGAATACATAC ATACATACTGAT (5'→3')		
	cQE2/cE1s ACTGATGC QCACTT ATGTATG ET ATGTATGACTA (3'←5')		
13	E1 TGACTACEGGTGAATACATAC ATACATACTGAT (5'→3')		
	cQE1/cE1s ACTGATG QCCACTT ATGTATG ET ATGTATGACTA (3'←5')		
 <p>E duplex</p>	-	NE TGACTACGGTGA ATACATACATACATACTGAT (5'→3')	
		cNE/cE3s ACTGATGCC ACTE TATGTATGTATGTATGACTA (3'←5')	
	-	NE TGACTACGGTGAATAC ATACATACATACTGAT (5'→3')	
	cNE/cE2s ACTGATGCC ACTT ATG ET ATGTATGTATGACTA (3'←5')		
-	NE TGACTACGGTGAATACATAC ATACATACTGAT (5'→3')		
	cNE/cE1s ACTGATGCC ACTT ATGTATG ET ATGTATGACTA (3'←5')		
 <p>EQ duplex</p>	-	E4 TGACTACGGTEGAATACATACATACATACTGAT (5'→3')	
		cQE4/cNEs ACTGATGCCA QCTT ATGTATGTATGTATGACTA (3'←5')	
	-	E3 TGACTACGGETGAATACATACATACATACTGAT (5'→3')	
		cQE3/cNEs ACTGATGCC QACTT ATGTATGTATGTATGACTA (3'←5')	
	-	E2 TGACTACGEGTGAATACATACATACATACTGAT (5'→3')	
		cQE2/cNEs ACTGATGC QCACTT ATGTATGTATGTATGACTA (3'←5')	
	-	E1 TGACTACEGGTGAATACATACATACATACTGAT (5'→3')	
	cQE1/cNEs ACTGATG QCCACTT ATGTATGTATGTATGACTA (3'←5')		
2	NE TGACTACGGT GA ATACATACATACATACTGAT (5'→3')		
	cQE4/cE3s ACTGATGCCA QC T ET ATGTATGTATGTATGACTA (3'←5')		
3	NE TGACTACGG TGA ATACATACATACATACTGAT (5'→3')		
	cQE3/cE3s ACTGATGCC QA C TE TATGTATGTATGTATGACTA (3'←5')		



Q-E duplex	4	NE cQE2/cE3s	TGACTACG GTGA ATACATACATACATACTGAT (5'→3') ACTGATGCQCACT ETATGTATGTATGTATGACTA (3'←5')
	5	NE cQE1/cE3s	TGACTAC GGTGA ATACATACATACATACTGAT (5'→3') ACTGATGCQCACT ETATGTATGTATGTATGACTA (3'←5')
	6	NE cQE4/cE2s	TGACTACGGT GAATAC ATACATACATACTGAT (5'→3') ACTGATGCCA CTTATGETATGTATGTATGACTA (3'←5')
	7	NE cQE3/cE2s	TGACTACGG TGAATAC ATACATACATACTGAT (5'→3') ACTGATGCCA CTTATGETATGTATGTATGACTA (3'←5')
	8	NE cQE2/cE2s	TGACTACG GTGAATAC ATACATACATACTGAT (5'→3') ACTGATGCQCACT TTATGETATGTATGTATGACTA (3'←5')
	9	NE cQE1/cE2s	TGACTAC GGTGAATAC ATACATACATACTGAT (5'→3') ACTGATGCQCACT TTATGETATGTATGTATGACTA (3'←5')

Table S4-2. Sequences of EQ-E, E, EQ, Q-E duplexes prepared in this study.

	bp	Sequence	τ_1 (ns)	τ_2 (ns)	α_1	α_2	χ^2	Φ_{T1}	Φ_{T2}
	2	E4/cQE4/cE3s	-*	-*	-	-	-	0.82	-
	3	E3/cQE3/cE3s	0.36	7.51	0.67	0.33	1.22	0.71	0.96
	4	E2/cQE2/cE3s	0.25	7.63	0.58	0.42	1.08	0.76	0.97
	5	E1/cQE1/cE3s	0.43	7.27	0.56	0.44	1.08	0.72	0.95
	6	E4/cQE4/cE2s	3.12	7.45	0.64	0.36	1.20	0.57	0.66
EQ-E duplex	7	E3/cQE3/cE2s	7.51	-	1	-	1.10	0.22	0.19
	8	E2/cQE2/cE2s	8.46	-	1	-	1.31	0.18	0.09
	9	E1/cQE1/cE2s	7.76	-	1	-	1.20	0.22	0.17
	10	E4/cQE4/cE1s	7.88	-	1	-	1.22	0.25	0.19
	11	E3/cQE3/cE1s	8.66	-	1	-	1.22	0.15	0.11
	12	E2/cQE2/cE1s	9.74	-	1	-	1.18	0.03	0.00
	13	E1/cQE1/cE1s	9.74	-	1	-	1.18	0.00	0.00
E duplex	-	NE/cNE/cE3s	8.87	-	1	-	1.20	-	-
	-	NE/cNE/cE2s	9.31	-	1	-	1.32	-	-
	-	NE/cNE/cE1s	9.74	-	1	-	1.14	-	-
Q-E duplex	3	NE/cQE3/cE3s	7.33	-	1	-	1.06	-	-
	4	NE/cQE2/cE3s	7.27	-	1	-	1.17	-	-
	5	NE/cQE1/cE3s	7.39	-	1	-	1.27	-	-

Table S4-3. Sequences of EQ-E, E, EQ, Q-E duplexes prepared in this study.

Sequence			
	4E cQ	GCCTETGAEAGAETGAETGCTACGATGTTCTAAATGCC CGGA ACT TCT ACT Q ACGATGCTACAAGATTACGG	(5'→3') (3'←5')
	1E-1 cQ	GCCTTGAAGATGAETGCTACGATGTTCTAAATGCC CGGA ACTTCTACTQ ACGATGCTACAAGATTACGG	(5'→3') (3'←5')
	1E-2 cQ	GCCTTGAAGAETGA TGCTACGATGTTCTAAATGCC CGGA ACTTCT ACTQ ACGATGCTACAAGATTACGG	(5'→3') (3'←5')
	1E-3 cQ	GCCTTGAEGATGA TGCTACGATGTTCTAAATGCC CGGA ACT TCTACTQ ACGATGCTACAAGATTACGG	(5'→3') (3'←5')
	1E-4 cQ	GCCTETGAAGATGA TGCTACGATGTTCTAAATGCC CGGA ACTTCTACTQ ACGATGCTACAAGATTACGG	(5'→3') (3'←5')
	4E cN	GCCTETGAEAGAETGAETGCTACGATGTTCTAAATGCC CGGA ACT TCT ACT ACGATGCTACAAGATTACGG	(5'→3') (3'←5')
	1E-1 cN	GCCTTGAAGATGAETGCTACGATGTTCTAAATGCC CGGA ACTTCTACT ACGATGCTACAAGATTACGG	(5'→3') (3'←5')
	1E-2 cN	GCCTTGAAGAETGATGCTACGATGTTCTAAATGCC CGGA ACTTCT ACTACGATGCTACAAGATTACGG	(5'→3') (3'←5')
	1E-3 cN	GCCTTGAEGATGATGCTACGATGTTCTAAATGCC CGGA ACT TCTACTACGATGCTACAAGATTACGG	(5'→3') (3'←5')
	1E-4 cN	GCCTETGAAGATGATGCTACGATGTTCTAAATGCC CGGA ACTTCTACTACGATGCTACAAGATTACGG	(5'→3') (3'←5')

Table S4-4. Duplex stability and lifetimes of duplexes tethering perylene.



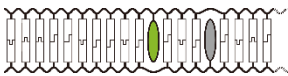







		$T_m / ^\circ\text{C}$	τ_1 (ns)	τ_2 (ns)	α_1	α_2	χ^2
4E/cQ		80.9	1.19	3.80	0.27	0.73	1.06
1E-1/cQ		74.2	-	-	-	-	-
1E-2/cQ		73.4	8.06	-	1	-	1.03
1E-3/cQ		74.4	9.74	-	1	-	1.23
1E-4/cQ		74.2	9.22	-	1	-	1.28
4E/cN		77.9	8.40	-	1	-	1.23
1E-1/cN		71.6	9.39	-	1	-	1.01
1E-2/cN		71.5	9.05	-	1	-	1.17
1E-3/cN		72.6	9.74	-	1	-	1.28
1E-4/cN		72.3	8.36	-	1	-	1.20

Table S4-5. Rate constants of perylenes used for the simulation.

k_{d1}	$1.00 \times 10^{11} \text{ s}^{-1}$
k_{d2}	$1.24 \times 10^8 \text{ s}^{-1}$
k_{d3}	$1.03 \times 10^8 \text{ s}^{-1}$
k_{d4}	$1.08 \times 10^8 \text{ s}^{-1}$
k_{12}	$2.94 \times 10^9 \text{ s}^{-1}$
k_{13}	$1.63 \times 10^8 \text{ s}^{-1}$
k_{14}	$2.32 \times 10^7 \text{ s}^{-1}$
k_{21}	$2.94 \times 10^9 \text{ s}^{-1}$
k_{23}	$2.20 \times 10^9 \text{ s}^{-1}$
k_{24}	$2.05 \times 10^8 \text{ s}^{-1}$
k_{31}	$1.63 \times 10^8 \text{ s}^{-1}$
k_{32}	$2.20 \times 10^9 \text{ s}^{-1}$
k_{34}	$1.32 \times 10^9 \text{ s}^{-1}$
k_{41}	$2.32 \times 10^7 \text{ s}^{-1}$
k_{42}	$2.05 \times 10^8 \text{ s}^{-1}$
k_{43}	$1.32 \times 10^9 \text{ s}^{-1}$

Chapter 5. Quantitative analyses of homo FRET between two pyrenes

5-1 Abstract

In chapter 5, we report energy transfer between the identical chromophores (homo FRET), following chapter 4. However, we treat pyrene as another chromophore, and the big difference is that we analyze homo FRET that occurs at the same time as hetero FRET.

Homo-FRET has been difficult to analyze since neither emission intensity nor lifetime changes with the occurrence of energy transfer. Herein we used a DNA scaffold and a quencher, anthraquinone, to analyze homo FRET between pyrene moieties. Homo-FRET was detected by monitoring quenching of pyrene emission and the decrease in the fluorescence lifetime of pyrene. Homo-FRET efficiencies could be calculated by excluding effects of hetero FRET. The experimentally determined efficiencies showed an excellent agreement with Förster theory. These results will inform design of novel molecular probes and light-harvesting antennae.

5-2 Introduction

In the case of energy transfer between two different chromophores, a process known as hetero-FRET, FRET efficiency can be easily determined by monitoring emission

intensity and/or lifetime. In sharp contrast, FRET between identical molecules, or homo-FRET, is usually difficult to analyze because neither fluorescence intensity nor lifetime are altered due to the energy transfer.

In chapter 4, we report a method that employs a DNA scaffold to analyze homo-FRET of perylene using a quencher.^[1] Our basic design is shown in Figure 5-1a. Two fluorophores and a quencher are introduced into the DNA scaffold. As a result, the quenched fluorophore works not as a donor but as an acceptor. Herein we used this system to analyze homo-FRET between pyrene moieties. Pyrene is widely used due to its high quantum yield and distinct excimer emission upon aggregation. Although several groups, including ours, have incorporated multiple pyrene moieties into DNA to prepare pyrene clusters^[2], homo-FRET of pyrene has not been investigated in detail.

Anthraquinone was previously reported to be a good quencher of pyrene.^[3] Pyrene and anthraquinone were introduced into DNA through D-threoninol because this linker allows control of the orientation of molecules.^[4] In contrast to perylene, hetero-FRET from pyrene to anthraquinone must be taken into account because the absorption spectrum of anthraquinone has a small overlap with emission spectrum of pyrene (Figure 5-1a). In order to assess homo-FRET efficiency quantitatively, a series of duplexes were prepared (Table S5-1). Each set in the series involved four duplexes (Figure 5-1b). The **PQ-P**

duplex has a pyrene-anthraquinone pair that are not separated by any base pairs and a pyrene separated from the anthraquinone by 2 to 13 base pairs; in these duplexes both homo- and hetero-FRET occur. The **P** duplex that has a single pyrene was used as a control since self-quenching does not occur with pyrene residues are separated by more than 1bp^[2-1]. The **PQ** duplex has an adjacent pyrene-anthraquinone pair. Finally, the **Q-P** duplex contains one anthraquinone and one pyrene separated by 2 to 13 base pairs. When two dyes are introduced into base pairing position as **PQ** duplex, each dye is stacked with the neighboring base pair at 5' sides as illustrated in Figure 5-1a^[9]. Therefore, the distance between pyrene and anthraquinone is the same as that between **PQ-P** and **Q-P** duplexes. These duplexes were prepared by hybridizing three strands. In chapter2, we report that orientation dependence of hetero-FRET kept intact in the case of nicked duplex. The number of base pairs between two pyrenes can be changed from 2 bp to 13 bp by hybridizing strands tethering dyes at different positions (Table S5-1).

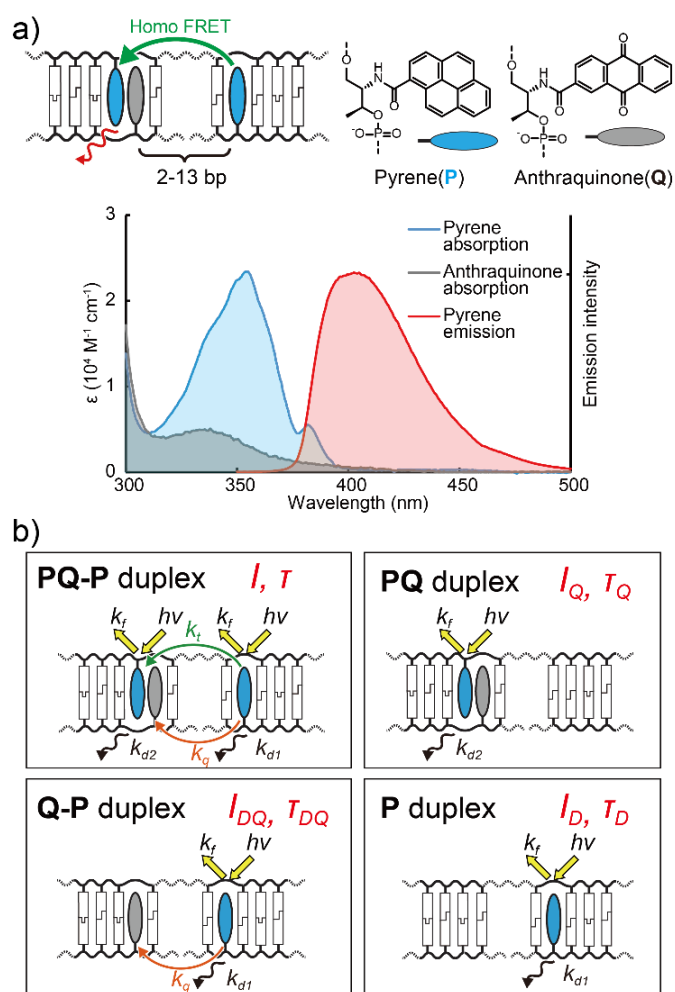


Figure 5-1.

a) Schematic illustration of analyses of homo-FRET using DNA scaffolds. UV/Vis absorption and normalized emission spectra of pyrene and anthraquinone in DNA are also shown. b) Illustration of **PQ-P**, **PQ**, **Q-P**, and **P** duplexes. Photochemical parameters of each duplex are also shown schematically.

5-3 Results and discussions

5-3-1 Melting temperatures (T_m s) of duplexes

Melting analyses revealed that all duplexes had melting temperatures (T_m s) higher

than 40°C (Table S2), indicating that the duplexes are stably formed below 20°C. Because the dyes are intercalated between base pairs, the T_{ms} of duplexes containing dyes were higher than the T_{ms} of the native duplexes.

5-3-2 Emission spectra of each set of duplexes

Emission spectra of each set of duplexes with 2 to 13 base pairs between dyes were measured (representative results of duplexes with dyes separated by 5 base pairs are shown in Figure 5-2).

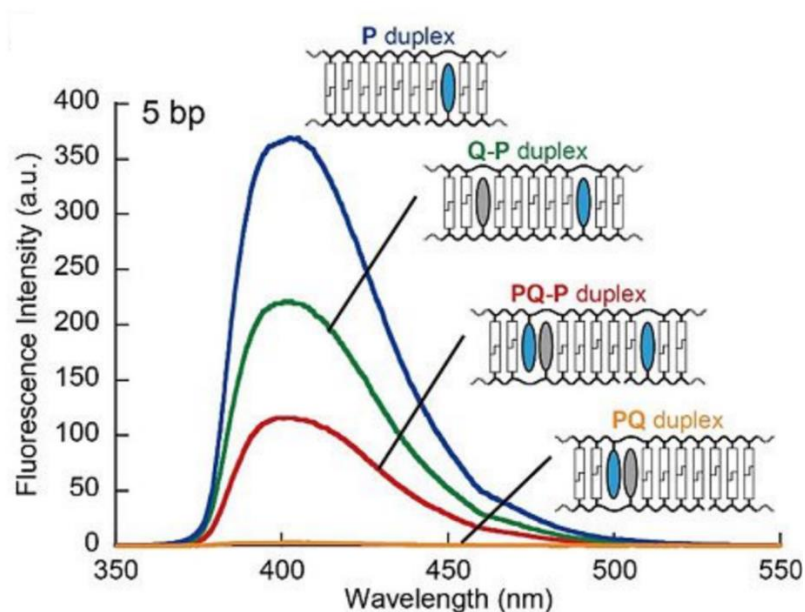


Figure 5-2.

Emission spectra of **PQ-P**, **PQ**, **Q-P**, and **P** duplexes with 5-base-pair separation.

The **P** duplexes had the highest emission, whereas **PQ** duplexes showed no emission indicating that anthraquinone is an efficient quencher of pyrene (Figure 5-3).

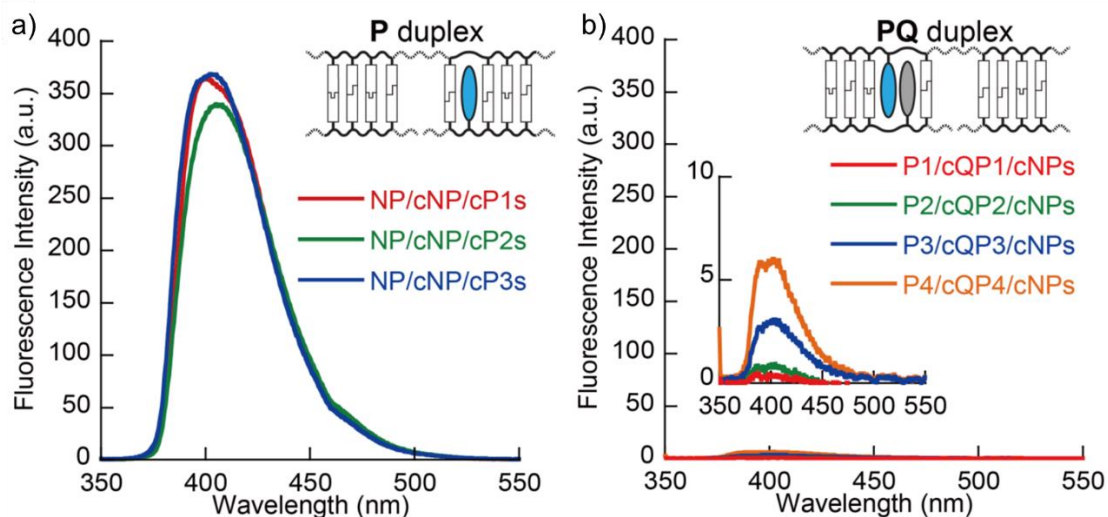


Figure 5-3.

Emission spectra of (a) **P** and (b) **PQ** duplexes. Magnified spectra of **PQ** duplexes are also shown

The quenching is probably due to electronic coupling and/or excitonic interaction because slight hypochromism was observed upon clustering (Figure 5-4).^[6]

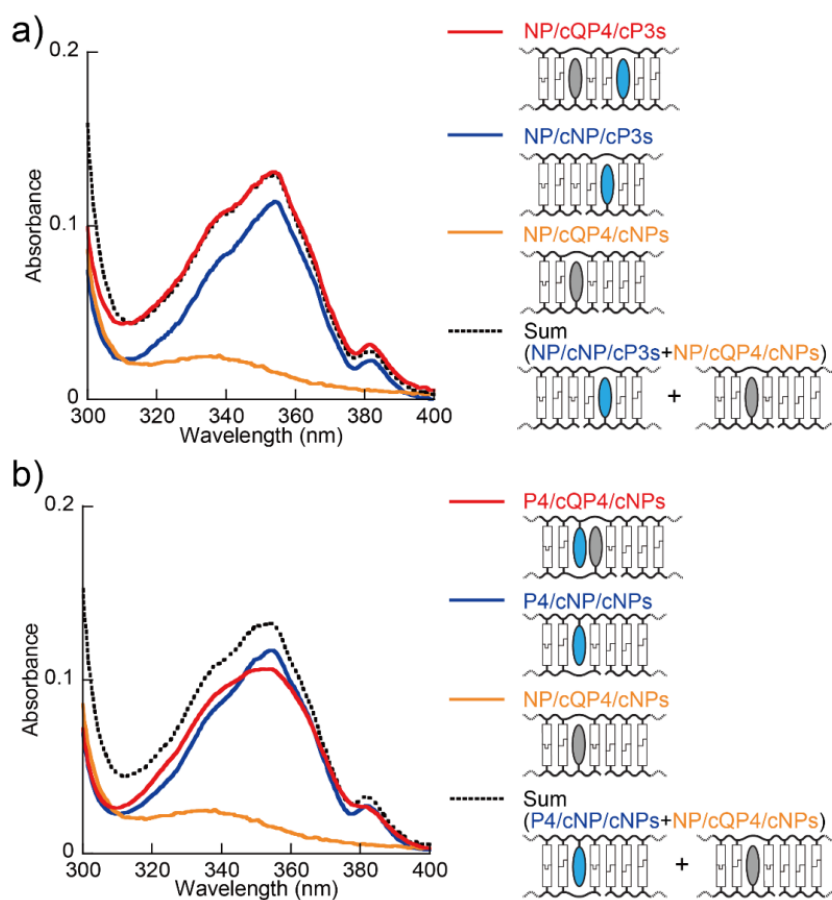


Figure 5-4.

Effects of excitonic interaction between pyrene and anthraquinone on the absorption spectra in the case of (a) 2-base-pair separation and (b) cluster formation.

The **Q-P** duplexes showed lower emission than **P** duplexes due to hetero-FRET from pyrene to anthraquinone. The **PQ-P** duplexes exhibited even lower emission than **Q-P** duplex indicative of homo-FRET between the two pyrenes. The degree of quenching depended on the number of base pairs separating the anthraquinone-pyrene pair from the lone pyrene (Figure S5-1). When the number of separating base pairs was 12 or 13, the

intensity of **PQ-P** duplex was only slightly lower than that of corresponding **Q-P** duplex.

5-3-3 Lifetime measurements of each set of duplexes

The evidence of homo-FRET was also obtained from lifetime measurements.

Representative results with the 5-base-pair separation are shown in Figure 5-5.

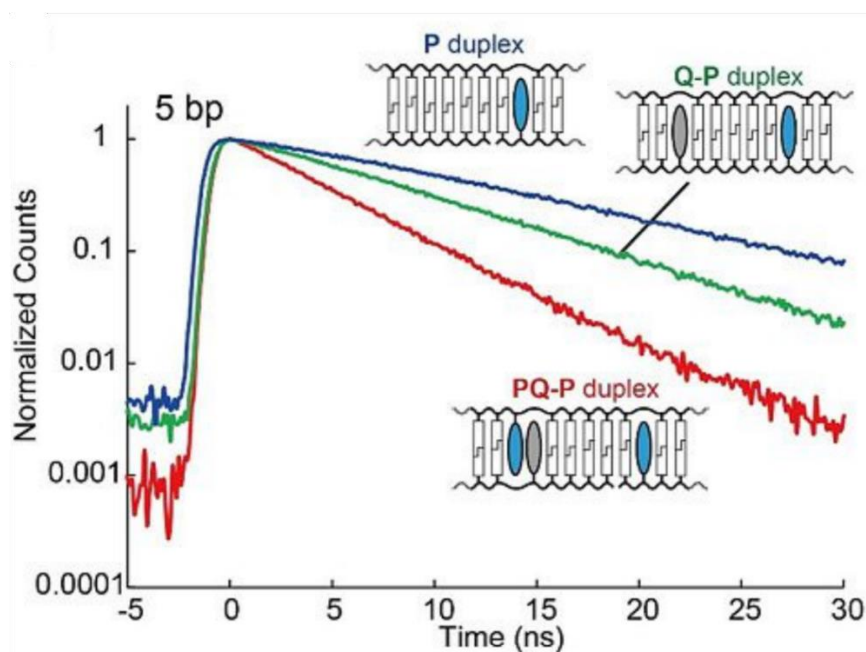


Figure 5-5.

Fluorescence decay curves of **PQ-P**, **PQ**, **Q-P**, and **P** duplexes with 5-base-pair separation.

The control **P** duplex with 5- base-pair separation had a fluorescent lifetime of 11.1 ns. The **Q-P** duplex decayed more rapidly with a lifetime of 7.76 ns; this indicated that there is slight hetero-FRET between pyrene and anthraquinone. The lifetime further decreased to 4.56 ns for the **PQ-P** duplex. The difference between **Q-P** and **PQ-P** duplexes shows

that homo-FRET occurs efficiently when 5 base pairs separate the dye pair from the lone pyrene. The lifetime of **PQ** duplex could not be determined because of extremely fast decay; this was the case for all **PQ** duplexes. The data for all **P**, **Q-P**, and **PQ-P** duplexes are shown in Figure S5-2 and lifetimes are listed in Table 5-1.

Table 5-1. Lifetimes of PQ-P duplexes. ^[a]

bp	PQ-P duplex					Q-P duplex					P duplex		
	τ_1 (ns)	τ_2 (ns)	α_1	α_2	χ^2	τ_{DQ1} (ns)	τ_{DQ2} (ns)	α_1	α_2	χ^2	τ_D (ns)	α_1	χ^2
2	-[c]	-[c]	-	-	-	-[c]	-[c]	-	-	-	11.12	1	1.17
3	1.28	5.08	0.97	0.03	1.06	1.74	5.08	0.71	0.29	0.92	10.25	1	1.11
4	5.21	-	1	-	1.09	6.42	-	1	-	1.20	10.69	1	1.08
5	4.56	-	1	-	1.03	7.76	-	1	-	1.14	11.12	1	1.17
6	5.29	-	1	-	1.03	7.82	-	1	-	1.12	10.25	1	1.11
7	7.21	-	1	-	1.29	9.13	-	1	-	1.15	10.69	1	1.08
8	10.00	-	1	-	1.14	10.60	-	1	-	1.17	11.12	1	1.17
9	9.65	-	1	-	1.24	9.74	-	1	-	1.21	10.25	1	1.11
10	10.17	-	1	-	1.24	10.60	-	1	-	1.26	10.69	1	1.08
11	10.25	-	1	-	1.06	10.94	-	1	-	1.19	11.12	1	1.17
12	9.91	-	1	-	1.22	10.51	-	1	-	1.30	10.25	1	1.11
13	10.08	-	1	-	1.12	10.51	-	1	-	1.25	10.69	1	1.08

[a] α is amplitude of lifetime component and χ^2 is chi-squared value obtained by the fitting program. [b] Number of base pairs separating the pyrene–anthraquinone pair from the lone pyrene. [c] Lifetimes could not be determined due to fast decay.

For duplexes with 3-base-pair separation, the decay curves had two components. The

longer fraction was attributed to emission from pyrene in excess single strands. Therefore, we used the shorter lifetimes for the calculation of FRET efficiency. As the number of base pairs increased, the difference between lifetimes of **Q-P** and **P** duplexes decreased, indicating the decline of hetero-FRET efficiency. The difference between **PQ-P** and **Q-P** duplexes also decreased, demonstrating that homo-FRET efficiency decreased as the number of base pairs increased.

5-3-4 Quantitative analysis of energy migration between two pyrenes

The observed FRET efficiencies are due to both homo-FRET and hetero-FRET. In our duplex series, hetero-FRET efficiencies also depend on the number of base pairs. Therefore, we calculated the actual homo-FRET efficiencies by excluding the effects of hetero-FRET as detailed in the Experimental Section. Table 5-2 lists the efficiencies of homo-FRET, steady-state fluorescence values (Φ_{T1}), and fluorescent lifetimes (Φ_{T2}). The homo-FRET efficiency decreased as the number of base pairs increased; however, non-monotonous behavior was observed. For example, Φ_{T1} and Φ_{T2} of the set of duplexes with 5 base pairs between the dye pair and the isolated pyrene were higher than those of the duplexes with 4-base-pair spacing. Minima of efficiency were observed at 4- and 9-base-pair spacings. This 5- base-pair cycle corresponds to a half-turn of B-form duplex. Thus,

homo-FRET between pyrenes strongly depends on the relative orientations of dyes, similarly to hetero-FRET as reported in previous reports. ^[4a,7]

Table 5-2. Homo-FRET efficiencies PQ-P duplexes.

bp	Φ_{T1}	Φ_{T2}
2	0.95 ± 0.02	-
3	0.73 ± 0.03	0.68 ± 0.02
4	0.43 ± 0.03	0.28 ± 0.01
5	0.62 ± 0.00	0.50 ± 0.00
6	0.43 ± 0.04	0.38 ± 0.01
7	0.31 ± 0.04	0.24 ± 0.01
8	0.09 ± 0.01	0.06 ± 0.01
9	0.01 ± 0.01	0.01 ± 0.01
10	0.02 ± 0.02	0.04 ± 0.01
11	0.12 ± 0.05	0.06 ± 0.01
12	0.06 ± 0.03	0.06 ± 0.01
13	0.04 ± 0.01	0.04 ± 0.01

5-3-5 Comparison with Förster theory

The experimentally determined homo-FRET efficiencies were compared with values calculated from Förster theory. Experimental efficiencies showed excellent agreement with theoretical values based on fixed orientation (Figure 5-6).

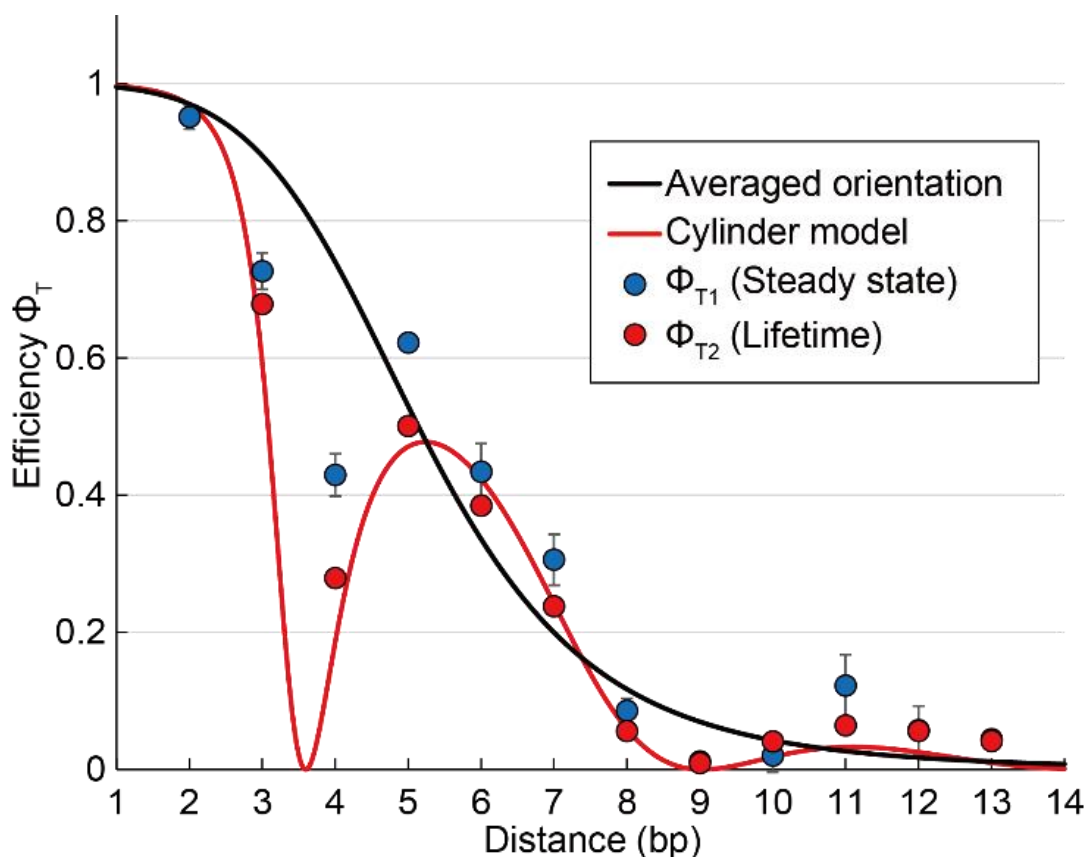


Figure 5-6.

Plots of homo-FRET efficiency versus the number of base pairs between the two pyrene moieties. Experimentally obtained efficiencies from emission intensities and lifetimes are shown in blue and red circles, respectively. Theoretically calculated values assuming random or fixed orientations are shown in black and red lines, respectively. Error bars are standard deviations of three independent fluorescence measurements.

There was better agreement with Φ_{T2} than Φ_{T1} . In the case of steady-state measurements, emission from species other than correctly formed duplex could affect FRET efficiency. For example, the presence of excess amount of quenched pyrene would raise apparent Φ_{T1} . Such effects can be excluded with lifetime measurements because lifetimes of such

species are usually different from those of correctly organized species; lifetimes of **PQ** duplexes are much shorter than those of **PQ-P** duplexes. Φ_{T1} was also determined at different temperatures and values were within experimental error and consistent with theory (Figure S5-3). Based on these results, we concluded that homo-FRET between pyrenes strictly obeys Förster theory. Förster distance assuming a random orientation of pyrene homo-FRET was calculated to be 22.9 Å, whereas that of perylene homo-FRET was 29.6 Å. The longer distance for perylene is due to the larger overlap between absorption and emission spectra than occurs in the spectra of pyrene (Chapter 4 Figure 4-6). These results indicate that homo-FRET efficiency can be tuned by selecting fluorophores with appropriate Stokes' shifts.

5-4 Conclusions

In conclusion, homo-FRET between pyrenes was investigated in detail using DNA scaffold. In contrast to perylene homo-FRET, which we evaluated in chapter 4, for pyrene, the hetero-FRET from pyrene to anthraquinone must be taken into account. We calculated homo-FRET efficiencies by ruling out effects of hetero-FRET. The calculated efficiencies agreed with calculated values based on Förster theory. These results clearly demonstrate that homo-FRET can be correctly evaluated even if hetero-FRET simultaneously occurs. Since the method that employs DNA scaffolds is easy and robust, it can be used to evaluate homo-FRET of various fluorophores quantitatively. Homo-FRET is a key process in natural and artificial photosynthesis and in molecular probes and photonic circuits in which energy can be transported without losing photon energy. The results described here should be useful in design of artificial light harvesting antennae and molecular probes.

5-5 Experimental section

Oligonucleotide synthesis

All conventional phosphoramidite monomers, CPG columns, reagents for DNA synthesis, and Poly-Pak II cartridges were purchased from Glen Research. Other reagents for the synthesis of phosphoramidite monomers were purchased from Tokyo Chemical Industry, Wako, and Aldrich. Native oligodeoxyribonucleotides (ODNs) were purchased from Integrated DNA Technologies or Hokkaido System Science Co., Ltd. ODNs tethering perylene or anthraquinone were synthesized on an automated DNA synthesizer (H-8-SE, Gene World). ODNs were purified by reversed-phase HPLC and characterized by MALDI-TOF MS (Autoflex II, Bruker Daltonics) and HPLC.

The MALDI-TOF MS data for the modified DNA were as follows: **P1**: Obsd. 8686 (Calcd. for [**P1**+H⁺]: 8686). **P2**: Obsd. 8684 (Calcd. for [**P2**+ H⁺]: 8686). **P3**: Obsd. 8686 (Calcd. for [**P3**+ H⁺]: 8686). **P4**: Obsd. 8687 (Calcd. for [**P4**+ H⁺]:8686). **cQP1**: Obsd. 4630 (Calcd. for [**cQP1**+ H⁺]: 4629). **cQP2**: Obsd. 4632 (Calcd. for [**cQP2**+H⁺]: 4629). **cQP3**: Obsd. 4630 (Calcd. for [**cQP3**+ H⁺]: 4629). **cQP4**: Obsd. 4629 (Calcd. for [**cQP4**+H⁺]: 4629). **cP1s**: Obsd. 4369 (Calcd. for [**cP1s**+H⁺]: 4370). **cE2s**: Obsd. 4367 (Calcd. for [**cP2s**+H⁺]: 4370). **cP3s**: Obsd. 4371 (Calcd. For [**cP3s**+ H⁺]: 4370).

Fluorescence measurements

Fluorescence spectra were measured on JASCO models FP-6500 or FP-8500. The excitation wavelength was 345 nm. Band widths were 3 nm (FP-6500) or 2.5 nm (FP-8500) for excitation and emission. Before measurements, sample solutions containing DNA duplex were heated at 80 °C, then slowly cooled down to 0 °C at a rate of 4 °C min⁻¹. Fluorescence spectra were measured at 80 to 0 °C at 10 °C intervals after 4 min incubations. Emission spectra were measured at 0 °C. Sample solutions contained 100 mM NaCl, 10 mM phosphate buffer, pH 7.0. Concentrations of ODNs were 1.0 μM for ODNs tethering pyrene (**P1-4** and **cP1s-cP3s**) and 1.5 μM for quencher strands (**cQP1-4** and **cNP**). For control measurements, concentrations of native strands **NP** and **cNP** were 1.0 μM and concentrations of **cNPs** strands were 1.5 μM. Fluorescence spectra were not normalized by extinction coefficients.

Fluorescence lifetime measurements

A pulse at 780 nm was generated by a Ti:sapphire laser system (Spectra-Physics, Tsunami; 3950-L2S, fwhm 150 fs, 82 MHz). The repetition rate was reduced to 4 MHz by a pulse selector (Spectra-Physics Model 3980). The exciting source was a laser with

wavelength converted to 390 nm by passage through SHG crystals. Fluorescence emission was captured by a streak camera (Hamamatsu C4334) operating in photon counting mode. Measurements were performed at room temperature. Decay curves were obtained from the integration of the photon counts in the spectral region from 400 to 500 nm in the streak image. The fluorescence decay curve was analyzed by using the U8167-01 program (Hamamatsu). The decay curves were fitted with the bi-exponential function $\alpha_1 \exp(-t/\tau_1) + \alpha_2 \exp(-t/\tau_2)$

Measurement of absorption spectra and melting temperatures

Absorption spectra were measured on a JASCO model V-530, V-550, or V-560. The sample solutions contained 100 mM NaCl, 10 mM phosphate buffer, pH 7.0, 5.0 μM each strand. Absorption spectra were measured at 0 °C. The melting curves were measured with a UV-1800 (Shimadzu) by monitoring 260 nm absorbance versus temperature. The T_m was determined from the maximum in the first derivative of the melting curve. Both the heating and the cooling curves were measured, and the calculated T_m agreed to within 1.0 °C. The temperature ramp was 0.5 °C min^{-1} . The sample solutions contained 100 mM NaCl, 10 mM phosphate buffer, pH 7.0, 1.0 μM .

Calculation of FRET efficiency

Energy transfer efficiency was calculated from steady-state fluorescence (Φ_{T1}) or fluorescent lifetimes (Φ_{T2}). The apparent homo-FRET efficiency, Φ_{T1}' , was experimentally calculated from the following Equation (1):

$$\Phi_{T1}' = \frac{I_{DQ} + I_Q - I}{I_{DQ} - I_Q} \quad (1)$$

where I , I_Q and I_D are emission intensities of **PQ-P** duplex, **PQ** duplex and **P** duplex, respectively (Figure 5-1). When energy transfer between two pyrenes does not occur, I should be equal to I_{DQ} plus I_Q so that Φ_{T1}' becomes zero. In contrast, when excitation energy of pyrene at distant position perfectly transfers to pyrene next to anthraquinone, the intensity of the pyrene should be the same as that of the quenched one. Therefore, I should be equal to $2 I_Q$. In this case, Φ_{T1}' becomes unity (Figure S5-4).

The apparent homo-transfer efficiency, Φ_{T1}' , is affected by hetero-transfer from pyrene to the adjacent anthraquinone, and hetero-transfer from the pyrene at the distant position to anthraquinone also affects Φ_{T1}' . In order to compare efficiencies of homo-FRET between different sequences, the actual efficiency Φ_{T1} was calculated from Equation (2):

$$\Phi_{T1} = \frac{\Phi_{T1}'}{\frac{I_{DQ}}{I_D}(1 - \Phi_{T1}') + \Phi_{T1}'} \quad (2)$$

where I_D is emission intensity of the **P** duplex.

The homo-FRET efficiency, Φ_{T2} , was determined from fluorescence lifetime measurements. For **P** duplexes that contain one fluorophore and no quencher, the fluorescent lifetime (τ_D) can be represented as follows [Eq. (3)]:

$$\frac{1}{\tau_D} = k_f + k_{d1} \quad (3)$$

where k_f and k_{d1} are an emissive rate constant and a non-radiative decay rate, respectively. The rate constants of homo-transfer (k_t) and hetero-transfer (k_q) must be taken into account in duplexes with two pyrenes and one anthraquinone. Lifetimes of **PQ** duplexes could not be determined in time-resolved fluorescence measurements with our apparatus. Emission intensities of **PQ** duplexes were much lower than those of **P** duplexes, indicating that quenching by anthraquinone occurs very rapidly. Therefore, we ignored the decay rate of the quenched pyrene (k_{d2}) because it is much larger than the other rate constant. Therefore, τ , which is a lifetime of **PQ-P**, can be represented using k_t and k_q [Eq. (4)]:

$$\frac{1}{\tau} = k_t + k_q + k_f + k_{d1} \quad (4)$$

where k_q , the rate constant of the hetero-transfer, can be calculated by measuring a fluorescent lifetime of **Q-P** duplex (τ_{DQ}) [Eq. (5)]:

$$\frac{1}{\tau_{DQ}} = k_q + k_f + k_{d1} \quad (5)$$

Apparent homo-transfer efficiency (Φ_{T2}') can be calculated from Equations (3–5) to give Equation (6):

$$\Phi_{T2}' = \frac{k_t}{k_t + k_q + k_f + k_{d1}} = 1 - \frac{\tau_D}{\tau_{DQ}} \quad (6)$$

Φ_{T2}' is also affected by hetero-transfer from pyrene to anthraquinone. The actual homo-transfer efficiency Φ_{T2} was calculated by excluding effects of hetero-transfer using

Equation (7):

$$\Phi_{T2} = \frac{k_t}{k_t + k_f + k_{d1}} = \frac{1 - \frac{\tau_D}{\tau_{DQ}}}{(1 - \frac{\tau_D}{\tau_{DQ}}) + \frac{\tau}{\tau_D}} = \frac{\Phi_{T2}'}{\frac{\tau_{DQ}}{\tau_D}(1 - \Phi_{T2}') + \Phi_{T2}'} \quad (7)$$

Theoretical calculation of energy transfer efficiencies based on Förster theory

Energy transfer efficiency was calculated from the following equations:

$$\Phi_T = \frac{1}{1 + (R/R_0)^6} \quad (8)$$

$$R_0 = 0.2108[J(\lambda)\kappa^2n^{-4}\Phi_D]^{1/6} \quad (9)$$

$$\kappa^2 = \cos^2\theta_T \quad (10)$$

where R is the distance between donor and acceptor, and R_0 is a Förster radius (the distance where $\Phi_T = 0.5$). $J(\lambda)$ is integral of spectral overlap between donor emission and acceptor absorption at λ nm. n is a refractive index, which is typically assumed to be 1.4 for biomolecules, and Φ_D is a fluorescence quantum yield of pyrene. The orientation factor, κ^2 , was calculated from the above equation, where θ_T is the angle between transition dipoles of donor and acceptor.

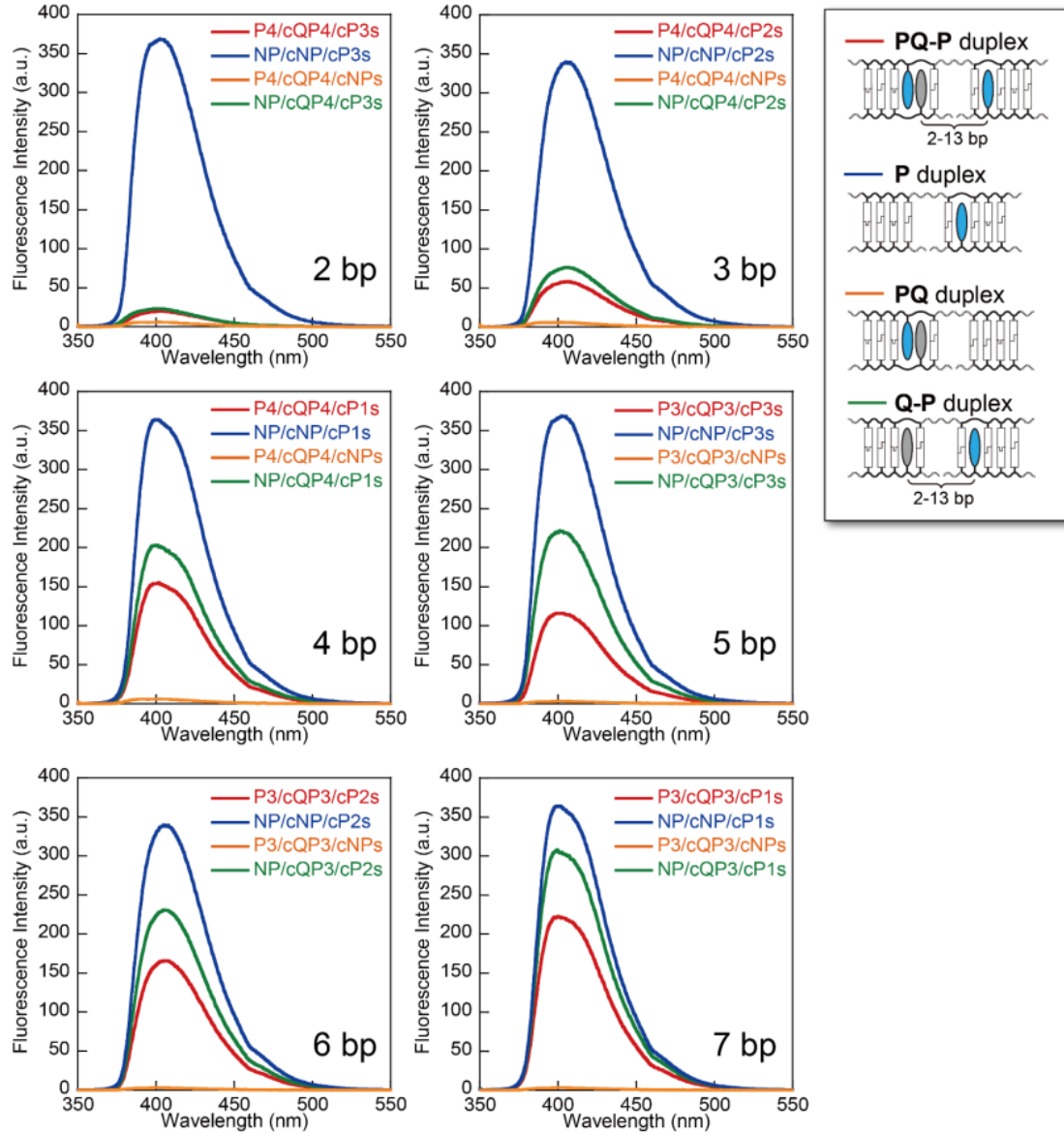
Theoretical transfer efficiency can be calculated from the distance and angle between two chromophores. Typical rise and twist angle of B-form duplex, 3.2 Å/base pair and 33°/base pair were used to calculate distance and angle between dyes (Figure S5-5). In our design, anthraquinone is located between two pyrenes. Therefore, we hypothesized that the distance between pyrene increased by 3.2 Å for each additional base pair between the dye pair and the lone pyrene. The dye angle, which is the sum of angles between fluorophores and neighboring base pairs, was assumed to be 4°, which was estimated from curve fitting and molecular modelling.

5-6 References

- [1] H. Kashida, H. Kawai, R. Maruyama, Y. Kokubo, Y. Araki, T. Wada, H. Asanuma, *Commun. Chem.* **2018**, *1*, 91
- [2] a) J. Gao, C. Strässler, D. Tahmassebi, E. T. Kool, *J. Am. Chem. Soc.* **2002**, *124*, 11590–11591; b) U. B. Christensen, E. B. Pedersen, *Nucleic Acids Res.* **2002**, *30*, 4918–4925; c) S. M. Langenegger, R. Häner, *Chem. Commun.* **2004**, 2792–2793; d) A. Okamoto, T. Ichiba, I. Saito, *J. Am. Chem. Soc.* **2004**, *126*, 8364–8365; e) P. J. Hrdlicka, B. R. Babu, M. D. Sorensen, N. Harrit, J. Wengel, *J. Am. Chem. Soc.* **2005**, *127*, 13293–13299; f) A. Trifonov, M. Raytchev, I. Buchvarov, M. Rist, J. Barbaric, H. A. Wagenknecht, T. Fiebig, *J. Phys. Chem. B* **2005**, *109*, 19490–19495; g) H. Kashida, H. Asanuma, M. Komiyama, *Chem. Commun.* **2006**, 2768–2770; h) Y. J. Seo, H. Rhee, T. Joo, B. H. Kim, *J. Am. Chem. Soc.* **2007**, *129*, 5244–5247; i) V. L. Malinovskii, F. Samain, R. Häner, *Angew. Chem. Int. Ed.* **2007**, *46*, 4464–4467; *Angew. Chem.* **2007**, *119*, 4548–4551; j) M. Nakamura, Y. Murakami, K. Sasa, H. Hayashi, K. Yamana, *J. Am. Chem. Soc.* **2008**, *130*, 6904–6905; k) Y. N. Teo, J. N. Wilson, E. T. Kool, *J. Am. Chem. Soc.* **2009**, *131*, 3923–3933; l) H. Kashida, H. Azuma, R. Maruyama, Y. Araki, T. Wada, H. Asanuma, *Angew. Chem. Int. Ed.* **2020**, *59*, 11360–11363; m) C. B. Winiger, S. M. Langenegger, G. Calzaferri, R. Häner, *Angew. Chem. Int. Ed.* **2015**, *54*, 3643–3647; *Angew. Chem.* **2015**, *127*, 3714–3718
- [3] T. Doi, T. Sakakibara, H. Kashida, Y. Araki, T. Wada, H. Asanuma, *Chem. Eur. J.*, **2015**, *21*, 15974–15980.
- [4] a) T. Kato, H. Kashida, H. Kishida, H. Yada, H. Okamoto, H. Asanuma, *J. Am. Chem. Soc.* **2013**, *135*, 741–750; b) H. Kashida, A. Kurihara, H. Kawai, H. Asanuma, *Nucleic Acids Res.* **2017**, *45*, e105; c) H. Kashida, Y. Kokubo, K. Makino, H.

- Asanuma, *Org. Biomol. Chem.* **2019**, *17*, 6786–6789.
- [5] T. Fujii, H. Kashida, H. Asanuma, *Chem. Eur. J.* **2009**, *15*, 10092–10102.
- [6] a) P. D. Cunningham, Y. C. Kim, S. A. Díaz, S. Buckhout-White, D. Mathur, I. L. Medintz, J. S. Melinger, *J. Phys. Chem. B* **2018**, *122*, 5020–5029; b) J. S. Huff, P. H. Davis, A. Christy, D. L. Kellis, N. Kandadai, Z. S. D. Toa, G. D. Scholes, B. Yurke, W. B. Knowlton, R. D. Pensack, *J. Phys. Chem. Lett.* **2019**, *10*, 2386–2392; c) Y. Hara, T. Fujii, H. Kashida, K. Sekiguchi, X. Liang, K. Niwa, T. Takase, Y. Yoshida, H. Asanuma, *Angew. Chem. Int. Ed.* **2010**, *49*, 5502–5506; *Angew. Chem.* **2010**, *122*, 5634–5638
- [7] a) F. D. Lewis, L. Zhang, X. Zuo, *J. Am. Chem. Soc.* **2005**, *127*, 10002–10003; b) A. Iqbal, S. Arslan, B. Okumus, T. J. Wilson, G. Giraud, D. G. Norman, T. Ha, D. M. J. Lilley, *Proc. Natl. Acad. Sci. USA* **2008**, *105*, 11176–11181; c) K. Börjesson, S. Preus, A. H. El-Sagheer, T. Brown, B. Albinsson, L. M. Wilhelmsson, *J. Am. Chem. Soc.* **2009**, *131*, 4288–4293; d) S. Preus, K. Kilså, F.-A. Miannay, B. Albinsson, L. M. Wilhelmsson, *Nucleic Acids Res.* **2013**, *41*, e18; e) T. Fessl, David M. J. Lilley, *Biophys. J.* **2013**, *105*, 2175–2181; f) M. S. Wranne, A. F. Füchtbauer, B. Dumat, M. Bood, A. H. El-Sagheer, T. Brown, H. Gradén, M. Grøtli, L. M. Wilhelmsson, *J. Am. Chem. Soc.* **2017**, *139*, 9271–9280.

5-7 Appendixes



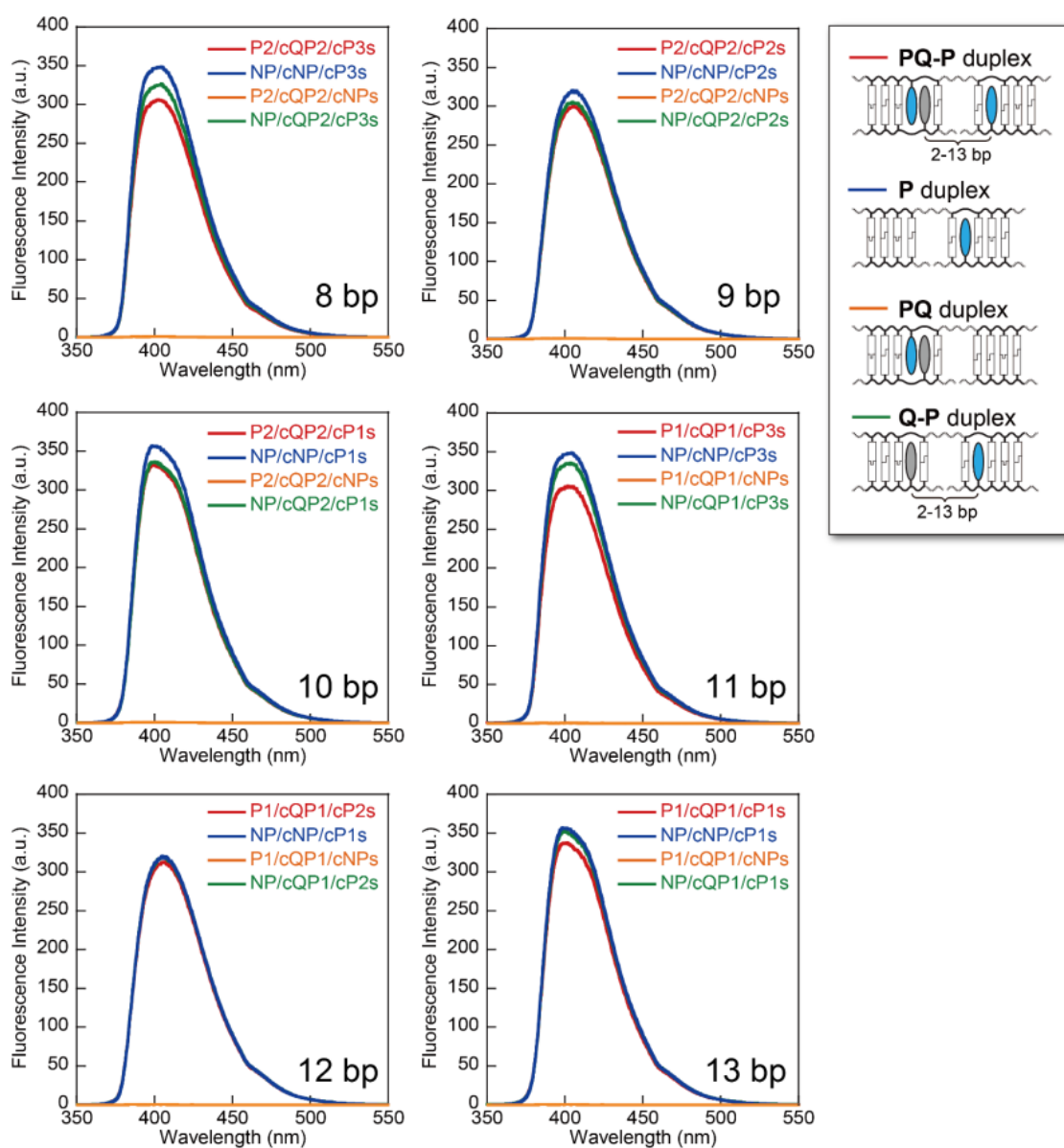
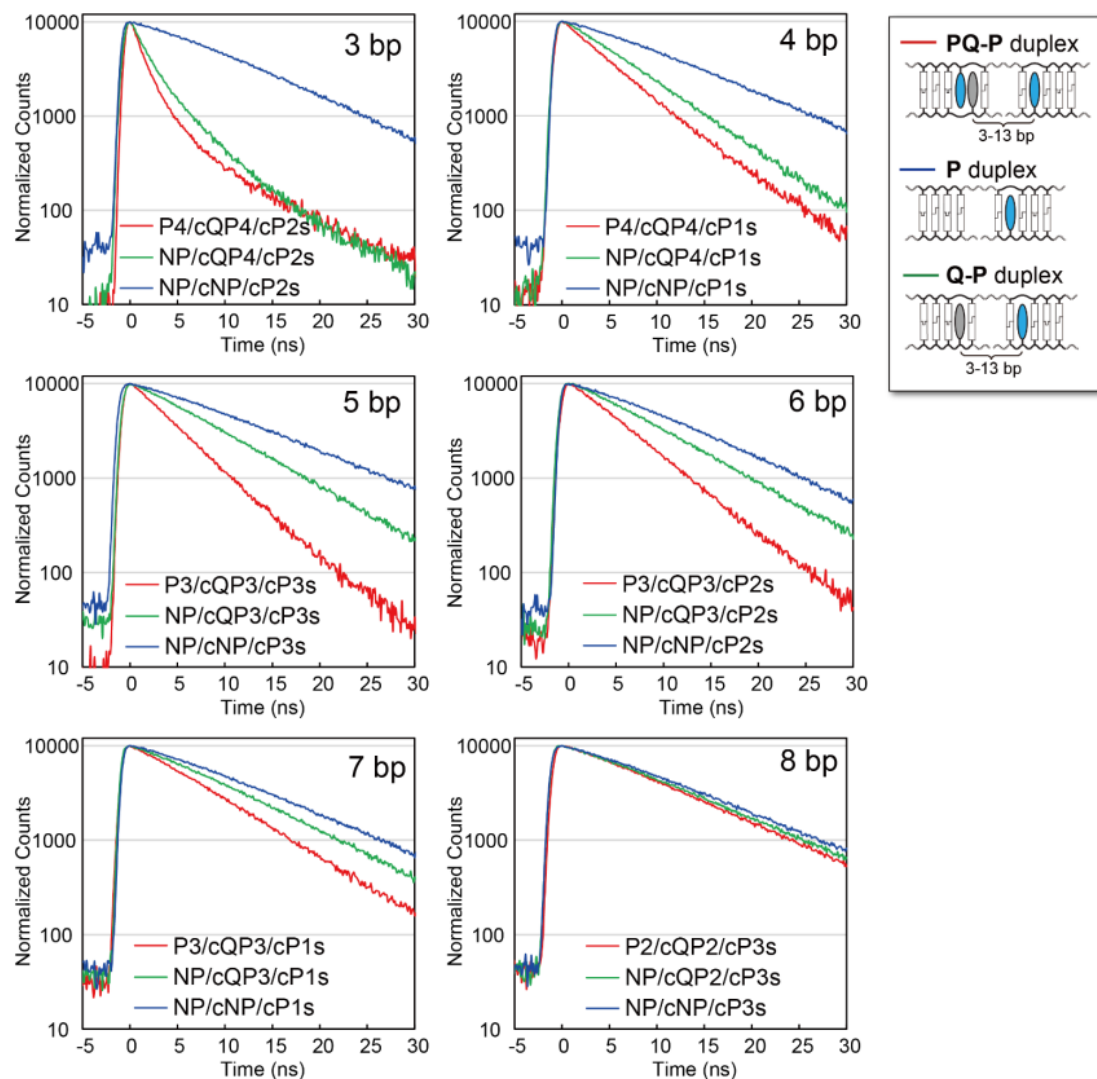


Figure S5-1. Emission spectra of **PQ-P** (red lines), **P** (blue lines), **PQ** (orange lines), and **Q-P** duplexes (green lines) with indicated separations in base pairs (bp) between the pyrene-anthraquinone pair and the lone pyrene.



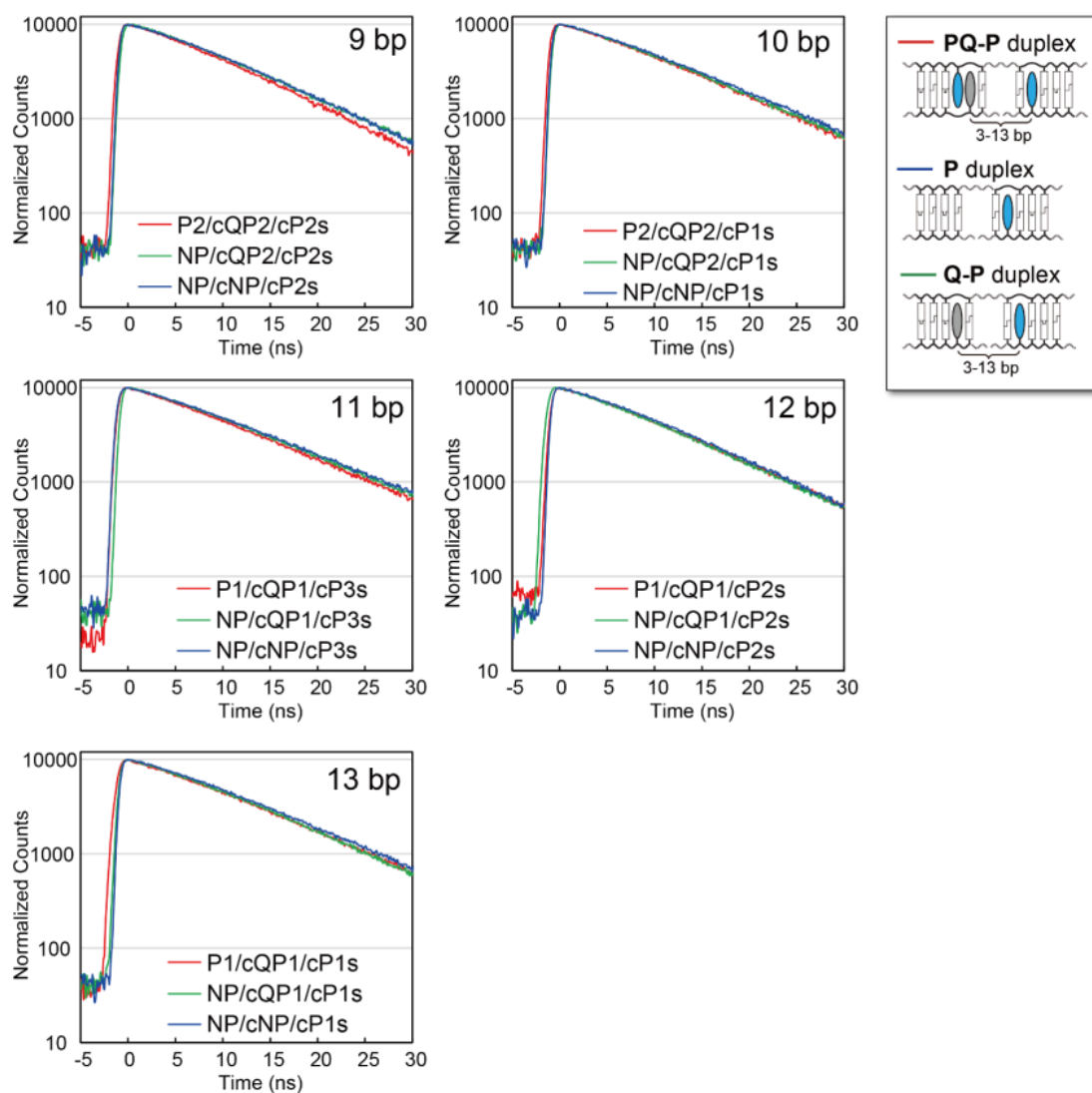


Figure S5-2. Fluorescence lifetime measurements of **PQ-P** (red lines), **P** (blue lines) and **Q-P** duplexes (green lines) with indicated separations in base pairs (bp) between the pyrene-anthraquinone pair and the lone pyrene.

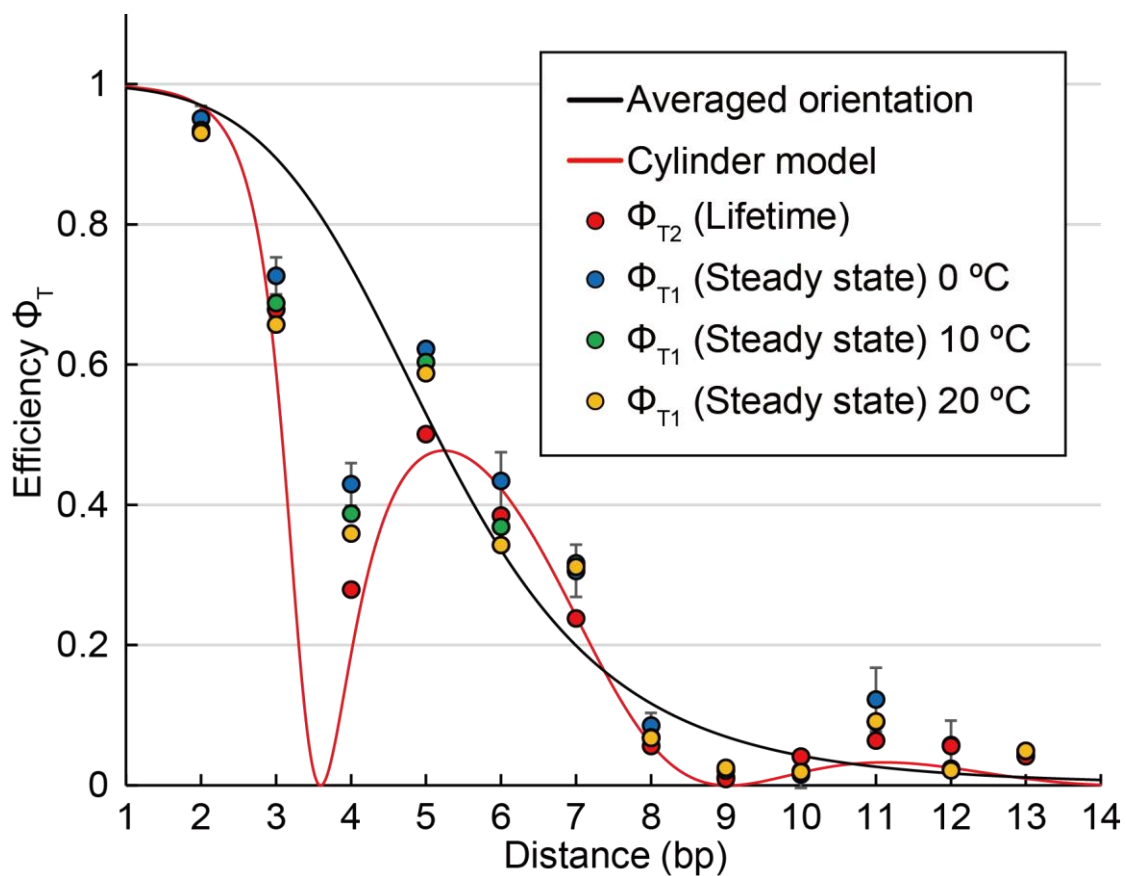


Figure S5-3. Effects of temperature on homo-FRET efficiency of pyrene. Error bars of Φ_{T1} show standard deviation of three independent measurements.

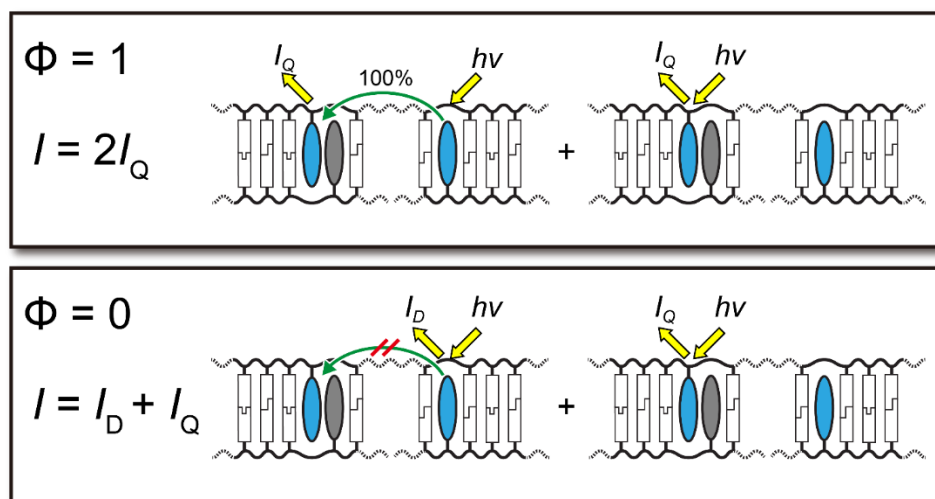


Figure S5-4. Schematic illustration of total emission observed from PQ-P duplex.

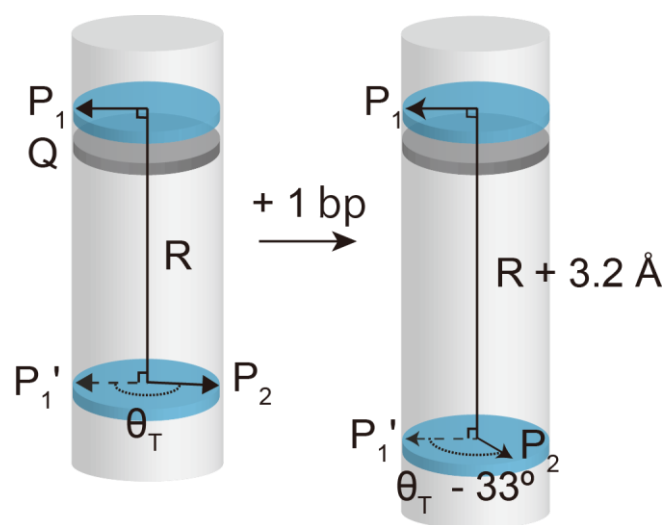
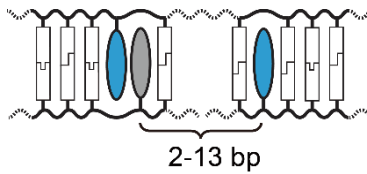
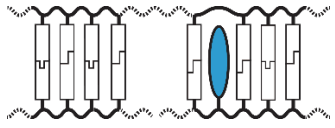
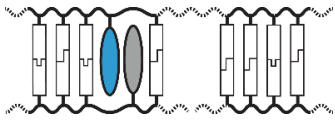


Figure S5-5.

Cylinder model of DNA duplex to calculate homo FRET efficiency theoretically.

Table S5-1. Sequences of pyrene modified DNA used in this study

	Distance	Sequence	
 <p>2-13 bp</p> <p>PQ-P duplex</p>	2 bp	P4 CAGGCTAGATAAT PAT ATAAGTGACCTC (5'→3') cQP4/cP3s GTCCGATCTATTA QTATP TTCCTGGAG (3'←5')	
	3 bp	P4 CAGGCTAGATAAT PATA TAAGTGACCTC (5'→3') cQP4/cP2s GTCCGATCTATTA QTATP TTCCTGGAG (3'←5')	
	4 bp	P4 CAGGCTAGATAAT PATAT AAGTGACCTC (5'→3') cQP4/cP1s GTCCGATCTATTA QTATP TTCCTGGAG (3'←5')	
	5 bp	P3 CAGGCTAGAT PAATAT ATAAGTGACCTC (5'→3') cQP3/cP3s GTCCGATCTA QTTATAP TTCCTGGAG (3'←5')	
	6 bp	P3 CAGGCTAGAT PAATATA TAAGTGACCTC (5'→3') cQP3/cP2s GTCCGATCTA QTTATAP TTCCTGGAG (3'←5')	
	7 bp	P3 CAGGCTAGAT PAATATAT AAGTGACCTC (5'→3') cQP3/cP1s GTCCGATCTA QTTATAP TTCCTGGAG (3'←5')	
	8 bp	P2 CAGGCTA PGATAATAT ATAAGTGACCTC (5'→3') cQP2/cP3s GTCCGAT QCTATTATAP TTCCTGGAG (3'←5')	
	9 bp	P2 CAGGCTA PGATAATATA TAAGTGACCTC (5'→3') cQP2/cP2s GTCCGAT QCTATTATAP TTCCTGGAG (3'←5')	
	10 bp	P2 CAGGCTA PGATAATATAT AAGTGACCTC (5'→3') cQP2/cP1s GTCCGAT QCTATTATAP TTCCTGGAG (3'←5')	
	11 bp	P1 CAGG PCTAGATAATAT ATAAGTGACCTC (5'→3') cQP1/cP3s GTCC QGATCTATTATAP TTCCTGGAG (3'←5')	
	12 bp	P1 CAGG PCTAGATAATATA TAAGTGACCTC (5'→3') cQP1/cP2s GTCC QGATCTATTATAP TTCCTGGAG (3'←5')	
	13 bp	P1 CAGG PCTAGATAATATAT AAGTGACCTC (5'→3') cQP1/cP1s GTCC QGATCTATTATAP TTCCTGGAG (3'←5')	
	 <p>P duplex</p>	-	NP CAGGCTAGATAATATAT AAGTGACCTC (5'→3') cNP/cP1s GTCCGATCTATTAT ATAP TTCCTGGAG (3'←5')
-		NP CAGGCTAGATAATATA TAAGTGACCTC (5'→3') cNP/cP2s GTCCGATCTATTAT ATP TTCCTGGAG (3'←5')	
-		NP CAGGCTAGATAATAT ATAAGTGACCTC (5'→3') cNP/cP3s GTCCGATCTATTAT APT TTCCTGGAG (3'←5')	
 <p>PQ duplex</p>	-	P4 CAGGCTAGATAAT PATATA AAGTGACCTC (5'→3') cQP4/cNPs GTCCGATCTATTA QTATAT TTCCTGGAG (3'←5')	
	-	P3 CAGGCTAGAT PAATATATA AAGTGACCTC (5'→3') cQP3/cNPs GTCCGATCTA QTTATATAT TTCCTGGAG (3'←5')	
	-	P2 CAGGCTA PGATAATATATA AAGTGACCTC (5'→3') cQP2/cNPs GTCCGAT QCTATTATATAT TTCCTGGAG (3'←5')	
	-	P1 CAGG PCTAGATAATATATA AAGTGACCTC (5'→3') cQP1/cNPs GTCC QGATCTATTATATAT TTCCTGGAG (3'←5')	
	-		

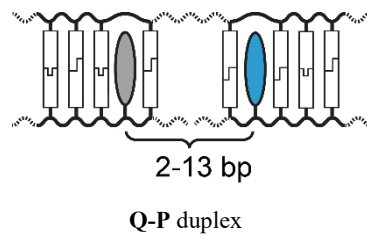
	Distance	Sequence	
	2 bp	NP cQP4/cP3s	CAGGCTAGATAAT AT ATAAGTGACCTC (5'→3') GTCCGATCTATTAQTATPTTCACTGGAG (3'←5')
	3 bp	NP cQP4/cP2s	CAGGCTAGATAAT ATA TAAGTGACCTC (5'→3') GTCCGATCTATTAQTATPTTCACTGGAG (3'←5')
	4 bp	NP cQP4/cP1s	CAGGCTAGATAAT ATAT AAGTGACCTC (5'→3') GTCCGATCTATTAQTATPTTCACTGGAG (3'←5')
	5 bp	NP cQP3/cP3s	CAGGCTAGAT AATAT ATAAGTGACCTC (5'→3') GTCCGATCTAQTATTATPTTCACTGGAG (3'←5')
	6 bp	NP cQP3/cP2s	CAGGCTAGAT AATATA TAAGTGACCTC (5'→3') GTCCGATCTAQTATTATPTTCACTGGAG (3'←5')
	7 bp	NP cQP3/cP1s	CAGGCTAGAT AATATAT AAGTGACCTC (5'→3') GTCCGATCTAQTATTATPTTCACTGGAG (3'←5')
	8 bp	NP cQP2/cP3s	CAGGCTA GATAATAT ATAAGTGACCTC (5'→3') GTCCGATQCTATTATATPTTCACTGGAG (3'←5')
	9 bp	NP cQP2/cP2s	CAGGCTA GATAATATA TAAGTGACCTC (5'→3') GTCCGATQCTATTATATPTTCACTGGAG (3'←5')
	10 bp	NP cQP2/cP1s	CAGGCTA GATAATATAT AAGTGACCTC (5'→3') GTCCGATQCTATTATATPTTCACTGGAG (3'←5')
	11 bp	NP cQP1/cP3s	CAGG CTAGATAATAT ATAAGTGACCTC (5'→3') GTCCQGATCTATTATATPTTCACTGGAG (3'←5')
	12 bp	NP cQP1/cP2s	CAGG CTAGATAATATA TAAGTGACCTC (5'→3') GTCCQGATCTATTATATPTTCACTGGAG (3'←5')
	13 bp	NP cQP1/cP1s	CAGG CTAGATAATATAT AAGTGACCTC (5'→3') GTCCQGATCTATTATATPTTCACTGGAG (3'←5')

Table S5-2. Melting temperatures of duplexes used in this study..

Sequence			$T_m / ^\circ\text{C}$
P1 cQP1	CAGG P CTAGATAAATATATAAGTGACCTC GTCC Q GATCTATTAT	(5'→3') (3'←5')	45.0
P2 cQP2	CAGGCTA P GATAAATATATAAGTGACCTC GTCCGAT Q CTATTAT	(5'→3') (3'←5')	53.5
P3 cQP3	CAGGCTAGAT P AATATATAAGTGACCTC GTCCGATCTA Q TTAT	(5'→3') (3'←5')	53.2
P4 cQP4	CAGGCTAGATAAAT P ATATAAGTGACCTC GTCCGATCTATTA Q T	(5'→3') (3'←5')	51.9
P1 cNP	CAGG P CTAGATAAATATATAAGTGACCTC GTCC GATCTATTAT	(5'→3') (3'←5')	44.1
P2 cNP	CAGGCTA P GATAAATATATAAGTGACCTC GTCCGAT CTATTAT	(5'→3') (3'←5')	48.4
P3 cNP	CAGGCTAGAT P AATATATAAGTGACCTC GTCCGATCTA TTAT	(5'→3') (3'←5')	48.5
P4 cNP	CAGGCTAGATAAAT P ATATAAGTGACCTC GTCCGATCTATTA T	(5'→3') (3'←5')	47.8
NP cQP1	CAGG CTAGATAAATATATAAGTGACCTC GTCC Q GATCTATTAT	(5'→3') (3'←5')	45.8
NP cQP2	CAGGCTA GATAAATATATAAGTGACCTC GTCCGAT Q CTATTAT	(5'→3') (3'←5')	48.9
NP cQP3	CAGGCTAGAT AATATATAAGTGACCTC GTCCGATCTA Q TTAT	(5'→3') (3'←5')	51.3
NP cQP4	CAGGCTAGATAAAT ATATAAGTGACCTC GTCCGATCTATTA Q T	(5'→3') (3'←5')	51.8
NP cNP	CAGGCTAGATAAATATATAAGTGACCTC GTCCGATCTATTAT	(5'→3') (3'←5')	45.4
NP cP1s	CAGGCTAGATAAATATAT AAGTGACCTC AT P TTCACTGGAG	(5'→3') (3'←5')	47.6
NP cP2s	CAGGCTAGATAAATATA TAAGTGACCTC AT P ATTCACTGGAG	(5'→3') (3'←5')	43.8
NE cP3s	CAGGCTAGATAAATAT ATAAGTGACCTC A P TATTCACTGGAG	(5'→3') (3'←5')	47.1
NE cNPs	CAGGCTAGATAAATATATAAGTGACCTC ATATTCACTGGAG	(5'→3') (3'←5')	43.1

List of Publications

Journal Articles

- 1) "Orientation-dependent FRET system reveals differences in structures and flexibilities of nicked and gapped DNA duplexes" Hiromu Kashida, Ayako Kurihara, Hayato Kawai, Hiroyuki Asanuma, *Nucleic Acids Res.*, **2017**, *45*, e105.
- 2) "Quantitative evaluation of energy migration between identical chromophores enabled by breaking symmetry" Hiromu Kashida, Hayato Kawai, Ryoko Maruyama, Yuta Kokubo, Yasuyuki Araki, Takehiko Wada, Hiroyuki Asanuma, *Communications Chemistry*, **2018**, *1*, 91.
- 3) "Quantitative Analyses of Forster Resonance Energy Transfer between Identical Pyrene Chromophores (Homo-FRET) In DNA Scaffolds" Hiromu Kashida, Hayato Kawai, Hidenori Azuma, Yasuyuki Araki, Takehiko Wada, Hiroyuki Asanuma, *ChemPhotoChem*, **2021**, *5*, 167-172.
- 4) "Perylene-Cy3 FRET System to Analyze Photoactive DNA Structures" Hayato Kawai, Tetsuya Doi, Yuka Ito, Tatsuya Kameyama, Tsukasa Torimoto, Hiromu Kashida, Hiroyuki Asanuma, *Chem. Eur. J.*, **2021**, *27*, 12845-12850.

List of Presentations

International Conference

"Structural analysis of modified DNA by using FRET system" Hayato Kawai, Tetsuya Doi, Hiromu Kashida, Hiroyuki Asanuma, The 11th SPSJ International Polymer Conference, December 13-16 Fukuoka (Japan), The Society of Polymer Science, Japan

Internal Conference

9 presentations. Omitted.

List of Awards

- 1) 第 9 回バイオ関連化学シンポジウム学生ポスター賞(Organic & Biomolecular Chemistry)、「FRET の配向依存性を利用した DNA 二重鎖中における色素会合体の構造解析」、2015 年 9 月 11 日、日本化学会—生体機能関連化学部会・バイオテクノロジー部会
- 2) 日本化学会東海支部長賞、2017 年 3 月、日本化学会東海支部

Acknowledgements

The present article is a thesis for application of doctoral degree at the Department of Biomolecular Engineering, Graduate School of Engineering, Nagoya University. All the study work was carried out under direction of Professor Hiroyuki Asanuma from April 2014 to March 2022.

I would like to express my sincere gratitude to Prof. Hiroyuki Asanuma and Associate Professor Hiromu Kashida who provided a number of helpful comments and valuable suggestions which were necessary for improvement of this study. I also especially thank Associate Professor Yukiko Kamiya and Assistant Professor Keiji Murayama who provided a lot of comments for my investigation.

I would also like to thank my coworkers Dr. Tetsuya Doi, Ms. Ayako Kurihara, Ms. Ryoko Maruyama, Mr. Yuta Kokubo Mr. Hidenori Azuma, Ms. Yuka Ito and other members of Asanuma Laboratory for their contribution to this study. Especially, I would thank Ms. Ayako Kurihara for providing me her valuable data in Chapter 2 and Ms. Ryoko Maruyama who provided her valuable data in Chapter 4.

Finally, I would like to give special thanks to Professor Tsukasa Torimoto and Professor Kentaro Tanaka for giving helpful comments and suggestion on this thesis.